INFORMATION TO USERS

This manuscript has been reproduced from the microfilm master. UMI films the text directly from the original or copy submitted. Thus, some thesis and dissertation copies are in typewriter face, while others may be from any type of computer printer.

The quality of this reproduction is dependent upon the quality of the copy submitted. Broken or indistinct print, colored or poor quality illustrations and photographs, print bleedthrough, substandard margins, and improper alignment can adversely affect reproduction.

In the unlikely event that the author did not send UMI a complete manuscript and there are missing pages, these will be noted. Also, if unauthorized copyright material had to be removed, a note will indicate the deletion.

Oversize materials (e.g., maps, drawings, charts) are reproduced by sectioning the original, beginning at the upper left-hand corner and continuing from left to right in equal sections with small overlaps. Each original is also photographed in one exposure and is included in reduced form at the back of the book.

Photographs included in the original manuscript have been reproduced xerographically in this copy. Higher quality 6" x 9" black and white photographic prints are available for any photographs or illustrations appearing in this copy for an additional charge. Contact UMI directly to order.

U·M·I

University Microfilms International
A Bell & Howell Information Company
300 North Zeeb Road, Ann Arbor, MI 48106-1346 USA
313/761-4700 800/521-0600

Order Number 9130390

Effect of high-temperature and fiber distribution on matrix microcracking and toughness of ceramic matrix composites

Xu, Yongli, Ph.D.

City University of New York, 1991

U·M·I
300 N. Zeeb Rd.
Ann Arbor, MI 48106

EFFECT OF HIGH TEMPERATURE AND FIBER DISTRIBUTION ON MATRIX MICROCRACKING AND TOUGHNESS OF CERAMIC MATRIX COMPOSITES

by

YONGLI XU

A dissertation submitted to the Graduate Faculty in Engineering in partial fulfilment of the requirements for the degree of Doctor of Philosophy, The City University of New York.

1991

This manuscript has been read and accepted for the Graduate Faculty in Engineering in satisfaction of the dissertation requirement for the degree of Doctor of Philosophy.

4/9/91
Date

Feridun Delale
Chair of Examining Committee

4/9/91
Date

Gerard L. Cohen
Executive Officer

Prof. Feridun Delale (Chair)

Prof. Stephen C. Cowin

Prof. Mumtaz Kassir

Prof. Ali M. Sadegh

Prof. Benjamin Been-Ming Liaw

Prof. Alan Lau
Supervisory Committee

The City University of New York

ABSTRACT

EFFECT OF HIGH TEMPERATURE AND FIBER DISTRIBUTION ON MATRIX MICROCRACKING AND TOUGHNESS OF CERAMIC MATRIX COMPOSITES

by

Yongli Xu

Adviser: Professor Feridun Delale

The ceramic material has long been recognized as a material of potential uses owing to its very appealing features such as stability under high temperature and lightness. Nevertheless, due to low strength and fracture toughness, its structural use was limited. Through these years extensive efforts have been made to improve the toughness and strength of ceramic materials and ceramic composites are developed.

In this dissertation microcracking in ceramic matrix composites is studied. It is believed that behaviors of microscopic microcracks in the ceramic matrix composite have significant effect on the overall toughness and strength of the material. The aim of this study is to investigate effect of fiber distribution, and temperature on matrix microcracking and toughness of the material, because ceramic matrix composites are expected to work under high temperature circumstances.

In chapter II, III and IV, two theoretical models of microcracking (two-fiber model and ring model) are proposed and used for the analyses of microcracking. Stress intensity factors or strain energy release rates are calculated for radial, interfacial and matrix cracks for both mechanical and thermal loading. Effect of fiber distribution and mismatch of mechanical constants of fiber and matrix materials are investigated.

In chapter V, experimental results are reported. Effect of temperature on toughness of ceramic matrix materials (SiC and CAS II) is studied experimentally by using micro-indentation technique. Further, effect of fiber distribution as well as temperature on matrix microcracking are investigated. Experimental results are compared with theoretical predictions.

In chapter VI, fiber debonding tests are reported. Debonding test data are used for the calculation of bonding strength of fiber-matrix interfaces in conjunction with a theoretical model and finite element procedure. A formula for the evaluation of the bonding strength under elevated temperature using shear stress criterion is proposed.

To my wife Nanying,
my parents, my sisters and
my brothers.

ACKNOWLEDGEMENTS

I wish to express my sincere appreciation to my advisor, Professor Feridun Delale for his support, guidance and fellowship through the course of this research. His profound knowledge, sharpness and efficiency deeply impressed me and he will always be an example to me in my pursuit of a professional career.

I would like specially thank professor Benjamin Been-Ming Liaw for his help in my experimental work.

I also wish to extend my gratitude to Dean Gerard G. Lowen and other members of my supervisory committee for all the arrangements, their time and interest.

The study was sponsored by AFSOR under grant ASFOR-87-0288, part of the equipment used in the investigation was acquired through NSF equipment grants, MSM-85060495 and MSM-8805710. All the financial supports are gratefully acknowledged.

TABLE OF CONTENTS

LIST OF TABLES

LIST OF FIGURES

CHAPTER I
INTRODUCTION

I.1 BACKGROUND AND OBJECTIVES

In developing light-weight, high-temperature-resistant materials which are indispensible in some important industries such as aerospace and engine industries, ceramics have drawn much more attention than any other materials owing to some of their very appealing properties such as low environmental degradation, lightness and high resistance to oxidation under high temperatures. However, as is known to all, monolithic ceramics are very brittle and fragile, in other words, they have very low toughness which is the main impediment that prevented them for years from wide engineering applications. Having recognized their potential use, extensive efforts have been made through the years to improve toughness and strength of ceramic materials. For instance, structuralization of ceramic materials is one of such measures, namely, construction of whisker reinforced ceramic composites, fiber reinforced ceramic composites, laminates, etc. Thanks to such efforts and especially owing to some important breakthroughs in technologies for manufacturing and processing ceramic composites some ceramic matrix composites exhibit considerably high strength and toughness, and have been successfully employed as structural materials[1].

Since brittleness is the vital weakness of ceramics, naturally toughness of the material is always of special concern in the development of ceramic composites. From the viewpoint of fracture mechanics it is believed that the fracture failure of brittle materials usually originates from some imperfections in the material. For ceramic materials such imperfections could be voids or microcracks formed in the manufacturing process due to some

reasons such as fiber-matrix thermal expansion mismatch, phase transformation, or thermal anistropy, etc. The deleterious effect of voids on the mechanical properties of ceramic materials has been extensively studied and documented in [2-9], therefore the present study focuses on the effect of microcracking on the toughness and strength of ceramic matrix composites. Although according to some authors[2], a controlled amount of microcracks can even improve toughness of ceramic materials, it is generally believed that microcracking has detrimental effect on the toughness of ceramic matrix composites.

The failure mechanism of ceramic matrix composites is very intricate due to the existence of fibers. But observation of tensile tested specimen reveals that failure of the ceramic composite generally starts in the matrix and occures in successive stages, i.e., multiple matrix cracking(microcracks propagate and join up and develope into multiple matrix cracks), fiber breaking, fiber pullout, and final fracture failure (see Fig.1). This observation, if perfectly true, is extremely important and significant because it discloses that behavior of microcracks including factors that influence microcracking must have substantial bearing on the overall strength and toughness of ceramic composites.

According to their geometries, microcracks can be classified as matrix cracks, radial cracks and interfacial cracks (see Fig.2). Among these cracks matrix cracks and radial cracks are considered more hazardous than interfacial cracks, because interfacial cracks at worst would just cause complete debonding and disable involved fibers, while matrix cracks and radial cracks would possibly join up to form multiple cracks and lead to catastrophic fracture failure.

As far as microcrack propagation is concerned, fiber-matrix bonding strength at the interface is also very important. It is found that a weak bonding will make crack deflection possible, i.e., if fibers have a not-very-strong bond with matrix at the interfaces, when a crack propagates towards a fiber it would cause fiber debonding but then possibly be arrested there (crack deflection) (see Fig.3).

In this dissertation microcracking in ceramic matrix composites is studied (Nicalon/SiC specimen is used in experiments). Based on above analysis, also bearing in mind the fact that ceramic matrix composites are expected to work under high temperatures, the aim of this study is to investigate effect of temperature and fiber distribution on matrix microcracking and toughness of ceramic matrix composites. It is hoped that study will reveal an insight in analyzing microcracking in ceramic matrix composites.

Study is conducted from following aspects:

a) theoretical analysis is conducted by using microcracking models. Based on observation of some ceramic composite specimens under optical and scanning electron microscopes two theoretical models of microcracking are proposed and used in the analysis. The first one is two-fiber model which defines two equal-sized circular fibers embedded in infinite matrix. Both radial and interfacial cracks (interfacial crack is actually partial debonding of the fiber-matrix interface) are considered. The purpose of two-fiber model is to analyze the effect of fiber interaction on microcracking. The second theoretical model is ring model which describes a crack in an infinitely extended matrix and surrounded

by a circularly distributed array of fibers (a ring-shaped composite zone is formed by the surrounding fibers and matrix). Effect of fiber distribution in the ring model is reflected on volume fraction of fibers for the composite in the ring in an average sense.

b) parallel to theoretical analysis, experiments are performed. First using micro-indentation technique and monolithic SiC specimens, we determine fracture toughness of matrix material(Nicalon/SiC composite), and then study temperature effect on toughness of the matrix material. Next, using micro-indentation technique again and Nicalon/SiC composite specimens, we study the effect of temperature and fiber distribution on matrix cracking. Experimental results are compared with theoretical results.

c) debonding tests (Nicalon/SiC specimen) are performed; fiber-matrix interfaces are forcefully debonded to obtain critical loads at debonding initiaion. Data are then used to evaluate bonding strength of fiber-matrix interfaces.

Following a briefing on modeling of microcracking in chapter II, theoretical analysis using two-fiber model is given in chapter III. Approximate approaches for the evaluation of stress intensity factors or strain energy release rates (for both radial and interfacial cracks) are developed by using single-fiber solution and the combination of finite element and singular integral equation techniques.

Theoretical analysis using ring model is given in chapter IV, exact analytical solutions for stress intensity factors of matrix cracks (for both mechanical and thermal loading) are obtained by using singular integral equation technique.

Effect of temperature and fiber distribution on matrix microcracking was also studied experimentally. Experimental results, i.e., "apparent critical stress intensity factors" versus "local volume fraction of fibers" for temperature ranging from room temperature to 800°C are given in chapter IV. Experimental results are compared with theoretical anticipation. The concept of "apparent critical stress intensity factor" is of evident practical significance for the estimation of microcrack propagation in ceramic matrix composites.

Results of debonding tests (Nicalon/SiC specimen) are given in Chapter VI, and a finite element procedure is developed to relate debonding load to stresses on the fiber-matrix interface; critical shear stress or shear bonding strength is calculated. A generic formula which includes the effect of temperature for the evaluation of bonding strength in light of maximum shear stress criterion is also proposed.

I.2 REVIEW OF PREVIOUS WORK

Since monolithic ceramics, particulate ceramic composites and fiber reinforced ceramic composites all belong to ceramic materials with low toughness and microcracking being their common concern, information from microcracking study in monolithic ceramics and particulate composites is also useful for the study of microcracking in fiber reinforced composites. Nevertheless, due to its specific microstructure, microcracking in the fiber reinforced composite has its own unique charateristics. In this section the previous work on fiber reinforced ceramic composites is reviewed. Some important literature on microcracking in monolithic ceramics and particulate composites may be found in [10-28].

As for ceramic matrix composites (from now on throughout this dissertation, the term "ceramic matrix composites" will be used to refer to fiber reinforced ceramic matrix composites), although the relevent literature is extensive, most of the previous studies are concerned with the tensile and flextural strength of these materials. Tensile and bending tests were reported to have been done for a variety of ceramic matrix composite systems [29-34]. Toughness or mechanism of fractural failure of these materials were studied by means of in situ observation and/or fractographic analyses of failed specimens. Failure mechanism of ceramic-fiber/ceramic-matrix composites was discussed by D.B.Marshall and A.G.Evans [34]. In their study it was noted that failure under tension occurs in a succession of stages, namely, multiple matrix cracking, fiber pullout and fiber breaking. The study includes another extremely important observation that there may not be chemical bonding between fibers and matrix and that at the fiber-matrix interface loads are carried by frictional forces. Needless to say, this finding is extremely important in modeling of the fiber-matrix interface. The same study also explored the indentaton method [35] to measure the frictional and residual stresses. In another study by the same authors [36] mutiple matrix cracking problem was analyzed, the effect of fibers that bridge the cracked matrix is represented by closure tractions applied on the crack surfaces, the stress intensity factor for the mutiple matrix crack was evaluated. Fiber-matrix bonding strength problems were also studied by several other authors [37][38][39]. Fiber pullout or pushout tests were performed in these tests and fibers were forced to slip relative to matrix, the frictional force between fibers and matrix was measured and bonding strength was thus defined and calculated. Fiber debonding tests were reported to have been

performed in [40] and bonding strength at debonding initiation was defined and calculated by using finite element method.

As for analytical approach to microcracking problems, i.e., studying microcracking by using theoretical models, only a few papers were found. Complex variable method and singular integral equation are the major techniques used in those studies. Usually strain energy release rates or stress intensity factors were calculated, and in some study critical fiber size below which microcracks can practically be suppressed, was also calculated.

Among those studies microcracking due to residual stresses was studied by F. Delale [41] using single-fiber model. Strain energy release rates and critical fiber sizes were calculated for both radial and interfacial cracks geometries (see Fig.4).

C.Atkinson studied interaction between a radial crack and an inclusion embedded in an infinite media subjected to uniaxial tension at infinity [42](see Fig.5). F.Erdogan and G.D.Gupta extended C.Atkinson's discussion to more general cases and considered two collinear radial cracks with all possible configurations [43] (see Fig.6). Crack tip singularities for all possible crack configurations were analyzed and stress intensity factors were calculated. M.Toya considered debonding of a partially embedded inclusion in an infinite media subjected to biaxial loading at arbitrary orientation [44] (see Fig.7). Muskihilishivili's complex variable method was used, strain energy release rate of the interfacial crack was calculated.

As one may see from the brief summary given above, previous analytical studies on microcracking in fiber reinforced composites are all based on single-fiber model without considering the influence of neighboring fibers. The advantage and usefulness of single-fiber model lies mainly in the fact that its simplicity lends itself to a relatively simple analysis and one may thus

determine without elaborate calculation the major factors influencing microcracking. Nevertheless a close examination of ceramic composite specimens under the electron microscope reveals that in the real material fibers may be closely packed, therefore effect of fiber interaction ought to be taken into consideration in the study of microcracking. In addition effect of temperature on microcracking has barely been studied. Therefore emphasis in this study is placed on effect of fiber distribution and temperature on matrix microcracking and toughness of the material.

CHAPTER II
MODELING OF MICROCRACKING

From observations of ceramic composite specimens under optical and scanning electron microscopes, it is found that distribution of fibers in the materials is quite random and fibers have circular cross sections but varies in their diameters (see Fig.8). Since modeling based on some real particular distribution of fibers in the composite is not only extremely complicated but also lacks generality, thus modeling of microcracking is done in this study by just simulating some typical patterns of fiber distributions that one may find in ceramic composites. From the observation one may find isolated single fibers, isolated two fibers, circularly distributed array of fibers, and random but closely clustered fibers, etc. In this study, the following two models are proposed for analysis of microcracking:

II.1. Two-fiber model

Two-fiber model describes two equal-sized fibers embedded in infinitely extended matrix (see Fig.9). Cracks under consideration may either emanate from one fiber in radial direction (radial crack) or lie along fiber-matrix interface (interfacial crack). Two-fiber model is not only the simulaton of a pattern of fiber distributions in the composite material, but also the simplest way to study interaction between fibers and a crack. Assuming the distance between two fibers as $2\delta R$ (where R is average radius of fibers, δ is a dimensionless parameter), by varying δ and comparing results with that from single-fiber model effect of neighboring fiber on stress distribution or microcrack propagation may be

determined. In addition, analyses based on two fiber model may be used to estimate geometrically much more complicated cases.

II-1. Ring model

Ring model defines a matrix crack in an infinitely extended composite material and surrounded by an array of circularly distributed fibers (see Fig.10). Ring model consists of three regions defined as follows:

Region 1: circular region of matrix defined by $r \leq a$ in plane polar coordinates, a radial crack lies in the matrix at $\theta=0$, $-a<a_1 \leq x \leq b_1<a$.

Region 2: annular domain, ring of composite defined by $a \leq r \leq b$, material in the domain is assmued isotropic with Young's modulus E_2, Possion's ratio ν_2 and thermal expansion coefficient α_2 being determined by virtue of the rule of mixture as follows:

$$E_2 = E_f \frac{nR^2}{b^2 - a^2} + E_m \frac{b^2 - a^2 - nR^2}{b^2 - a^2} \qquad (2\text{-}1)$$

$$\nu_2 = \nu_f \frac{nR^2}{b^2 - a^2} + \nu_m \frac{b^2 - a^2 - nR^2}{b^2 - a^2} \qquad (2\text{-}2)$$

$$\alpha_2 = \alpha_f \frac{nR^2}{b^2 - a^2} + \alpha_m \frac{b^2 - a^2 - nR^2}{b^2 - a^2} \qquad (2\text{-}3)$$

where n is number of fibers in the ring, a and b are radii of inner and outer circular boundaries respectively. R is average radius of fibers.

Region 3: composite material, infinitely extended domain defined as $b \leq r$. Material in this region is assumed mechanically transversely isotropic and thermally isotropic. Young's modulus, Possion's ratio and thermal expansion coefficient of the material are determined by following formulas (fiber aligned along x_3 direction) (see Fig.10b):

$$E_3 = V_f E_f + (1-V_f) E_m \qquad (2\text{-}4)$$

$$E = \frac{1}{\frac{V_f}{E_f} + \frac{(1-V_f)}{E_m}} \qquad (2\text{-}5)$$

$$\nu = \nu_{31} = V_f \nu_f + (1-V_f)\nu_m \qquad (2\text{-}6)$$

$$\alpha = V_f \alpha_f + (1-V_f)\alpha_m \qquad (2\text{-}7)$$

where V_f is overall volume fraction of fibers, E_f and E_m are Young's moduli of fibers and matrix respectively, ν_f and ν_m are Poisson's ratios of fibers and matrix, α_f and α_m are thermal expansion coefficients of fibers and matrix respectively. E is Young's modulus in x_1-x_2 plane (see Fig. 10b), E_3 is Young's modulus in x_3 direction, ν being Poisson's ratio in x_1-x_2 plane,

ν_{31} being Poisson's ratio for transverse strain in any direction in x_1-x_2 plane due to stress in x_3 direction (see Fig. 10b), accordingly we have following relation

$$\frac{\nu_{31}}{E_3} = \frac{\nu_{13}}{E} \qquad (2\text{-}8)$$

The effect of surrounding fibers in ring model is accounted for in an average sense. The extent of such effect depends on the width of the ring and the number of fibers n in the ring. When number of fibers in the ring or the width of the ring is changed, volume fraction of fibers $V_{f\text{-}ring}$ in the ring is changed, thus Young's modulus E_2, Possion's ratio ν_2 and thermal expansion coefficient α_2 will all be changed, and effect of the ring (fiber cluster) will be different. By comparing results from different $V_{f\text{-}ring}$, effect of neighboring fibers can be assessed.

CHAPTER III

SOLUTION OF TWO-FIBER MODEL PROBLEM-- ANALYTICAL APPROACH I

III.1. Introduction

As is defined and discussed in chapter II, two-fiber model consists of two equal-sized fibers embedded in an infinite matrix with a spacing $2\delta R$ between them. (R is radius of fiber, δ is a dimensionless parameter, see Fig.9). Two crack configurations are considered in this analysis: (a) a radial crack and (b) an interfacial crack as shown in Figs 9(a) and 9(b) respectively. The loading could either be mechanical or thermal one. Due to the complexity of the geometry, numerical and approximate methods have been used. To approach the model problems, first the stress fields for the uncracked geometry are determined using finite element technique, then by superposition, solution of the original problem can be translated into that of a perturbation crack problem in which the only loads are the crack surface pressures which are equal to the negative of stresses in the uncracked geometry case (see Fig.11) (since for crack problem we are mostly concerned with propagation of the cracks, and as far as crack tip singularity is concerned the perturbation problem is identical to the original one, therefore instead of original problem, we can alternatively solve a perturbation problem). After that, for radial crack case an approximate approach for the evaluation of the stress intensity factors or strain energy release rates is developed using single fiber solution and singular integral equation technique. For interfacial crack case an approximate approach for the calculation of strain energy release rate is developed using single-fiber solution and analogy technique.

III.2. Solution of uncracked geometry

To find out the stress distribution in the matrix and at fiber-matrix interface in uncracked geometry, finite element technique is used and the finite element mesh is shown in Fig.12. By symmetry only a quarter of model is used in the calculation, and of course certain restraints such as vanishing shear stresses and normal displacements as well as zero rotation angles along the two cut-out lines are imposed. By changing the spacing (center distance) between the two fibers and comparing the stress fields thus obtained, effect of interaction of the two fibers on the stress field can be determined. By assuming different values for the mechanical constants and comparing stress fields thus obtained the effect of mismatch of mechanical properties between fiber and matrix materials can be assessed. Finite element computer procedures using ANSYS [45] which gives stresses and displacements for in-plane mechanical and thermal loadings have been developed, the accuracy of FEM solutions was checked by comparing with some available analytical results. For instance when the two fibers are far away results were compared with the single-fiber solution. When Young's moduli of fibers are assigned a very small value, problem is reduced to an infinite domain containing two holes, results were compared with analytical solution for unidirectional traction case. When fiber and matrix are of the same material results were compared with homogeneous media case. Stress distributions of two-fiber model due to mechanical or thermal loading are shown in Figs. 13-24. In either case effect of Young's modulus ratios and fiber spacing is investigated. It is found the stress distributions are strongly affected by fiber interaction, especially when the material is subjected to mechanical loading.

III.3. Radial crack case

For the radial crack, an approximate approach using single-fiber solution and singular integral equation technique is developed.

Dundurs and Mura's dislocation solution [46](infinite domain with an embedded inclusion and an edge dislocation, see Fig.25) is used as a Green's function, after integration a singular integral equation is obtained, the stress intensity factor or energy release rate at the crack tip is related to the solution of the singular integral equation and can be evaluated accurately by using collocation technique.

The approximation is due to the fact that the Green's function used in the approach is from the single-fiber case while the crack surfaces are still loaded with the stresses obtained from two-fiber model.

The formulation of a radial crack emanating from a single fiber embedded in an infinite matrix for uniaxial loading is given in [43]. Referring to [43], after some simplification, the problem in terms of the crack surface displacement derivative f(t) can be written as (see Fig.26):

$$\int_R^{R+c} \frac{f(x)}{t-x}\,dt + \int_R^{R+c} [k_{11_S}(x,t)+k_{11_f}(x,t)]f(t)dt = \frac{\pi(\kappa_m + 1)}{2\mu_m}\,p(x),$$

$$(R < x < R+c) \qquad (3\text{-}1)$$

where $f(x) = \frac{\partial}{\partial x}[v(x^+,0)-v(x^-,0)]$, $\qquad c<x<R+c,$

with the single-valueness condition:

$$\int_c^{R+c} f(x)dx = 0 \qquad (3\text{-}2)$$

where

$$k_{11_s}(x,t) = \frac{1}{t-s}\left[(A_1+ A_2) \frac{s}{2x} + \frac{A_1}{x^2}(3s^2 - R^2)(1- \frac{2s}{t})\right] +$$

$$A_1\left[(1-\frac{4s}{t})\frac{s(s^2 - R^2)}{x^2(t-s)^2} - \frac{s^3(s^2 - R^2)^2}{R^4 t(t-s)^3}\right] ;$$

$$k_{11_f}(x,t)= \frac{A_1R^2}{x^2}(\frac{2}{x} + \frac{1}{2t} - \frac{3R^2}{tx^2}) - [M(\kappa_f + 1) - 1]\frac{R^2}{2tx^2} ;$$

$$\text{with } s = \frac{R^2}{x} , \quad M = \frac{m(\kappa_m + 1)}{(\kappa_f+ m)(\kappa_f- 1+2m)} , \quad A_1 = \frac{1 - m}{1+ m\kappa_m} ,$$

$$A_2 = \frac{\kappa_f - m\kappa_m}{\kappa_f + m} ,$$

$$m = \frac{\mu_f}{\mu_m}, \quad \kappa_m = 3-4\nu_m, \quad \kappa_f = 3-4\nu_f \qquad (3\text{-}3)$$

For the problem under consideration the external load p(x) is replaced by the negative of the stress obtained for the uncracked two-fiber geometry.

To solve singular integral equation (3-1) with (3-2), the following normalization is performed:

$$x = \frac{c}{2}\rho + R + \frac{c}{2} \qquad \text{for } R < x < R+c \text{ and } -1 < \rho < 1;$$

$$t = \frac{c}{2}\tau + R + \frac{c}{2} \qquad \text{for } R < t < R+c \text{ and } -1 < \tau < 1;$$

thus

$$f(t) = g(\tau); \quad k_{11_s}(x,t) = K_{11_s}(\rho,\tau);$$

$$p(x) = q(\rho); \quad k_{11_f}(x,t) = K_{11_f}(\rho,\tau). \qquad (3\text{-}4)$$

eqs (3-1) and (3-2) become

$$\int_{-1}^{1} \frac{g(\tau)}{\tau-\rho}\, d\tau + \frac{c}{2}\int_{-1}^{1} [K_{11_s}(\rho,\tau) + K_{11_f}(\rho,\tau)]g(\tau)d\tau = \frac{\pi(\kappa_m + 1)}{2\mu_m} q(\rho), \quad -1 < \rho < 1 \qquad (3\text{-}5)$$

and

$$\int_{-1}^{1} g(\tau)d\tau = 0 \qquad (3\text{-}6)$$

The normalized crack surface displacement $g(\tau)$ is singular at $\tau = \pm 1$ and may be written as:

$$g(\tau) = \frac{G(\tau)}{\sqrt{1 - \tau}\ (1 + \tau)^{-\beta}} \qquad (3\text{-}7)$$

where $G(\tau)$ is a bounded function , $-1<\beta<0$, determined by [43] from the following equation:

$$2\cos\pi\beta + (A_1 + A_2) - 4A_1(\beta+1)^2 = 0 \qquad (3\text{-}8)$$

At the crack tip the stress intensity factor can be defined as:

$$k(c) = \lim_{x\to R+c} \sqrt{2(x-R-c)}\,\sigma_{yy}(x,0)\Big|_{matrix}$$

$$= -\frac{2\mu_m}{1 + \kappa_m}\sqrt{c}\ 2^{\beta}G(1) \qquad (3\text{-}9)$$

Noting that $K_I = \sqrt{\pi}\ k(c)$, then the strain energy release rate is found to be:

$$G_I = \frac{K_I^2(1-\nu_m^2)}{E_m} = \frac{\pi}{E_m}(1-\nu_m^2)k^2(c) \qquad (3\text{-}10)$$

$$\text{or } G_I = \frac{\pi}{E_m}(1-\nu_m^2)\,R\frac{c}{R}\left(\frac{k(c)}{\sqrt{c}}\right)^2 \qquad (3\text{-}11)$$

Defining $\frac{c}{R} = \epsilon$, $\frac{k(c)}{\sqrt{c}} = \frac{}{\sigma}\,k'(\epsilon)$ and $g(\epsilon) = \epsilon\,[k'(\epsilon)]^2$, eq (3-9) becomes:

$$G_I = \frac{\pi}{E_m}(1-\nu_m^2)\, R\bar{\sigma}^2 g(\epsilon) \qquad (3\text{-}12)$$

Note that the quantity $g(\epsilon)$ is dimensionless, and thus called the normalized strain energy release rate.

The numerical results are computed for various material properties and fiber spacings ($2\delta R$) and displayed in Figs 27 to 30.

The results indicate that (a) material properties have very little effect on the normalized strain energy release rate $g(\epsilon)$ as shown in Fig.29 (for radial crack case); (b) the spacing between the two fibers plays a significant role on whether crack arrest is possible or not (e. g. Fig.28 indicates that when δ is large, i.e., the fibers are far from each other, the normalized strain energy release rate passes through a maximum making crack arrest possible; on the other hand when δ is small, i.e., when the fibers are close to each other, there is no possibility of radial crack arrest); and (c) the variation of the normalized strain energy release rate $g(\epsilon)$ is drastically different between the single-fiber and two-fiber geometries.

III.4. Interfacial crack

For the interfacial crack case, again an approximate approach using Toya's single-fiber solution [44] and least square technique is developed. First it may be noted that Toya's solution (Fig.31(a)) can be considered as the superposition of an uncracked geometry case (Fig.31(b)) and a crack case in which the crack is loaded with the negative of stresses from the uncracked geometry case (Fig.31(c)). Then the strain energy release rate can be

computed by considering the perturbation problem shown in Fig.31(c) only.

Next the tangential and radial stresses at the fiber/matrix interface (of the considered case), obtained from finite element analysis, can be approximated in the least square sense to yield the crack surface tractions prescribed in Fig.31(c).

Stress fields for a single fiber embedded in infinite matrix subjected to biaxial traction N, T at arbitrary orientation (see Fig.31a) can be found to be:

$$\sigma_{rr}= \frac{N+T}{2}\left[1-4A\left(\frac{R}{r}\right)^2\right]- \frac{N-T}{2}\left[1+12B\left(\frac{R}{r}\right)^4 - 16B\left(\frac{R}{r}\right)^2\right]\cos 2(\theta-\varphi) \quad (3\text{-}13)$$

$$\sigma_{\theta\theta}= \frac{N+T}{2}\left[1+4A\left(\frac{R}{r}\right)^2\right]+ \frac{N-T}{2}\left[1+12B\left(\frac{R}{r}\right)^4\right]\cos 2(\theta-\varphi) \quad (3\text{-}14)$$

$$\tau_{r\theta}= \frac{N-T}{2}\left[-1+12B\left(\frac{R}{r}\right)^4 - 8B\left(\frac{R}{r}\right)^2\right]\sin 2(\theta-\varphi) \quad (3\text{-}15)$$

where,

$$A= \frac{(1-2\nu_f)\mu_m - (1-2\nu_m)\mu_f}{4[(1-2\nu_f)\mu_m + \mu_f]} \quad (3\text{-}16),$$

$$B= \frac{\mu_m - \mu_f}{4[\mu_m + (3 - 4\nu_m)\mu_f]} \quad (3\text{-}17),$$

at fiber-matrix interface, r=R, it becomes

$$\sigma_{rr} = \frac{N+T}{2}(1-4A) - \frac{N-T}{2}(1-4B)\cos 2(\theta-\varphi) \quad (3\text{-}18)$$

$$\sigma_{\theta\theta} = \frac{N+T}{2}(1+4A) + \frac{N-T}{2}(1+12B)\cos 2(\theta-\varphi) \quad (3\text{-}19)$$

$$\tau_{r\theta} = \frac{N-T}{2}(-1+4B)\sin 2(\theta-\varphi) \quad (3\text{-}20)$$

To find N_{eq}, T_{eq} and φ_{eq}, which yield stresses on the fiber-matrix interface in 31(c) with the amount approximately equal to that in the two-fiber model obtained by finite element method, least square technique is employed,

Assume

$$\Delta = \sum_{i=1}^{M} \left\{ \left[\left(\frac{N+T}{2}(1-4A) - \frac{N-T}{2}(1-4B)\cos 2(\theta_i-\varphi) - \sigma_{rri} \right]^2 + \right. \right.$$

$$\left. \left[\frac{N-T}{2}(-1+4B)\sin 2(\theta_i-\varphi) - \tau_{r\theta i} \right]^2 \right\} \quad (3\text{-}21)$$

where σ_{rri}, $\tau_{r\theta i}$ are stresses of two-fiber model from finite element analysis. It is obvious that Δ is the sum of difference of normal and shear stresses (between that from single-fiber case and two-fiber case) at the interfacial collocation points. Then N_{eq}, T_{eq} and φ_{eq} can be determined in such a way that Δ be the minimun. To do this we take derivatives of Δ with respect to N, T, φ as follows:

$$\frac{\partial \Delta}{\partial N}=0,$$

$$\frac{\partial \Delta}{\partial T}=0, \qquad (3\text{-}22)$$

$$\frac{\partial \Delta}{\partial \varphi}=0,$$

from the resulting simultaneous equations N_{eq}, T_{eq} and φ_{eq} can be determined.

For specific cases, i.e., when the crack lies along fiber-matrix interface symmetrically with respect to x axis or y axis , take $\varphi=0$. For example, if crack lies symmetrically with respect to x axis, using polar coordinates as is shown in Fig.32, let $\varphi=0$, replacing θ in eqns (3-21), (3-22) with $\pi-\theta$, then stresses on the fiber-matrix interface can be written as

$$\sigma_{rr}=\frac{N+T}{2}(1-4A)-\frac{N-T}{2}(1-4B)\cos 2\theta \qquad (3\text{-}23)$$

$$\tau_{r\theta}=\frac{N-T}{2}(-1+4B)\sin 2\theta \qquad (3\text{-}24)$$

and

$$\Delta=\sum_{i=1}^{M}\left\{\left[\left(\frac{N+T}{2}(1-4A)-\frac{N-T}{2}(1-4B)\cos 2\theta_i-\sigma_{rri}\right]^2+\right.\right.$$

$$\left.\left.\left[\frac{N-T}{2}(-1+4B)\sin 2\theta_i-\tau_{r\theta i}\right]^2\right\} \qquad (3\text{-}25)$$

then, to minimize Δ, taking derivatives with respect to N and T and equating them 0, we obtain:

$$\frac{\partial \Delta}{\partial N} = 2(S1.N + S2.T - S3) = 0$$

$$\frac{\partial \Delta}{\partial T} = 2(S2.N + S4.T - S5) = 0 \qquad (3\text{-}26)$$

where

$$S1 = \sum_{i=1}^{M} \left\{ \left[\frac{1}{2}(1-4A) - \frac{1}{2}(1-4B)\cos 2\theta_i \right]^2 + \left[\frac{1}{2}(-1+4B)\sin 2\theta_i \right]^2 \right\} \qquad (3\text{-}27)$$

$$S2 = \sum_{i=1}^{M} \left[\frac{1}{4}(1-4A)^2 - \frac{1}{4}(1-4B)^2 \right] \qquad (3\text{-}28)$$

$$S3 = \sum_{i=1}^{M} \left\{ \left[\frac{1}{2}(1-4A) - \frac{1}{2}(1-4B)\cos 2\theta_i \right] \sigma_{rri} + \frac{1}{2}(-1+4B)\sin 2\theta_i \tau_{r\theta i} \right\} \qquad (3\text{-}29)$$

$$S4 = \sum_{i=1}^{M} \left\{ \left[\frac{1}{2}(1-4A) + \frac{1}{2}(1-4B)\cos 2\theta_i \right]^2 + \left[\frac{1}{2}(-1+4B)\sin 2\theta_i \right]^2 \right\} \qquad (3\text{-}30)$$

$$S5 = \sum_{i=1}^{M} \left\{ \left[\frac{1}{2}(1-4A) - \frac{1}{2}(1-4B)\cos 2\theta_i \right] \sigma_{rri} - \frac{1}{2}(-1+4B)\sin 2\theta_i \tau_{r\theta i} \right\} \qquad (3\text{-}31)$$

thus, we have the following simultaneous eqns:

$$S2.N+S4.T=S5$$
$$S1.N+S2.T=S3 \qquad (3\text{-}32)$$

from which, N_{eq} and T_{eq} can be determined as follows:

$$T_{eq}=\left(\frac{S3}{S1}-\frac{S5}{S2}\right)/\left(\frac{S2}{S1}-\frac{S4}{S2}\right) \qquad (3\text{-}33)$$

$$N_{eq}=\frac{S3}{S1}-\frac{S2}{S1}T \qquad (3\text{-}34)$$

For single-fiber model and interfacial crack case, the strain energy release rate at the crack tip is given as [43]:

$$G = \frac{1}{4}kR\, A_0(1+4\lambda_0^2)\pi N_1 \bar{N}_1 \sin\alpha e^{2\lambda_0(\pi-\alpha)} ;$$

where $N_1= (c_0- \frac{d_{-1}}{k}) + \frac{1-k}{k}(N - T)e^{[i(2\varphi-\alpha)i+2\lambda_0(\alpha-\pi)]}$;

$$A_0= \frac{k}{4}\left(\frac{1+\kappa_m}{\mu_m} + \frac{1+\kappa_f}{\mu_f}\right);$$

$$c_0= G_0+ iH_0;$$

$$G_0= \{ \frac{1}{2}(N + T)[1-(\cos\alpha + 2\lambda_0\sin\alpha)e^{2\lambda_0(\pi-\alpha)}] -$$

$$\frac{1}{2}(1-k)(1+4\lambda_0^2)(N \quad - T \quad)\sin^2\alpha\cos 2\varphi\} \;/$$

$$\{\ 2 - k - k(\cos\alpha + 2\lambda_0\sin\alpha)e^{2\lambda_0(\pi-\alpha)}\}$$

where

$$H_0 = \{\ \frac{1}{2}(1-k)(1+4\lambda_0^2)(N \quad - T \quad)\sin^2\alpha\sin 2\varphi$$

$$+ \frac{4\mu_m\epsilon_\infty}{1+\kappa_m}[1+(\cos\alpha + 2\lambda_0\sin\alpha)e^{2\lambda_0(\pi-\alpha)}]\} \;/$$

$$k[1+(\cos\alpha + 2\lambda_0\sin\alpha)e^{2\lambda_0(\pi-\alpha)}]$$

with $$d_{-1} = \frac{1}{2}(N \quad + T \quad) + \frac{4\mu_m i\epsilon_\infty}{1+\kappa_m}$$

$$\lambda_0 = -(\ln\nu)/2\pi$$

$$k = \frac{\beta_0}{1+\nu}$$

$$\beta_0 = \frac{\mu_m(1+\kappa_f)}{(\mu_m + \kappa_m\mu_f)}$$

$$\nu = \frac{(\mu_f+\kappa_f\mu_m)}{(\mu_m+\kappa_m\mu_f)} \qquad (3\text{-}35)$$

where ϵ_∞ is the rotation at infinity, $\bar{N}_1$ is the complex conjugate of N_1, and R, α and φ are shown in Fig 31a. For a constant crack surface pressure $\bar{\sigma}$, in [41], it was shown that $T_{eq} = N_{eq} = \frac{\bar{\sigma}}{1-4A}$ and $\varphi = 0$, and the normalized strain energy release rate at the interface becomes:

$$G' = \frac{GE_m}{2(1+\nu_m)\,\bar{\sigma}^2 R} \qquad (3\text{-}36)$$

For the problem under consideration, T , N and angle φ in eqn (3-35) are replaced by N_{eq}, T_{eq} and φ_{eq}.

The numerical results are displayed in Figs 33 to 38 for thermal and mechanical loading, where the normalized strain energy release rate is plotted against the interfacial crack angle α. The material properties and the fiber spacings are varied and the results are compared with single-fiber case. It is found that mismatch of mechanical properties of the constituents and the spacing between fibers may affect the interfacial crack propagation considerably. Furthermore, contrary to the radial crack case, the variation of G' is qualitatively similar for both the single-fiber and the two-fiber cases, making interfacial crack arrest possible (see Figs.36 to 38).

CHAPTER IV
SOLUTION OF RING MODEL PROBLEM-- ANALYTICAL APPROACH II

IV.1. Introduction

The definition of the ring model has been given in chapter II, and its geometry is shown in Fig.10. Both mechanical and thermal loading are considered in this analysis and exact analytical solutions of stress intensity factors for matrix cracks are derived. To approach the problem, dislocation solution is sought first in section IV.2, then the dislocation solution is applied as a Green's function to solutions of crack problems in IV.3. Since a crack can be regarded as pile-up of dislocations in an appropriate way, by integrating the dislocation solution a singular integral equation is obtained. Stress intensity factors at the crack tips are related to the solution of the singular integral equation and can be evaluated accurately by using a collocation technique.

IV.2. Dislocation solution

The geometry for the considered problem, as is shown in Fig.39, consists of three domains, i.e., circular disk (matrix) containing an edge dislocation, circular ring (composite) and exterior infinite domain (composite). The materials for the circular disk and ring are isotropic, and the outside infinite domain transversely isotropic.

To formulate the problem under consideration, Michell's general solutions are employed for the three domains, i.e., general annulus solution for the circular ring and exterior solution for the outside infinite domain. For the internal circular domain, since a dislocation is embedded in it, the solution is constructed

by superposition of the following two, Michell's general interior domain solution [47] and an infinite plane containing an edge dislocation, the latter is obviously to account for the main feature of the edge dislocation. Stress field in the disk then can be obtained by the following superposition:

$$\sigma^{*}_{ij}(r,\theta)= \sigma_{ij}(r,\theta) + \sigma_{ij^{1}}(r,\theta) \qquad (i,j = r,\theta) \qquad (4\text{-}1)$$

where σ_{ij} and $\sigma_{ij^{1}}$ $(i,j=r,\theta)$ are stress fields for infinite plane containing an edge dislocation and that of the uncracked circular disk respectively.

(a) **Solution for infinite plane containing an edge dislocation**

Consider an infinite plane with an edge dislocation having a Burger's vector $b_y=-f$ located at the point $r=t$, $\theta=0$ (Fig.40). The plane elasticity problem may be solved by assuming that

$$\sigma_{r\theta}= 0, \quad 0 \le r < \infty \qquad \theta =0, \ \theta =\pi \qquad (4\text{-}2)$$

$$\frac{\partial}{\partial r}[u_{\theta}(r,0^{+})-u_{\theta}(r,0^{-})]= f\delta(r-t), \qquad 0 \le r < \infty \qquad (4\text{-}3)$$

Referring to [48], the Airy stress function of the problem may be expressed as (Fig.40)

$$\Psi_{1}(r,\theta) = - \frac{2\mu_{1}}{\pi(1+\kappa)} f r_{1} \log r_{1} \cos \theta_{1}$$

$$=-\frac{\mu_1}{\pi(1+\kappa)}\, f(r\cos\theta - t)\log(r^2+t^2-2rt\cos\theta) \qquad (4\text{-}4)$$

where μ_1 is shear modulus of disk material, $\kappa_1=3-4\nu_1$ for plane strain, $\kappa_1=(3-\nu_1)/(1+\nu_1)$ for the generalized plane stress (solution is sought for plain strain case in this study), ν_1 being the Poisson's ratio of disk material. From (4-4) stresses are obtained as follows

$$\sigma_{rr}(r,\theta)= \frac{1}{r}\frac{\partial\Psi_1}{\partial r} + \frac{1}{r^2}\frac{\partial^2\Psi_1}{\partial\theta^2}$$

$$=-\frac{2\mu_1 f}{\pi(1+\kappa_1)}\left[\frac{r\cos\theta - t - 2t\sin^2\theta}{r^2+t^2-2rt\cos\theta} - \frac{2t^2\sin^2\theta(r\cos\theta - t)}{(r^2+t^2-2rt\cos\theta)^2}\right] \qquad (4\text{-}5)$$

$$\sigma_{r\theta}(r,\theta)= -\frac{\partial}{\partial r}\left(\frac{1}{r}\frac{\partial\Psi_1}{\partial\theta}\right)$$

$$=\frac{2\mu_1 f}{\pi(1+\kappa_1)}\left[\frac{\sin\theta(2t\cos\theta - r)}{r^2+t^2-2rt\cos\theta} - \frac{2t\sin\theta(r\cos\theta - t)(r-t\cos\theta)}{(r^2+t^2-2rt\cos\theta)^2}\right] \qquad (4\text{-}6)$$

$$\sigma_{\theta\theta}(r,\theta)= \frac{\partial^2\Psi_1}{\partial r^2}$$

$$=-\frac{2\mu_1 f}{\pi(1+\kappa_1)}\left[\frac{2\cos\theta(r-t\cos\theta)+r\cos\theta - t}{r^2+t^2-2rt\cos\theta} - \frac{2(r\cos\theta - t)(r-t\cos\theta)^2}{(r^2+t^2-2rt\cos\theta)^2}\right] \qquad (4\text{-}7)$$

displacements can be found as

$$u_r(r,\theta) = -\frac{f}{\pi(1+\kappa_1)}\left[\frac{1-2\nu_1}{2}\cos\theta\log(r^2+t^2-2rt\cos\theta)\right.$$

$$\left.+\frac{trsin^2\theta}{r^2+t^2-2rt\cos\theta}-2(1-\nu_1)\tan^{-1}\left(\frac{r\cos\theta-t}{r\sin\theta}\right)\sin\theta\right] \qquad (4\text{-}8)$$

$$u_\theta(r,\theta) = \frac{f}{\pi(1+\kappa_1)}\left[\frac{1-2\nu_1}{2}\sin\theta\log(r^2+t^2-2rt\cos\theta)\right.$$

$$\left.+\frac{(r-t\cos\theta)r\sin\theta}{r^2+t^2-2rt\cos\theta}+2(1-\nu_1)\tan^{-1}\left(\frac{r\cos\theta-t}{r\sin\theta}\right)\cos\theta\right] \qquad (4\text{-}9)$$

In order to combine the infinite plane solution with the disk solution, we express stresses and displacements along the circle r=a in the plane in terms of the following Fouries series:

$$\sigma_{r\theta}(a,\theta) = \frac{\mu_1 f}{\pi(1+\kappa_1)}\sum_{1}^{\infty} A_n(t)\sin n\theta \qquad (4\text{-}10)$$

$$\sigma_{rr}(a,\theta) = -\frac{\mu_1 f}{\pi(1+\kappa_1)}\sum_{0}^{\infty} B_n(t)\cos n\theta \qquad (4\text{-}11)$$

$$u_r(a,\theta) = -\frac{f}{\pi(1+\kappa_1)}\sum_{0}^{\infty} C_n(t)\cos n\theta \qquad (4\text{-}12)$$

$$u_\theta(a,\theta) = -\frac{f}{\pi(1+\kappa_1)} \sum_1^\infty D_n(t)\sin n\theta \qquad (4\text{-}13)$$

where Fourier coefficients are given by

$$A_n(t) = \frac{\pi(1+\kappa_1)}{\mu_1 f} \frac{2}{\pi} \int_0^\pi \sigma_{r\theta}(a,\theta)\sin n\theta d\theta \qquad (4\text{-}14)$$

$$B_0(t) = -\frac{\pi(1+\kappa_1)}{\mu_1 f} \frac{1}{\pi} \int_0^\pi \sigma_{rr}(a,\theta)d\theta \qquad (4\text{-}15)$$

$$B_n(t) = -\frac{\pi(1+\kappa_1)}{\mu_1 f} \frac{2}{\pi} \int_0^\pi \sigma_{rr}(a,\theta)\cos n\theta \, d\theta \qquad (4\text{-}16)$$

$$C_0(t) = -\frac{\pi(1+\kappa_1)}{f} \frac{1}{\pi} \int_0^\pi U_r(a,\theta) \, d\theta \qquad (4\text{-}17)$$

$$C_n(t) = -\frac{\pi(1+\kappa_1)}{f} \frac{2}{\pi} \int_0^\pi U_r(a,\theta) \cos n\theta \, d\theta \qquad (4\text{-}18)$$

$$D_n(t) = -\frac{\pi(1+\kappa_1)}{f} \frac{2}{\pi} \int_0^\pi U_\theta(a,\theta) \sin n\theta \, d\theta \qquad (4\text{-}19)$$

while σ_{rr}, $\sigma_{r\theta}$, u_r and u_θ are given by (4-5),(4-6),(4-8) and (4-9).

Integrals in (4-14) to (4-19) can be evaluated in closed form, for example,

$$A_n(t) = \frac{\pi(1+\kappa_1)}{\mu_1 f}\frac{2}{\pi}\int_0^{\pi}\sigma_{r\theta}(a,\theta)\sin n\theta\, d\theta$$

$$=\frac{4}{\pi}\int_0^{\pi}\left[\frac{\sin\theta(2t\cos\theta - a)}{a^2 + t^2 - 2at\cos\theta} - \frac{2t\sin\theta(a\cos\theta - t)(a - t\cos\theta)}{(a^2 + t^2 - 2at\cos\theta)^2}\right]\sin n\theta\, d\theta$$

define $s=\frac{t}{a}$, then

$$A_n(t) = A_n(as) = G_1(s) + G_2(s) + G_3(s) \qquad (4\text{-}20)$$

with

$$G_1(s)= \frac{2}{\pi}\int_0^{\pi}\frac{s}{a}\,\frac{\sin 2\theta \sin n\theta}{1 - 2s\cos\theta + s^2}d\theta \qquad (4\text{-}21)$$

$$G_2(s)= -\frac{2}{\pi}\int_0^{\pi}\frac{2}{a}\,\frac{\sin\theta\, \sin n\theta}{1 - 2s\cos\theta + s^2}d\theta \qquad (4\text{-}22)$$

$$G_3(s)= \frac{2}{\pi}\int_0^{\pi}\frac{s\,\sin n\theta}{a(1 - 2s\cos\theta + s^2)^2}\,[\sin 2\theta(1 - 2s\cos\theta + s^2) +$$

$$4\sin\theta(s - \cos\theta)(1 - s\cos\theta)]d\theta \qquad (4\text{-}23)$$

Using tables in [48], from (4-21) and (4-22), we obtain:

$$G_1(s)= \frac{s^{n-1}}{a}(1+s^2) \qquad (4\text{-}24)$$

$$G_2(s)= -\frac{2s^{n-1}}{a} \qquad (4\text{-}25)$$

note that,

$$G_3(s) = s\frac{d}{ds}[G_1(s) + G_2(s)]$$

$$= \frac{s^{n-1}}{a}[n(s^2 - 1) + (s^2+1)] \qquad (4\text{-}26)$$

then,

$$A_n(t) = A_n(as) = \frac{s^{n-1}}{a}[n(s^2 - 1) + 2s^2] \quad (n\geq 2) \qquad (4\text{-}27)$$

or

$$A_n(t) = \frac{(n+2)t^{n+1}}{a^{n+2}} - \frac{nt^{n-1}}{a^n} \quad (n\geq 2) \qquad (4\text{-}28)$$

In a similar manner, we obtain

$$A_1(t) = \frac{3t^2}{a^3} - \frac{2}{a} \qquad (4\text{-}29)$$

$$B_0(t) = -\frac{2t}{a^2} \qquad (4\text{-}30)$$

$$B_1(t) = -\frac{3t^2}{a^3} + \frac{2}{a} \qquad (4\text{-}31)$$

$$B_n(t) = -\frac{(n+2)t^{n+1}}{a^{n+2}} + \frac{(n+2)t^{n-1}}{a^n} \quad (n\geq 2) \qquad (4\text{-}32)$$

For another example,

$$C_n(t) = -\frac{\pi(1+\kappa_1)}{f}\frac{2}{\pi}\int_0^{\pi} u_r(a,\theta)\,\cos n\theta\,d\theta \qquad (n\geq 2)$$

$$= \frac{2}{\pi}\int_0^{\pi}\Big[\frac{1-2\nu_1}{2}\cos\theta\log(a^2+t^2-2at\cos\theta) + \frac{t\sin^2\theta}{a^2+t^2-2at\cos\theta} -$$

$$2(1-\nu_1)\tan^{-1}\Big(\frac{a\cos\theta-t}{a\sin\theta}\Big)\sin\theta\Big]\cos n\theta\,d\theta \qquad (4\text{-}33)$$

Define

$$C_n(t) = \frac{2}{\pi}\,[C_{n1}(t) + C_{n2}(t) + C_{n3}(t)] \qquad (n\geq 2) \qquad (4\text{-}34)$$

with

$$C_{n1}(t) = \int_0^{\pi}\frac{1-2\nu_1}{2}\cos\theta\log(a^2+t^2-2at\cos\theta)\,\cos n\theta\,d\theta \qquad (4\text{-}35)$$

$$C_{n2}(t) = -\int_0^{\pi} 2(1-\nu_1)\tan^{-1}\Big(\frac{a\cos\theta-t}{a\sin\theta}\Big)\sin\theta\cos n\theta\,d\theta \qquad (4\text{-}36)$$

$$C_{n3}(t) = \int_0^{\pi}\frac{t\sin^2\theta\,\cos n\theta}{a^2+t^2-2at\cos\theta}\,d\theta \qquad (4\text{-}37)$$

Among them $C_{n3}(t)$ can be readily found to be

$$C_{n3}(t)= \frac{\pi}{4}\left(\frac{t^{n+1}}{a^{n+1}} - \frac{t^{n-1}}{a^{n-1}}\right) \qquad (n\geq 2) \qquad (4\text{-}38)$$

but for $C_{n1}(t)$ and $C_{n2}(t)$, it would be convenient first to find their derivatives $C'_{n1}(t)$ and $C'_{n2}(t)$ (prime means derivatives with respect to t), then find $C_{n1}(t)$ and $C_{n2}(t)$ by integrations.

For example,

$$C_{n1}(t)= \int_0^{\pi} \frac{1-2\nu_1}{2}\cos\theta\log(a^2+t^2-2at\cos\theta)\,\cos n\theta\, d\theta$$

note that,

$$\frac{\partial}{\partial t}C_{n1}(t)= \frac{1-2\nu_1}{2}\int_0^{\pi} \frac{2\cos\theta(t-a\cos\theta)\cos n\theta}{a^2+t^2-2at\cos\theta}\, d\theta$$

which can be readily evaluated

$$= -\frac{(1-2\nu_1)\pi}{4}\left(\frac{t^{n-2}}{a^{n-1}} + \frac{t^{n}}{a^{n+1}}\right) \qquad (n\geq 2) \qquad (4\text{-}39)$$

by integration

$$C_{n1}(t)= \int_0^t \frac{\partial}{\partial t}C_{n1}(t)\,dt + C_{n1}(0)$$

$$= -\frac{(1-2\nu_1)\pi}{4}\left[\frac{t^{n-1}}{(n-1)a^{n-1}} + \frac{t^{n+1}}{(n+1)a^{n+1}}\right] \qquad (n\geq 2) \qquad (4\text{-}40)$$

for

$$C_{n2}(t)= -\int_0^{\pi} 2(1-\nu_1)\tan^{-1}\frac{a\cos\theta-t}{a\sin\theta}\,\sin\theta\cos n\theta\, d\theta$$

also note that,

$$\frac{\partial}{\partial t}C_{n2}(t) = 2(1-\nu_1)\int_0^{\pi} \frac{a\sin^2\theta\ \cos n\theta}{a^2 + t^2 - 2at\cos\theta}\, d\theta$$

$$= \frac{2(1-\nu_1)}{t} C_{n3}(t)$$

$$= \frac{(1-\nu_1)\pi}{2}\left(\frac{t^n}{a^{n+1}} - \frac{t^{n-2}}{a^{n-1}}\right) \qquad (n\geq 2) \qquad (4\text{-}41)$$

then $$C_{n2}(t) = \int_0^t \frac{\partial}{\partial t} C_{n2}(t)\, dt + C_{n2}(0)$$

since from equation (4-36):

$$C_{n2}(0) = -2(1-\nu_1)\int_0^{\pi} \tan^{-1}(c\tan\theta)\sin\theta\cos n\theta\ d\theta$$

$$= -\frac{(1-\nu_1)\pi}{2}\left[\frac{1+(-1)^{n+1}}{n+1} - \frac{1+(-1)^{n+1}}{n-1}\right] \qquad (4\text{-}42)$$

thus,

$$C_{n2}(t) = \frac{(1-\nu_1)\pi}{2}\left[\frac{t^{n+1}}{(n+1)a^{n+1}} - \frac{t^{n-1}}{(n-1)a^{n-1}}\right] -$$

$$\frac{(1-\nu_1)\pi}{2}\left[\frac{1+(-1)^{n+1}}{n+1} - \frac{1+(-1)^{n+1}}{n-1}\right] \qquad (4\text{-}43)$$

and,

$$C_n(t)= \frac{2}{\pi} [C_{n1}(t) + C_{n2}(t) + C_{n3}(t)] \qquad (n\geq 2)$$

$$=\frac{1}{2}\left(-\frac{(n+2-4\nu_1)t^{n-1}}{2(n-1)a^{n-1}} + \frac{(n+2)t^{n+1}}{(n+1)a^{n+1}}\right) + \frac{2(1+(-1)^{n+1})}{n^2 - 1}(1-\nu_1) \qquad (4\text{-}44)$$

In a similar way we obtain

$$C_0(t)= \frac{t}{a} \qquad (4\text{-}45)$$

$$C_1(t)= \frac{3}{4}\frac{t^2}{a^2} - (1-\nu_1) + (1-2\nu_1)\log a \qquad (4\text{-}46)$$

$$D_1(t)= \frac{3}{4}\frac{t^2}{a^2} - (2-\nu_1) - (1-2\nu_1)\log a \qquad (4\text{-}47)$$

$$D_n(t)=\frac{1}{2}\left(-\frac{(n-4+4\nu_1)t^{n-1}}{(n-1)a^{n-1}} + \frac{(n+2)t^{n+1}}{(n+1)a^{n+1}}\right)-2(1-\nu_1)n\,\frac{(1+(-1)^{n+1})}{n^2 - 1} \qquad (4\text{-}48)$$

b. Disk solution

For the problem under consideration stresses and displacements should satisfy the following symmetry conditions:

$$\sigma_{rr}(r,\theta) = \sigma_{rr}(r,-\theta) \qquad (4\text{-}49)$$

$$\sigma_{\theta\theta}(r,\theta) = \sigma_{\theta\theta}(r,-\theta) \qquad (4\text{-}50)$$

$$\sigma_{r\theta}(r,\theta) = -\sigma_{r\theta}(r,-\theta) \qquad (4\text{-}51)$$

$$u_r(r,\theta) = u_r(r,-\theta) \qquad (4\text{-}52)$$

$$u_\theta(r,\theta) = -u_\theta(r,-\theta) \qquad (4\text{-}53)$$

Using Michell's general solution, taking regularity of solutions and symmetry conditions into consideration, stresses and displacements for the disk solution can be assumed as

$$\sigma_{rr1}(r,\theta)=2c_{01}+2d_{11}r\cos\theta-\sum_{2}^{\infty}\ [a_{n1}n(n-1)r^{n-2}+\ b_{n1}(n+1)(n-2)r^{n}]\cos n\theta \qquad (4\text{-}54)$$

$$\sigma_{\theta\theta1}(r,\theta) = 2c_{01}+6d_{11}r\cos\theta+\sum_{2}^{\infty}\ [a_{n1}n(n-1)r^{n-2}+ b_{n1}(n+1)(n+2)r^{n}]\cos n\theta \qquad (4\text{-}55)$$

$$\sigma_{r\theta1}(r,\theta)=2d_{11}r\sin\theta+\sum_{2}^{\infty}\ [a_{n1}n(n-1)r^{n-2}+ b_{n1}n(n+1)r^{n}]\sin n\theta \qquad (4\text{-}56)$$

correspondingly, displacements can be written as

$$u_{r1}(r,\theta)=\frac{1-\nu_1^2}{E_1}\left\{\frac{2(1-2\nu_1)}{1-\nu_1}c_{01}r+\frac{(1-4\nu_1)}{1-\nu_1}\ d_{11}r^2\cos\theta\ +\ \sum_{2}^{\infty}\ [(-\ \frac{n}{1-\nu_1}a_{n1}r^{n-1}\right.$$

$$+ b_{n1}\left(\frac{2(1-2\nu_1)-n}{1-\nu_1}\right)r^{n+1}]\cos n\theta\Big\} + (1+\nu_1)\alpha_1\Delta T r + S_2\cos\theta \quad (4\text{-}57)$$

$$u_{\theta 1}(r,\theta) = \frac{1-\nu_1^2}{E_1}\Big\{ \frac{(5-4\nu_1)}{1-\nu_1} d_{11} r^2 \sin\theta + \sum_{2}^{\infty} [\left(\frac{n}{1-\nu_1} a_{n1} r^{n-1} + \right.$$

$$\left. b_{n1}\left(\frac{n+4-4\nu_1}{1-\nu_1}\right)r^{n+1}]\sin n\theta\right\} - S_2\sin\theta \quad (4\text{-}58)$$

c. Ring solution

By the same analysis stresses in the ring can be assumed as

$$\sigma_{rr2}(r,\theta) = \frac{b_{02}}{r^2} + 2c_{02} + \left(-\frac{2c_{12}}{r^3} + 2d_{12}r\right)\cos\theta - \frac{(3+\nu_2)}{4\pi}\frac{(R_y\sin\theta + R_x\cos\theta)}{r} -$$

$$\sum_{2}^{\infty} [a_{n2}n(n-1)r^{n-2} + b_{n2}(n+1)(n-2)r^n + c_{n2}n(n+1)r^{-(n+2)} +$$

$$d_{n2}(n-1)(n+2)r^{-n}]\cos n\theta \quad (4\text{-}59)$$

$$\sigma_{\theta\theta 2}(r,\theta) = -\frac{b_{02}}{r^2} + 2c_{02} + \left(\frac{2c_{12}}{r^3} + 6d_{12}r\right)\cos\theta + \frac{(1-\nu_2)}{4\pi}\frac{(R_y\sin\theta + R_x\cos\theta)}{r} +$$

$$\sum_{2}^{\infty} [a_{n2}n(n-1)r^{n-2} + b_{n2}(n+1)(n+2)r^n + c_{n2}n(n+1)r^{-(n+2)} +$$

$$d_{n2}(n-1)(n-2)r^{-n}]\cos n\theta \qquad (4\text{-}60)$$

$$\sigma_{r\theta 2}(r,\theta)=-(\frac{2c_{12}}{r^3} - 2d_{12}r)\sin\theta-\frac{(1-\nu_2)}{4\pi}\frac{(R_y\cos\theta+R_x\sin\theta)}{r} +$$

$$\sum_{1}^{\infty}[a_{n2}n(n-1)r^{n-2}+b_{n2}n(n+1)r^{n}-c_{n2}n(n+1)r^{-(n+2)}-d_{n2}n(n-1)r^{-n}]\sin n\theta$$

(4-61)

where R_x and R_y are components of resultant force acting on the inside of the annulus, and for our case $R_x=R_y=0$.

Displacements in the ring can be written as

$$u_{r2}(r,\theta)=\frac{1-\nu_2^2}{E}\left\{-\frac{b_{02}}{1-\nu_2}\frac{1}{r}+\frac{2(1-2\nu_2)}{1-\nu_2}c_{02}r+(\frac{c_{12}}{1-\nu_2}\frac{1}{r^2} +\right.$$

$$\left.\frac{(1-4\nu_2)}{1-\nu_2}d_{12}r^2)\cos\theta + \sum_{2}^{\infty}[(-\frac{n}{1-\nu_2}a_{n2}r^{n-1}- b_{n2}(\frac{n-2+4\nu_2}{1-\nu_2})r^{n+1}+\right.$$

$$\left.\frac{n}{1-\nu_2}c_{n2}r^{-n-1}+ d_{n2}(\frac{n+2-4\nu_2}{1-\nu_2})r^{-n+1}]\cos n\theta\right\} + (1+\nu_2)\alpha_2\Delta Tr + S_3\cos\theta$$

(4-62)

$$u_{\theta 2}(r,\theta)=\frac{1-\nu_2^2}{E_2}\left\{(\frac{c_{12}}{1-\nu_2}\frac{1}{r^2} + \frac{(5-4\nu_2)}{1-\nu_2}d_{12}r^2)\sin\theta+ \sum_{2}^{\infty}[-\frac{n}{1-\nu_2}a_{n2}r^{n-1}+\right.$$

$$b_{n2}\left(\frac{n+4-4\nu_2}{1-\nu_2}\right)r^{n+1}+\frac{n}{1-\nu_2}c_{n2}r^{-n-1}+d_{n2}\left(\frac{n-4+4\nu_2}{1-\nu_2}\right)r^{-n+1}]\sin n\theta\Big\} -$$

$$S_3\sin\theta \qquad (4\text{-}63)$$

d. Infinite domain

In the same fashion, stresses in the outside infinite domain can be written as

$$\sigma_{rr3}(r,\theta)=\frac{XX+YY}{2}+\frac{XX-YY}{2}\cos 2\theta-\frac{(3+\nu)}{4\pi}\frac{(R_y\sin\theta+R_x\cos\theta)}{r}+$$

$$\frac{b_{03}}{r^2}-\frac{2c_{13}}{r^3}\cos\theta-\sum_{2}^{\infty}[c_{n3}n(n+1)r^{-(n+2)}+$$

$$d_{n3}(n-1)(n+2)r^{-n}]\cos n\theta \qquad (4\text{-}64)$$

$$\sigma_{\theta\theta 3}(r,\theta)=\frac{XX+YY}{2}-\frac{XX-YY}{2}\cos 2\theta+\frac{(1-\nu)}{4\pi}\frac{(R_y\sin\theta+R_x\cos\theta)}{r}-$$

$$\frac{b_{03}}{r^2}+\frac{2c_{13}}{r^3}\cos\theta+\sum_{2}^{\infty}[c_{n3}n(n+1)r^{-(n+2)}+$$

$$d_{n3}(n-1)(n-2)r^{-n}]\cos n\theta \qquad (4\text{-}65)$$

$$\sigma_{r\theta 3}(r,\theta) = -\frac{XX-YY}{2}\sin 2\theta - \frac{2c_{13}}{r^3}\sin\theta - \frac{(1-\nu)}{4\pi}\frac{(R_y\cos\theta+R_x\sin\theta)}{r} -$$

$$\sum_{2}^{\infty}\left[c_{n3}n(n+1)r^{-(n+2)} + d_{n3}n(n-1)r^{-n}\right]\sin n\theta \qquad (4\text{-}66)$$

where XX and YY represent cartesian components of stresses acting at infinity, R_x and R_y are cartesian components of resultant force acting on the boundary r=b, and for the considered case, $R_x=R_y=XX=YY=0$.

For transversely isotropic materials, general constitutive equations are as follows:

$$\begin{vmatrix} \epsilon_{rr3} \\ \epsilon_{\theta\theta 3} \\ \epsilon_{zz3} \\ \gamma_{\theta z3} \\ \gamma_{zr3} \\ \gamma_{r\theta 3} \end{vmatrix} = \begin{vmatrix} \frac{1}{E} & -\frac{\nu}{E} & -\frac{\nu_{31}}{E_3} & 0 & 0 & 0 \\ -\frac{\nu}{E} & \frac{1}{E} & -\frac{\nu_{31}}{E_3} & 0 & 0 & 0 \\ -\frac{\nu_{31}}{E_3} & -\frac{\nu_{31}}{E_3} & \frac{1}{E_3} & 0 & 0 & 0 \\ 0 & 0 & 0 & \frac{1}{G_3} & 0 & 0 \\ 0 & 0 & 0 & 0 & \frac{1}{G_3} & 0 \\ 0 & 0 & 0 & 0 & 0 & \frac{2(1+\nu)}{E} \end{vmatrix} \begin{vmatrix} \sigma_{rr3} \\ \sigma_{\theta\theta 3} \\ \sigma_{zz3} \\ \tau_{\theta z3} \\ \tau_{zr3} \\ \tau_{r\theta 3} \end{vmatrix} + \begin{vmatrix} \alpha \\ \alpha \\ \alpha \\ 0 \\ 0 \\ 0 \end{vmatrix} \Delta T$$

Definition for the five engineering constants are as follows:

E : Young's modulus in x_1-x_2 plane (see Fig.10)

E_3: Young's modulus in x_3 direction (see Fig.10)

ν : Poisson's ratio in x_1-x_2 plane (see Fig.10)

ν_{31} : Poisson's ratio for transverse strain in any direction in x_1-x_2 plane due to stress in x_3 direction (see Fig.10).

Accordingly we have relation $\frac{\nu_{31}}{E_3} = \frac{\nu_{13}}{E}$

G_3: shear modulus in plane parallel to x_3 axis.

Since the model is applied to a fiber reinforced composite material with fiber being aligned along x_3 direction, these engineering constants can be determined by following formulas:

$$E_3 = V_f E_f + (1-V_f)E_m \qquad (4\text{-}67)$$

$$E = \frac{1}{\frac{V_f}{E_f} + \frac{(1-V_f)}{E_m}} \qquad (4\text{-}68)$$

$$\nu = \nu_{31} = V_f \nu_f + (1-V_f)\nu_m \qquad (4\text{-}69)$$

$$\alpha = V_f \alpha_f + (1-V_f)\alpha_m \qquad (4\text{-}70)$$

where V_f is the overall volume fraction of fibers, E_f, E_m being Young's modulus of fiber and matrix respectively, ν_f, ν_m being Poisson's ratio of fiber and matrix respectively, α_f, α_m being thermal expansion coefficient of fiber and matrix respectively. Note that this domain is assumed thermally isotropic.
For plain strain case, $\epsilon_{zz3}=0$, we obtain

$$\epsilon_{zz3} = -\frac{\nu_{31}}{E_3}\sigma_{rr3} - \frac{\nu_{31}}{E_3}\sigma_{\theta\theta 3} + \frac{1}{E_3}\sigma_{zz3} + \alpha_3\Delta T = 0 \qquad (4\text{-}71)$$

therefore,

$$\sigma_{zz3} = (\sigma_{rr3} + \sigma_{\theta\theta 3})\nu_{31} - E_3\alpha_3\Delta T \qquad (4\text{-}72)$$

$$\epsilon_{rr3} = -\frac{1}{E}\sigma_{rr3} - \frac{\nu}{E}\sigma_{\theta\theta 3} - \frac{\nu_{31}}{E_3}\sigma_{zz3} + \alpha_3\Delta T \qquad (4\text{-}73)$$

$$\epsilon_{\theta\theta 3} = \frac{1}{E}\sigma_{\theta\theta 3} - \frac{\nu}{E}\sigma_{rr3} - \frac{\nu_{31}}{E_3}\sigma_{zz3} + \alpha_3\Delta T \qquad (4\text{-}74)$$

substituting (4-72) into (4-73) and (4-74), we obtain

$$\epsilon_{rr3} = \frac{1}{E'}(\sigma_{rr3} - \nu'\sigma_{\theta\theta 3}) + (1+\nu_{31})\alpha_3\Delta T \qquad (4\text{-}75)$$

$$\epsilon_{\theta\theta 3} = \frac{1}{E'}(\sigma_{\theta\theta 3} - \nu'\sigma_{rr3}) + (1+\nu_{31})\alpha_3\Delta T \qquad (4\text{-}76)$$

$$\text{where } E' = \frac{E}{1 - \frac{E}{E_3}\nu_{31}^2}, \qquad \nu' = \frac{\nu + \frac{E}{E_3}\nu_{31}^2}{1 - \frac{E}{E_3}\nu_{31}^2} \tag{4-77}$$

it can readily be shown that

$$\frac{1 + \nu'}{E'} = \frac{1 + \nu}{E}$$

thus displacements can be found as follows:

$$u_{r3}(r,\theta) = \frac{1}{E'}\left\{-\frac{b_{03}}{r}(1+\nu') + \frac{c_{13}}{r^2}(1+\nu')\cos\theta + \sum_{2}^{\infty}[c_{n3}n(1+\nu')r^{-(n+1)}\right.$$

$$\left. + d_{n3}((n+2)+\nu'(n-2))r^{1-n}]\cos n\theta\right\} + (1+\nu_{31})\alpha_3\Delta T + S_4\cos\theta \tag{4-78}$$

$$u_{\theta 3}(r,\theta) = \frac{1}{E'}\left\{-\frac{c_{13}}{r^2}(1+\nu')\sin\theta + \sum_{2}^{\infty}[\, c_{n3}n(1+\nu')r^{-(n+1)} + \right.$$

$$\left. d_{n3}((n - 4 + n\nu'))r^{1-n}]\sin n\theta\right\} - S_4\sin\theta \tag{4-79}$$

e. Boundary conditions

After assuming basic form of solutions, the unknown constants in those equations can be determined by simply substituting them into the following boundary and continuity conditions:

$$\sigma_{rr}(a,\theta) + \sigma_{rr1}(a,\theta) = \sigma_{rr2}(a,\theta) \tag{4-80}$$

$$\sigma_{r\theta}(a,\theta) + \sigma_{r\theta 1}(a,\theta) = \sigma_{r\theta 2}(a,\theta) \qquad (4\text{-}81)$$

$$u_r(a,\theta) + u_{r1}(a,\theta) = u_{r2}(a,\theta) \qquad (4\text{-}82)$$

$$u_\theta(a,\theta) + u_{\theta 1}(a,\theta) = u_{\theta 2}(a,\theta) \qquad (4\text{-}83)$$

$$\sigma_{rr2}(b,\theta) = \sigma_{rr3}(b,\theta) \qquad (4\text{-}84)$$

$$\sigma_{r\theta 2}(b,\theta) = \sigma_{r\theta 3}(b,\theta) \qquad (4\text{-}85)$$

$$u_{r2}(b,\theta) = u_{r3}(b,\theta) \qquad (4\text{-}86)$$

$$u_{\theta 2}(b,\theta) = u_{\theta 3}(b,\theta) \qquad (4\text{-}87)$$

where σ_{rr}, $\sigma_{r\theta}$, $\sigma_{\theta\theta}$, u_r and u_θ are given by eqns (4-5) to (4-9), σ_{rr1}, $\sigma_{r\theta 1}$, $\sigma_{\theta\theta 1}$, u_{r1} and $u_{\theta 1}$ are given by eqns (4-54) to (4-58), σ_{rr2}, $\sigma_{r\theta 2}$, $\sigma_{\theta\theta 2}$, u_{r2} and $u_{\theta 2}$ are given by eqns (4-59) to (4-63), σ_{rr3}, $\sigma_{r\theta 3}$, $\sigma_{\theta\theta 3}$, u_{r3} and $u_{\theta 3}$ are given by eqns (4-64) to (4-66) and (4-78) to (4-79).

Define

$$a_{nj} = -\frac{\mu_1 f}{\pi(1+\kappa_1)}\,\alpha_{nj}\,, \qquad b_{nj} = -\frac{\mu_1 f}{\pi(1+\kappa_1)}\,\beta_{nj}$$

$$c_{nj} = -\frac{\mu_1 f}{\pi(1+\kappa_1)}\,\gamma_{nj}\,, \qquad d_{nj} = -\frac{\mu_1 f}{\pi(1+\kappa_1)}\,\delta_{nj} \qquad \begin{matrix}(n=0,1,2,3,\ldots)\\(j=1,2,3)\end{matrix}$$

After substituting into eqns (4-80) to (4-87), we obtain

$$2\gamma_{01} - \frac{\beta_{02}}{a^2} - 2\gamma_{02} = -B_0 \qquad (4\text{-}88)$$

$$\frac{2(1-2\nu_1)(1+\nu_1)}{E_1}a\gamma_{01} + \frac{(1+\nu_2)}{E_2}\frac{1}{a}\beta_{02} - \frac{2(1-2\nu_2)(1+\nu_2)}{E_2}a\gamma_{02} =$$

$$-\frac{C_0}{\mu_1} - \frac{\pi(1+\kappa_1)[(1+\nu_2)\alpha_2-(1+\nu_1)\alpha_1]\Delta Ta}{f\mu_1} \qquad (4\text{-}89)$$

$$\frac{\beta_{02}}{b^2} + 2\gamma_{02} - \frac{\beta_{03}}{b^2} = 0 \qquad (4\text{-}90)$$

$$-\frac{(1+\nu_2)}{E_2}\frac{1}{b}\beta_{02} + \frac{2(1+\nu_2)(1-2\nu_2)}{E_2}b\gamma_{02} + \frac{(1+\nu')}{E'}\frac{1}{b}\beta_{03} =$$

$$-\frac{\pi(1+\kappa_1)[(1+\nu_{31})\alpha_3-(1+\nu_2)\alpha_2]\Delta Tb}{f\mu_1} \qquad (4\text{-}91)$$

$$2\delta_{11}a + \frac{2\gamma_{12}}{a^3} - 2\delta_{12}a = -B_1 \qquad (4\text{-}92)$$

$$2\delta_{11}a + \frac{2\gamma_{12}}{a^3} - 2\delta_{12}a = A_1 \qquad (4\text{-}93)$$

$$\frac{(1+\nu_1)(1-4\nu_1)}{E_1}a^2\delta_{11} - \frac{(1+\nu_2)}{E_2}\frac{1}{a^2}\gamma_{12} - \frac{(1-4\nu_2)(1+\nu_2)}{E_2}a^2\delta_{12} + S_I = -\frac{C_1}{\mu_1}$$

(4-94)

$$\frac{(1+\nu_1)(5-4\nu_1)}{E_1}a^2\delta_{11} - \frac{(1+\nu_2)}{E_2}\frac{1}{a^2}\gamma_{12} - \frac{(5-4\nu_2)(1+\nu_2)}{E_2}a^2\delta_{12} - S_I = -\frac{D_1}{\mu_1}$$

(4-95)

$$\frac{2\gamma_{12}}{b^3} - 2\delta_{12}b - \frac{\gamma_{13}}{b^3} = 0 \qquad (4\text{-}96)$$

$$\frac{(1+\nu_2)}{E_2}\frac{1}{b^2}\gamma_{12}+\frac{(1+\nu_2)(1-4\nu_2)}{E_2}b^2\delta_{12}-\frac{(1+\nu')}{E'}\frac{1}{b^2}\gamma_{13}+S_{II}=0 \qquad (4\text{-}97)$$

$$\frac{(1+\nu_2)}{E_2}\frac{1}{b^2}\gamma_{12}+\frac{(1+\nu_2)(5-4\nu_2)}{E_2}b^2\delta_{12}-\frac{(1+\nu')}{E'}\frac{1}{b^2}\gamma_{13}-S_{II}=0 \qquad (4\text{-}98)$$

$$n(1-n)a^{n-2}\alpha_{n1}+(n+1)(2-n)a^{n}\beta_{n1}+n(n-1)a^{n-2}\alpha_{n2}+(n+1)(n-2)a^{n}\beta_{n2}+$$
$$n(n+1)a^{-n-2}\gamma_{n2}+(n-1)(n+2)a^{-n}\delta_{n2}=-B_n \qquad (4\text{-}99)$$

$$n(n-1)a^{n-2}\alpha_{n1}+n(n+1)a^{n}\beta_{n1}-n(n-1)a^{n-2}\alpha_{n2}-n(n+1)a^{n}\beta_{n2}+$$
$$n(n+1)a^{-n-2}\gamma_{n2}+n(n-1)a^{-n}\delta_{n2}=A_n \qquad (4\text{-}100)$$

$$-\frac{1+\nu_1}{E_1}na^{n-1}\alpha_{n1}+\frac{1+\nu_1}{E_1}[2(1-2\nu_1)-n]a^{n+1}\beta_{n1}+\frac{1+\nu_2}{E_2}na^{n-1}\alpha_{n2}+\frac{1+\nu_2}{E_2}(n-$$

$$2+4\nu_2)a^{n+1}\beta_{n2}-\frac{1+\nu_2}{E_2}na^{-n-1}\gamma_{n2}-\frac{1+\nu_2}{E_2}(n+2-4\nu_2)a^{-n+1}\delta_{n2}=-\frac{C_n}{\mu_1}$$

(4-101)

$$\frac{1+\nu_1}{E_1}na^{n-1}\alpha_{n1}+\frac{1+\nu_1}{E_1}(n+4-4\nu_1)a^{n+1}\beta_{n1}-\frac{1+\nu_2}{E_2}na^{n-1}\alpha_{n2}-\frac{1+\nu_2}{E_2}(n+4-$$

$$4\nu_2)a^{n+1}\beta_{n2} - \frac{1+\nu_2}{E_2} na^{-n-1}\gamma_{n2} - \frac{1+\nu_2}{E_2}(n-4+4\nu_2)a^{-n+1}\delta_{n2} = -\frac{D_n}{\mu_1}$$

(4-102)

$$n(n-1)b^{n-2}\alpha_{n2} + (n+1)(n-2)b^{n}\beta_{n2} + n(n+1)b^{-n-2}\gamma_{n2} + (n-1)(n+2)b^{-n}\delta_{n2} - n(n+1)b^{-n-2}\gamma_{n3} - (n-1)(n+2)b^{-n}\delta_{n3} = 0 \qquad (4\text{-}103)$$

$$n(n-1)b^{n-2}\alpha_{n2} + n(n+1)b^{n}\beta_{n2} - n(n+1)b^{-n-2}\gamma_{n2} - n(n-1)b^{-n}\delta_{n2} + n(n+1)b^{-n-2}\gamma_{n3} + n(n-1)b^{-n}\delta_{n3} = 0 \qquad (4\text{-}104)$$

$$-\frac{1+\nu_2}{E_2} nb^{n-1}\alpha_{n2} - \frac{1+\nu_2}{E_2}(n-2+4\nu_2)b^{n+1}\beta_{n2} + \frac{1+\nu_2}{E_2} nb^{-n-1}\gamma_{n2} + \frac{1+\nu_2}{E_2}(n+2-4\nu_2)b^{-n+1}\delta_{n2} - \frac{1+\nu'}{E'} nb^{-n-1}\gamma_{n3} - \frac{n+2+(n-2)\nu'}{E'} b^{-n+1}\delta_{n3} = 0 \qquad (4\text{-}105)$$

$$\frac{1+\nu_2}{E_2} nb^{n-1}\alpha_{n2} + \frac{1+\nu_2}{E_2}(n+4-4\nu_2)b^{n+1}\beta_{n2} + \frac{1+\nu_2}{E_2} nb^{-n-1}\gamma_{n2} + \frac{1+\nu_2}{E_2}(n-4+4\nu_2)b^{-n+1}\delta_{n2} - \frac{1+\nu'}{E'} nb^{-n-1}\gamma_{n3} - \frac{n-4+n\nu'}{E'} b^{-n+1}\delta_{n3} = 0 \qquad (4\text{-}106)$$

$$(n=2,3,4,\ldots)$$

where A_n, B_n, C_n and D_n are known functions of t and given by eqns (4-28) to (4-32) and (4-44) to (4-48), consquently, coefficients

a_{nj}, b_{nj}, c_{nj} and d_{nj} (n=0,1,2,..., j=1,2,3) calculated from eqns (4-88) to (4-106) will also be functions of t.

Examining those equations it can be seen that for n=0 or n≥2, there are equal number of equations and unknown constants for each n, therefore these unknown constants can be uniquely determined, but when n=1, there are 7 equations but only 6 unknowns. It is conceivable that one of the 7 equations must be redundent. This is, in fact, suggested by the pair equations (4-92) and (4-93), because the two equations indicate that if

$$A_1+B_1=0 \qquad (4\text{-}107)\ ,$$

then they are identical, and one of them will be redundent. Referring to (4-14) and (4-16), it may be seen that

$$A_1+B_1=\frac{\pi(1+\kappa_1)}{\mu_1 f}\ \frac{1}{\pi a}\int_0^{2\pi}[\sigma_{r\theta}(a,\theta)\sin\theta-\sigma_{rr}(a,\theta)\cos\theta]a\ d\theta \qquad (4\text{-}108)$$

Consider now an infinite plane containing an edge dislocation at r=t, θ=0, it is clear that the integral in (4-108) is nothing but the x component of the resultant of stresses acting on the circle r=a. Since the dislocation problem is a self-equilibrating case, the resultant force on the boundary r=a must be zero and thus proves the validity of (4-107).

After determining all the coefficients, stresses and displacements for all the three domains are determined by eqns (4-5)-(4-9), (4-54)-(4-66) and (4-78) to (4-79). Remember that stresses and displacements in the disk should be the combination of eqns (4-5)-(4-9) and eqns (4-54)-(4-58) in light of eqn (4-1).

IV.3. Crack problem

To find stress intensity factors for the matrix cracks in the ring model, first by superposition, original problem is reduced to a perturbation problem in which the only loading is the pressure on the crack surfaces (see Fig.41). If a crack lies (in the ring model) at $\theta=0$, $-a\le a_1\le x\le b_1\le a$, then in the perturbation case, we have the following condition:

$$\sigma_{r\theta}= 0, \quad 0 \le r < \infty \qquad \theta =0, \text{ or } \theta =\pi \tag{4-109}$$

$$\sigma_{\theta\theta}(r,0)=P(r), \qquad a_1\le x\le b_1 \ , \ \theta =\pi \tag{4-110}$$

$$u_\theta(r,0)=0, \quad -\infty < x \le a_1 \text{ or } b_1 \le x < \infty, \qquad \theta =0 \tag{4-111}$$

where p(r) is equal to the negative of $\sigma_{\theta\theta}$ in the corresponding uncracked geometry (see Fig.41c).

Now assume that the crack is formed by distributing the dislocations along the line $\theta=0$, $a_1<r<b_1$ with f as a funtion of t, then $\sigma_{\theta\theta}(r,\theta)$ in the disk may be evaluated by integrating while using dislocation solution (4-7) and (4-55) as Green's function. Specially, for $\theta=0$, r=x from (4-110) we find

$$\int_{a_1}^{b_1} \frac{f(t)}{t-r}\, dt + \int_{a_1}^{b_1} k(r,t)f(t)\, dt=\frac{\pi(1+\kappa_1)}{2\mu_1} P(r), \quad a_1<r<b_1 \tag{4-112}$$

where the Fredhom kernel is

$$k(r,t)=\frac{1}{2}\left\{ 2\ \gamma_{01} + 6\delta_{11}r + \sum_{2}^{\infty} [n(n-1)r^{n-2}\alpha_{n1} + (n+1)(n+2)r^{n}\beta_{n1}]\right\}$$

(4-113)

and α_{n1}, β_{n1} $(n=2,3,\ldots,)$, γ_{01} and δ_{11} are known functions of t which are determined by eqns (4-88) to (4-106). If the crack is an embedded crack, (i.e., if $-a<a_1<b_1<a$) then from the definition of f(t), it follows that

$$\int_{a_1}^{b_1} f(t)\ dt = 0 \qquad (4\text{-}114)$$

The stress intensity factor of the matrix crack is related to the solution of the singular integral equation. If the crack is an embedded crack the index of the singular integral equation (4-114) is +1 and the function f(r) can be written as the following form

$$f(r)=\frac{F(r)}{[(r-a_1)(b_1-r)]^{1/2}} \qquad (a_1<r<b_1) \qquad (4\text{-}115)$$

where F(r) is a bounded function. After evaluating F(r), the stress intensity factor at the crack tips $r=a_1$ and $r=b_1$ may be defined and obtained as follows:

$$k(a_1) = \lim_{r\to a_1} \sqrt{2(a_1-r)}\ \sigma_{\theta\theta}(r,0)$$

$$= \frac{2\mu_1}{1+\kappa_1} \lim_{r\to a_1} \sqrt{2(r-a_1)}\, f(r) = \frac{2\mu_1}{1+\kappa_1} \frac{F(a_1)}{\sqrt{(b_1-a_1)/2}} \qquad (4\text{-}116)$$

$$k(b_1) = \lim_{r\to b_1} \sqrt{2(r-b_1)}\, \sigma_{\theta\theta}(r,0)$$

$$= -\frac{2\mu_1}{1+\kappa_1} \lim_{r\to b_1} \sqrt{2(b_1-r)}\, f(r) = \frac{2\mu_1}{1+\kappa_1} \frac{F(b_1)}{\sqrt{(b_1-a_1)/2}} \qquad (4\text{-}117)$$

IV.4. Numerical results and discussion

The singular integral equation (4-112) with (4-114) can be solved numerically by Gaussian quadrature method.
First, equations are normalized by assuming

$$r = \frac{b_1-a_1}{2}\rho + \frac{b_1+a_1}{2}, \quad \text{where, } a_1 < r < b_1 \ , \ -1 < \rho < 1;$$

$$t = \frac{b_1-a_1}{2}\tau + \frac{b_1+a_1}{2}, \quad \text{where, } a_1 < t < b_1, \ -1 < \tau < 1;$$

$$f(t) = g(\tau); \quad k(r,t) = K(\rho,\tau);$$

$$p(r) = q(\rho) \ . \qquad (4\text{-}118)$$

eqns (4-112) and (4-114) hence become

$$\int_{-1}^{1} \frac{g(\tau)}{\tau-\rho} d\tau + \frac{(b_1-a_1)}{2} \int_{-1}^{1} K(\rho,\tau) g(\tau) d\tau = \frac{\pi(\kappa_m + 1)}{2\mu_m} q(\rho), \quad -1 < \rho < 1 \tag{4-119}$$

and

$$\int_{-1}^{1} g(\tau) d\tau = 0 \tag{4-120}$$

The function $g(\tau)$ is singular at $\tau = \pm 1$ and may be written as follows [49]:

$$g(\tau) = \frac{G(\tau)}{(1-\tau^2)^{1/2}} \tag{4-121}$$

where $G(\tau)$ is a bounded function.

At the crack tip the stress intensity factor can then be calculated by the following eqns:

$$k(a_1) = -\frac{\sqrt{2\mu_m}}{1+\kappa_m} \sqrt{(b_1-a_1)}\, G(-1) \tag{4-122}$$

$$k(b_1) = -\frac{\sqrt{2\mu_m}}{1+\kappa_m} \sqrt{(b_1-a_1)}\, G(1) \tag{4-123}$$

Using Labato-Chebyshev numerical integration method, following a standard procedure in [50], [51], the integral equation can be

solved by reducing it to a set of linear algebraic simultaneous equations as follows, from which G(1) and G(-1) can be evaluated accurately:

$$\sum_{k=0}^{n} \lambda_k \frac{G(\tau_k)}{\tau_k-\rho_k} + \frac{(b_1-a_1)}{2} \sum_{k=0}^{n} \lambda_k K(\tau_k, \rho_k) G(\tau_k) = \frac{2\mu_m}{1+\kappa_m} q(\rho_k), \quad (4\text{-}124),$$

where

$$\lambda_k = \begin{cases} \frac{\pi}{2(n-1)}, & \text{when } k=1,n, \\ \frac{\pi}{n-1}, & \text{when } k=2,3,\ldots,n-1, \end{cases} \quad (4\text{-}125)$$

τ_k's, ρ_k's are roots of Chebyshev polynomials as follows:

$$T_{n-1}(\rho_r)=0, \quad r=1,2,\ldots,n-1, \quad (4\text{-}126)$$

$$(1-\tau_k^2)U_{n-2}(\tau_k)=0, \quad k=1,2,\ldots,n-2, \text{ and } \tau_k=\pm 1, \quad (4\text{-}127)$$

Results are compared with available analytical solutions for specific cases for verification of the solution. For example, when Young's moduli in ring and external infinite domain are set a very small value, considered problem is reduced to a cracked disk case, for which the solutions for various loadings have been given by Tweed and Rooke, Bowie, Isida, Erdogan and Delale, et al., comparison are made for both radial and edge cracks with various loadings [58] and listed in Table 1. For another specific case, if the infinite domain of the problem has the same mechanical

constants as the ring domain, considered problem is reduced to a single fiber embedded in infinite matrix with a fiber crack, comparison is made with Erdogan's solution [43] and listed in Table 2.

Analysis of matrix microcracking for mechanical and thermal loadings is conducted using ring model. Superposition technique is used, i.e., first the uncrack geometry case is solved, then by superposition the considered case is transformed into a perturbation case, in which the only loading is self-equilibrating crack surface pressure. Solutions for uncracked geometry cases can be found in Appendix I.

To study effect of fiber distribution on microcracking, different crack geometries (different crack lengths), volume fractions of fibers for the composite in the ring, various widths of the ring and volume fractions of fibers for the composite in the infinite domain are considered. Extensive results are obtained and exhibited in tabular and graphical forms in Figs 42-49 and Tables 3-10.

Results for the ring model subjected to uniaxial traction at infinity are displayed in Figs 42-45 and listed in Tables 3-6. Among them, Effect of $V_{f\text{-}ring}$ (volume fraction of fibers for the composite in the ring) and mismatch of fiber and matrix materials on the microcracking is presented in Figs. 42-43 and Tables 3-4. It can be seen in Fig.42 that for "reverse" composite material (i.e., if $E_m > E_f$), when crack is a short one, or not very close to the surrounding fibers, its tendency to propagate will be diminishing with increasing $V_{f\text{-}ring}$, (i.e., with decreasing stiffness of the ring material), but if the crack is relatively long, or close to surrounding fibers, it will tend to propagate with increasing $V_{f\text{-}ring}$, (i.e., with decreasing stiffness of the

ring material). Effect of $V_{f\text{-ring}}$ on microcracking for $E_f > E_m$, is given in Fig. 43 and Table 4. It is observed that for all sizes of cracks they will be less tending to propagate with increasing $V_{f\text{-ring}}$ (i.e., with increasing stiffness of the ring material). When the crack is relatively long or close to nearby fibers such effect becomes more evident. Effect of the width of the ring on microcracking (for uniaxial traction case) is displayed in Fig.44 and listed in Table 5. It is found that such effect is evident for b/a within 2-3. However, for b/a>4 the increasing width has hardly any effect on the normalized stress intensity factors. This also tells that effect of surrounding fibers in ceramic composites on the microcracking to a great extent is due to those situated within a local area of b/a<3. Effect of $V_{f\text{-overall}}$ (volume fraction of fibers in the infinite domain, this is also the volume fraction of fibers of the composite) on the microcracking is displayed in Fig.45 and listed in Table 6. It is observed that for $V_{f\text{-overall}}$ ranging from 0.0-1.0 the effect is evident, but usually for ceramic composite, $V_{f\text{-overall}}$ is between 30%-40%, therefore such effect is only about 10%.

Results of ring model under thermal loading are displayed in Figs 46-49 and listed in Tables 7-10. Among them, effect of $V_{f\text{-ring}}$ as well as mismatch of constituent materials on microcracking are displayed in Figs 46-47 and listed in Tables 7-8. It is observed that the effect of $V_{f\text{-ring}}$ is significant, but such effect is evenly exerted on all sizes of cracks, i.e., for long cracks or short cracks, such effect is almost the same. Effect of the width of the ring on microcracking is given in Fig.48 and Table 9. It is observed that such effect is significant for b/a < 5, after that the increasing b/a has hardly any effect on

normalized stress intensity factors. Effect of $V_{f\text{-overall}}$ on normalized stress intensity factors is displayed in Fig.49 and listed in Table 10. It is observed that unlike mechanical loading case, the $V_{f\text{-overall}}$ has sizable effect on normalized stress intensity factors.

CHAPTER V

EXPERIMENTAL APPROACH

USING MICRO-INDENTATION TECHNIQUE TO INVESTIGATE EFFECT OF TEMPERATURE AND FIBER DISTRIBUTION ON MATRIX MICROCRACKING AS WELL AS TOUGHNESS OF THE MATERIAL

Parallel to theoretical analysis, experiments are carried out using Nicalon/SiC composite specimens to investigate effect of temperature and fiber distribution on matrix microcracking and toughness of the composite material.

Two sets of experiments are conducted in this study. The first one is using micro-indentation technique and specimens of monolithic ceramic matrix materials (SiC and CAS II) to determine the fracture toughness K_{Ic} of matrix materials, and further to study effect of temperature on fracture toughness K_{Ic} of the matrix materials. The second set uses micro-indentation technique again and specimens of ceramic matrix composite (Nicalon/SiC ceramic composite) to study the effect of fiber distribution and temperature on matrix microcracking. Experimental results are compared with theoretical predications.

V.1. Set up of experiments

Part of the experiment set-up is shown in Fig. 50. An ATS series 3320 split-tube laboratory furnace (Applied Test Systems, Inc., Butler, PA) and a diamond Vickers indenter (Wilson Instruments, Inc., Bridgeport, CT) are used for heating specimens and carrying out micro-indentations at elevated temperatures. The furnace can be set up to any desired temperature within allowed range and be heated up to 3000 $^{\circ}$F in 30 minutes. Temperature in the

furnace is measured by two type B platinum/platinum-30% rhodium thermocouples and real-time LCD displayed on the panel of the furnace controller.

The Vickers indenter is glued at the tip of an alumina cylindrical bar (inside the furnace) using high-temperature cement. The other end of the cylindrical bar is attached to a vernier screw mechanism (outside the furnace), which is designed to raise or lower the cylindrical bar as well as the indenter precisely. In the indentation test the specimen is placed on a refractory base, the indenter is moved downward by turning the screw mechanism and indent the specimen. The indentation load is measured by an ultra precision, 10-lb super-mini load cell and displayed on the panel of the load cell readout (Interface, Inc., scoattsdale, AZ).

In addition a NIKON UM-2 universal microscope is used for measuring the length of the indentation-generated microcracks, and Tukon 300 microhardness tester with the Vickers indenter (Wilson Instruments, Inc., Bridgeport, CT) is used for room temperature tests.

V.2. Effect of temperature on toughness of ceramic matrix materials

Indentation technique [59][60] is employed in this experiment for determination of fracture toughness of matrix materials (SiC and CAS II). Further, effect of temperature on fracture toughness of matrix materials is investigated.

Equipment for the test is the series 3320 split-tube laboratory furnace and the Vickers diamond indenter. Specimens are monolithic SiC purchased from Amercom, Inc. Chatsworth, CA. and monolithic CAS II from Corning, Inc., New York. The SiC specimen consists of a 1/2"x1/2"x1/8" graphite base coated with a 0.02"

layer of SiC by the CVD (Chemical Vapor Deposition) technology (see Fig.51). Specimens are mounted in bakelite molds and polished for the preparation of the tests. They are polished in two steps: 7.5 micron grit diamond paste is used first in the lapping process, then 1.0 micron grit diamond paste is used for improving the finish of the testing surface.

For each test the specimen is first heated up to and kept at desired temperature for certain amount of time, then indented with certain load. The indentation-generated semi-penny-like crack (see Fig.52) is measured for its length under the NIKON UM2 universal microscope, and toughness of the material can be calculated by using the following formula [61]:

$$K_{Ic} = \frac{1}{\pi^{3/2}\tan\psi}\left(\frac{P}{D^{3/2}}\right) \qquad (5\text{-}1)$$

where P is the applied load, D the half crack length and ψ is half of the indenter's vertex angle (for Vickers indenter, $\psi = 68^{\circ}$). Details about the indentation technique can be found in [18],[61] by Lawn et al.

To study the effect of temperature on toughness of ceramic matrix materials, tests was conducted under various temperatures ranging from room temperature 25°C to 800°C. The toughness of SiC (and CAS II) for changing temperatures are presented in Fig.53. It is observed that the toughness of the ceramic matrix material SiC (as well as CAS II) decreases significantly with increasing temperature.

V.3. Effect of temperature and fiber distribution on matrix cracking

As is stated before matrix microcracking is one of the major detrimental factors for low toughness of ceramic matrix composites. Parallel to analytical work, experiments are also conducted to investigate the effect of fiber distribution as well as temperature on the matrix microcracking. Micro-indentation technique is used again, the facilities are still the series 3320 split-tube laboratory furnace and the Vickers diamond indenter. The specimen is 1/2"x1/2"x1/8" Nicalon/SiC composite with fibers aligned normal to the testing surface (Nicalon is SiC yarn from Nippon Carbon Co.) The specimen (purchased from Amercom, Inc., Chatsworth, CA) is prepared in a way similar to that for monolithic SiC specimens as described in the preceding section.

In the experiment microcracks were generated in the matrix of the composite at various temperatures ranging from room temperature to 800 $^{\circ}$C. To ascertain the effect of fiber distribution, indentations were also performed at locations with different densities of fiber distribution and the fracture toughness was calculated still using formula (5-1). It must be pointed out that the formula (5-1) is only applicable to homogeneous brittle materials, but here it is used as if fibers did not exist. Therefore the toughness thus obtained contains the effect of the fiber distributions, and it is defined as "apparent fracture toughness" of the matrix material. (The practical significance of "apparent fracture toughness" will be explained later in this section.) The effect of surrounding fibers is introduced and defined by local volume fraction of fibers. Local volume fraction of fiber reflects the fiber distribution density in the vinicity of the crack. To measure the local volume fraction of fibers, a square

sample cell containing the indentation imprint and surrounding fibers is selected. The size of the cell is taken in proportion to crack length (say, if the crack length is 2a, then b/a=3, 2b is the side length of the square cell) (see Fig. 54). The local volume fraction of fibers is then defined as the ratio of the total cross sectional areas of all the fibers in the cell to the area of the cell. The experimentally obtained apparent fracture toughness versus local volume fraction of fibers for temperatures of 25°C, 250°C , 600°C and 800°C are presented in Figs 55-58 and summarized in Fig.59, in which the experimental data are presented as regressional straight lines.

It is observed that the "apparent fracture toughness" of SiC decreases with increasing local volume fraction of fibers and also decreases with increasing temperature. This means that it is easier to generate microcracks in Nicalon/SiC composites or if already there is a microcrack it is more likely to propagate at a location where the density of fibers is larger or when the temperature is higher.

The result that the "apparent fracture toughness" of the matrix material (SiC) decreases with increasing local volume fraction is not supprising and actually expected, since Nicalon/SiC composite is so-called "reverse" composite, meaning that the matrix is stiffer than the fibers. Here the Young's modulus of the matrix material (SiC) is $E_m=55\times10^6$ psi and the Young's modulus of fibers (Nicalon) is $E_f=26\times10^6$ psi. (If fibers are stiffer than matrix material, apparent K_{IC} is expected to increase with increasing local volume fraction of fibers, which will be seen later in this section.)

V.4. The theoretical model

A theoretical model, shown in Fig.60, is used to predict the experimental results (see also [62]). The mechanical constants used in the analysis for the Nicalon/SiC composite are as follows:

MAtrix material (SiC):

Young's modulus: $E_m = 55 \times 10^6$ psi,

Possion's ratio: $\nu_m = 0.2$,

Thermal expansion coefficient: $\alpha_f = 4.3 \times 10^{-4} / {}^\circ C$.

Fiber material (Nicalon):

Young's modulus: $E_f = 26 \times 10^6$ psi,

Possion's ratio: $\nu_f = 0.2$,

Thermal expansion coefficient: $\alpha_f = 3.0 \times 10^{-4} / {}^\circ C$.

Mechanical constants of the composite in the ring can be determined by rule of mixture using a volume fraction of fibers equivalent to that in the cell. Uniform pressure $\sigma_\circ$ is applied on the crack edges to simulate indentation force. Temperature effect is also accounted for as thermal loading.

Since for a given composite material the mechanical constants of the constituents are known, from the dimensional analysis, it can be shown that the stress intensity factor of the crack in the model problem can be written as

$$K_I = \sigma_\circ \sqrt{\pi\, a}\; f(V_f,\ R/a,\ \Delta T) \qquad (5\text{-}2)$$

where V_f is the local volume fraction of fibers, $\sigma_\circ$ is the pressure on the crack surface, R is the fiber radius, a is the half crack length. Note that when $\sigma_\circ$ reaches the critical value $(\sigma_\circ)_c$, K_I becomes the critical stress intensity factor of the matrix material $(K_{Ic})_{matrix}$. Thus the "apparent fracture toughness", for this case can be written as:

$$(K_{Ic})_{app} = (\sigma_\circ)_c \sqrt{\pi\, a}\ , \qquad (5\text{-}3)$$

which can also be expressed in terms of V_f , R/a and ΔT as:

$$(K_{Ic})_{app} = \frac{(K_{Ic})_{matrix}}{f(V_f,\ R/a,\ \Delta T)} \qquad (5\text{-}4)$$

where $$f(V_f,\ R/a,\ \Delta T) = \frac{K_I}{\sigma_\circ \sqrt{\pi a}}\ , \qquad (5\text{-}5)$$

is the normalized stress intensity factor.

The stress intensity factor K_I is determined by using analytical solution as well as finite element technique. A finite element procedure using the finite element code ABAQUS (Hibbit, Karlsson & Sorensen, Inc., Providence, RI) is developed and the finite element model is shown in Fig.61. The results for R/a=0.55, temperature ranging from 25°C to 800°C are displayed in Figs.62-65 and summerized in Fig.66. Each of them is plotted against corresponding experimental result. It is observed that the

theoretical results match the experimental results exceptionally well.

For the same model and same loading (uniform pressure p), the results $\frac{k1(a1)}{p\sqrt{c}}$ (normalized stress intensity factors) versus $V_{f\text{-ring}}$ (volume fraction of fibers for the composite in the ring) for different crack lengths and different E_m/E_f are given in Table 11-12 and displayed in Figs 67-68. It can be seen by the same reasoning that when $E_f > E_m$, apparent K_{IC} would increase with the increasing $V_{f\text{-local}}$(local volume fraction of fibers), in other words, if fibers are stiffer than matrix material, it is more difficult to generate a crack at a spot where the density of fiber distribution is higher.

The concept of "apparent fracture toughness" of matrix has obvious practical significance for the estimation of crack propagation and thus is useful for the design of the ceramic matrix composite(see Fig.69). With the concept of "apparent fracture toughness" the propagation of a matrix crack may be easily assessed without going through solution of an extremely complicated elasticity problem, i.e., to estimate possible propagation of a crack in the ceramic matrix composite, one can simply find the K_I which is the stress intensity factor for the same crack geometry but in the homogeneous case, then compare it with $K_{Ic\text{-app}}$ which can be obtained from experiments, for instance, using the results given in Figs 55-58. Homogeneous crack problems usually will not pose any difficulty and many of the solutions have been documented in handbooks.

CHAPTER VI
DEBONDING TESTS TO DETERMINE FIBER-MATRIX BONDING STRENGTH AT DEBONDING INITIATION

Debonding tests are performed to determine fiber-matrix bonding strength at debonding initiation. Equipment for the purpose is Tukon 300 microhardness tester and Vickers indenter, the specimen is Nicalon/SiC composite. Since usually debonding force is much less than that which will induce a microcrack in fibers, therefore Vickers indenter was used, instead of using some specifically-designed probes, to push the fiber and force fibers debond from matrix. In debonding tests indenter presses the center of the fiber and load is applied incrementally until complete debonding takes place, when a dark circle highlightening the fiber-matrix interface can be observed.

After a number of debonding tests, it is found through a regressional analysis (actually it is expected from dimensional analysis) that the debonding loads are proportional to the crosssectional areas of the debonded fibers (see Fig.70). This finding indicates that the results of debonding tests will be consistent no matter what size of fibers are taken for the test as well as for the calculation of the bonding strength.

A finite element procedure was developed using ANSYS code to relate the critical loading to the stresses on fiber-matrix interface (see Fig.71). Axisymmetric elements are used in the FEM model and a concentrated force or distributing pressure is specified at the center of the fiber. Results are compared with Boussinesq's solution when the fiber is assigned with the same mechanical constants as the matrix to check the accuracy of the FEM

solution. In this aspect, a similar model was developed in [40] for study of the interfacial strength of fiber reinforced composites.

Normalized stresses on the fiber-matrix interface due to the concentrated load are given in Fig.72, and the effect of temperature on the interfacial stress distribution is presented in Fig.73.

Using maximum shear stress criterion, fiber-matrix bonding strength at the fiber-matrix interface can be evaluated by the following formula:

$$\tau_{rz(critical)} = K_1 \frac{P_{cr}}{R^2} + K_2 \alpha_m E_m \Delta T \quad (6\text{-}1)$$

where for given materials, K_1, K_2 can be determined by finite element analysis, for example, for Nicalon/SiC composite, $K_1 \simeq 0.1$, $K_2 \simeq 0.095$. P_{cr} is the critical load at debonding initiation, E_m Young's modulus of matrix, α_m thermal expansion coefficient of matrix, R the radius of the tested fiber, Δ T the change in temperature.

VII. CLOSURE

VII.1. Concluding remarks

As a result of the study on microcracking in ceramic matrix composites the following conclusions may be made:

1) Indentation tests reveal that temperature affects the toughness of ceramic matrix materials considerably. For the selected tested materials(SiC and CAS II) it is observed that the toughness of the ceramic matrix materials declines with increasing temperature. This means that when temperature goes up it is easier to generate cracks in matrix, consquently toughness of the ceramic matrix composites will decline.

2) Both experimental and theoretical studies show that fiber distribution has significant effect on stress distribution and microcrack propagation in the ceramic matrix composite. It is observed that for a "reverse composite", i.e., if $E_m > E_f$, it is easier to generate a crack in matrix at a location with a higher desenty of fiber distribution. Nevertheless, it is expected that if $E_m < E_f$, it is more difficult to generate a crack at locations with higher fiber distribution densities, in other words, the material appears tougher than its monolithic form due to the existence of fibers.

3) Concepts of Apparent K_{IC} and local volume fraction of fibers, proposed in this study, have obvious practical significance for the estimation of microcrack propagation.

4) Analyses of microcracking based on two-fiber model indicate that neighboring fibers have significant effect on radial and interfacial microcracking only when neighboring fiber stays very close. It is found that when $\delta>3$, i.e., the spacing between fibers is larger than 3 times the fiber diameter such effect is negligible. Single fiber solution will work farely well under such circumstances. But if fibers are close, say $\delta<3$, it seems that interfacial crack arrest is still possible, while radial crack arrest seems unlikely once crack propagation initiates.

5) Analyses of microcracking based on ring model show that effect of neighboring fibers on matrix crack propagation is significant only when $b/a < 3$ for uniaxial traction, and $b/a<5$ for thermal loading.

6) Debonding tests are performed and a formula for the calculation of bonding strength of fiber-matrix interfaces in conjunction with maximum shear stress criterion (with temperature effect being included) is proposed.

VII.2. Future development

Much work can be done for the further study of microcracking in ceramic matrix composites, for instance, in the immediate future, improvement may be made from the following aspects:

1) It is worth trying again to find exact analytical solutions for the two-fiber model problems. It seems likely that there exist closed form solutions for two-fiber model problems.

2) Effect of fiber distribution can be taken into consideration in the further study of bonding strength of fiber-matrix interfaces at debonding initiation.

3) "sizing effect" can be considered. In the manufacturing of ceramic composites, fibers are coated with a thin layer of material usually referred to as "sizing" (see Fig. 74). It is believed that this layer may have a significant effect on the bonding strength of fiber-matrix interfaces, as well as interfacial crack propagation. Therefore it should be incorporated into the analytical model.

4) different geometries of matrix cracks in ring model may be considered, for example, an arc crack or arbitrarily oriented linear matrix crack can be considered.

Table 1. Comparison with Bowie and Neal's results (circular disk containing a central crack subjected to uniform external tension)

a/R	Bowie and Neal's Results	Present Results
0.04	1	1.0024
0.1	1.02	1.015
0.2	1.06	1.06
0.4	1.24	1.2432
0.6666	1.74	1.7425
0.7407	1.98	1.9794
0.8	2.24	2.2385
0.8333	2.43	2.4313
0.8696	2.71	2.7085
0.91	3.17	3.179

Table 2. Comparison with Erdogan's results. (single fiber embedded in infinite matrix subjected to uniaxial traction with a crack in the fiber)

a1/a	b1/a	$\mu_m/\mu_f=3$				$\mu_m/\mu_f=1/3$			
		$\frac{k1(a1)}{\sigma_0\sqrt{c}}$		$\frac{k1(b1)}{\sigma_0\sqrt{c}}$		$\frac{k1(a1)}{\sigma_0\sqrt{c}}$		$\frac{k1(b1)}{\sigma_0\sqrt{c}}$	
		Erdogan's Results	Present Results	Erdogan's Results	Present Results	Erdogan's Results	Present Results	Erdogan's Results	Present Results
-0.1	0.1	1.283	1.2834	1.283	1.2834	0.6046	0.6046	0.6046	0.6046
-0.25	0.25	1.332	1.3317	1.332	1.3317	0.5796	0.5796	0.5796	0.5796
-0.5	0.5	1.491	1.4907	1.491	1.4906	0.5144	0.5144	0.5144	0.5144
-0.75	0.75	1.752	1.7518	1.752	1.7517	0.4437	0.4438	0.4437	0.4437
-0.9	-0.75	0.5886	0.5886	0.595	0.595	1.324	1.324	1.309	1.3089
-0.9	-0.5	0.5416	0.5417	0.5684	0.5685	1.451	1.4506	1.376	1.3765
-0.9	-0.25	0.5032	0.5034	0.5452	0.5452	1.572	1.5709	1.438	1.4383
-0.9	0	0.4719	0.472	0.5219	0.5219	1.684	1.6822	1.501	1.501
-0.9	0.25	0.445	0.4456	0.4969	0.4969	1.79	1.7861	1.572	1.5718
-0.9	0.5	0.422	0.4227	0.4682	0.4682	1.89	1.8845	1.664	1.6639
-0.9	0.75	0.402	0.4025	0.43	0.4303	1.99	1.9822	1.822	1.8214
-0.9	0.9	2.062	2.0483	2.062	2.0483	0.39	0.3913	0.39	0.3913

Table 3. Normalized stress intensity factors vs. normalized crack lengths for various volume fractions of fibers in the ring.

b/a=2 Em/Ef= 3

c/a	$\frac{k1(a1)}{\sigma_0\sqrt{c}}$					
	*Vf=0.0	Vf=0.2	Vf=0.4	Vf=0.6	Vf=0.8	Vf=1.0
0.05	1	0.9976	0.9881	0.9671	0.9264	0.8496
0.1	1	0.9982	0.9894	0.9691	0.9293	0.8532
0.15	1	0.9992	0.9915	0.9725	0.934	0.8592
0.2	1	1.0005	0.9943	0.977	0.9403	0.8672
0.25	1	1.0022	0.9979	0.9826	0.9481	0.8773
0.3	1	1.0041	1.0019	0.989	0.9572	0.889
0.35	1	1.0062	1.0064	0.9962	0.9674	0.9023
0.4	1	1.0085	1.0113	1.0041	0.9784	0.9167
0.45	1	1.011	1.0165	1.0124	0.9903	0.9323
0.5	1	1.0135	1.0219	1.021	1.0027	0.9487
0.55	1	1.0161	1.0275	1.0301	1.0156	0.966
0.6	1	1.0188	1.0333	1.0394	1.0291	0.9841
0.65	1	1.0216	1.0393	1.0492	1.0432	1.0032
0.7	1	1.0246	1.0458	1.0597	1.0583	1.0237
0.75	1	1.0278	1.0528	1.0712	1.075	1.0465
0.8	1	1.0316	1.0609	1.0844	1.0944	1.0731
0.85	1	1.0362	1.071	1.101	1.1187	1.1067
0.9	1	1.0424	1.0848	1.1241	1.1533	1.1552

*V_f means V_{f-ring}

Table 4. Normalized stress intensity factors vs. normalized crack lengths for various volume fractions of fibers in the ring (uniaxial traction at infinity)

Em/Ef=1/3 b/a=2

c/a	$\frac{kl(al)}{\sigma_0 \sqrt{c}}$					
	* Vf=0.0	Vf=0.2	Vf=0.4	Vf=0.6	Vf=0.8	Vf=1.
0.05	1	0.9855	0.9576	0.9259	0.8939	0.8629
0.1	1	0.984	0.955	0.9225	0.8899	0.8585
0.15	1	0.9816	0.9509	0.9171	0.8835	0.8514
0.2	1	0.9784	0.9453	0.9097	0.8749	0.8418
0.25	1	0.9744	0.9385	0.9008	0.8644	0.8301
0.3	1	0.9699	0.9306	0.8907	0.8525	0.8168
0.35	1	0.9648	0.922	0.8794	0.8393	0.8023
0.4	1	0.9594	0.9128	0.8675	0.8254	0.7868
0.45	1	0.9538	0.9032	0.855	0.8108	0.7707
0.5	1	0.9479	0.8932	0.8421	0.7958	0.7542
0.55	1	0.9418	0.883	0.8289	0.7805	0.7373
0.6	1	0.9356	0.8724	0.8154	0.7648	0.7202
0.65	1	0.9291	0.8616	0.8015	0.7488	0.7026
0.7	1	0.9223	0.8502	0.7869	0.7321	0.6844
0.75	1	0.9149	0.8379	0.7714	0.7144	0.6652
0.8	1	0.9066	0.8243	0.7543	0.695	0.6443
0.85	1	0.8967	0.8083	0.7345	0.6728	0.6206
0.9	1	0.8837	0.7877	0.7094	0.6449	0.5912

*V_f means $V_{f\text{-ring}}$

Table 5. Results from ring model
Normalized stress intensity factors vs.
normalized crack lengths for various ring widths
(uniaxial traction at infinity)

Em/Ef=1/3 Vf-ring=1 Vf-overall=0.0

b/a	$\frac{k1(a1)}{\sigma_0\sqrt{c}}$								
	c/a=0.1	c/a=0.2	c/a=0.3	c/a=0.4	c/a=0.5	c/a=0.6	c/a=0.7	c/a=0.8	c/a=0.9
2	0.8585	0.8418	0.8168	0.7868	0.7542	0.7202	0.6844	0.6443	0.5912
3	0.8104	0.7925	0.7661	0.7345	0.7008	0.6663	0.6312	0.5931	0.5441
4	0.7926	0.7743	0.7473	0.7151	0.6808	0.646	0.6107	0.5728	0.5248
5	0.7842	0.7657	0.7384	0.706	0.6714	0.6363	0.6009	0.563	0.5154
6	0.7796	0.761	0.7336	0.701	0.6663	0.631	0.5955	0.5576	0.5101
7	0.7768	0.7582	0.7307	0.698	0.6631	0.6278	0.5922	0.5543	0.5069
8	0.775	0.7564	0.7288	0.696	0.6611	0.6257	0.5901	0.5522	0.5048
9	0.7738	0.7551	0.7275	0.6947	0.6597	0.6243	0.5886	0.5507	0.5034
10	0.7729	0.7542	0.7266	0.6937	0.6587	0.6233	0.5875	0.5496	0.5023
11	0.7723	0.7535	0.7259	0.693	0.658	0.6225	0.5867	0.5488	0.5016
12	0.7718	0.753	0.7254	0.6925	0.6574	0.6219	0.5862	0.5482	0.501
13	0.7714	0.7526	0.725	0.692	0.657	0.6215	0.5857	0.5478	0.5005
14	0.7711	0.7523	0.7246	0.6917	0.6566	0.6211	0.5853	0.5474	0.5002
15	0.7708	0.7521	0.7244	0.6914	0.6563	0.6208	0.585	0.5471	0.4999
16	0.7706	0.7519	0.7242	0.6912	0.6561	0.6206	0.5848	0.5468	0.4996
17	0.7705	0.7517	0.724	0.691	0.6559	0.6204	0.5846	0.5466	0.4994
18	0.7703	0.7515	0.7238	0.6909	0.6558	0.6202	0.5844	0.5465	0.4993
19	0.7702	0.7514	0.7237	0.6907	0.6556	0.6201	0.5843	0.5463	0.4991
20	0.7701	0.7513	0.7236	0.6906	0.6555	0.62	0.5841	0.5462	0.499
21	0.77	0.7512	0.7235	0.6905	0.6554	0.6199	0.584	0.5461	0.4989
22	0.7699	0.7512	0.7234	0.6905	0.6553	0.6198	0.584	0.546	0.4988
23	0.7699	0.7511	0.7234	0.6904	0.6553	0.6197	0.5839	0.5459	0.4987
24	0.7698	0.751	0.7233	0.6903	0.6552	0.6196	0.5838	0.5458	0.4986
25	0.7698	0.751	0.7232	0.6903	0.6551	0.6196	0.5837	0.5458	0.4986

Table 6.
Results from ring model. b/a=2 E_f/E_m=3 c/a=0.75 $V_{f\text{-ring}}$=1 $V_{f\text{-overall}}$=0.0-1.0

Vf (overall)	$\frac{k1(a1)}{\sigma_0\sqrt{c}}$
0	0.6652
0.1	0.6556
0.2	0.6438
0.3	0.6298
0.4	0.6138
0.5	0.5952
0.6	0.5738
0.7	0.549
0.8	0.52
0.9	0.4854
1	0.4437

Table 7. Results from ring model

Normalized stress intensity factors vs normalized crack lengths.

b/a=2 Vf-overall=0.

$E_f/E_m=3$

c/a	$\frac{kl(al)}{E_m(\alpha_f-\alpha_m)\Delta T}$				
	*Vf=0.2	Vf=0.4	Vf=0.6	Vf=0.8	Vf=1.0
0.05	0.023	0.0882	0.189	0.3193	0.474
0.1	0.0229	0.088	0.1884	0.3181	0.472
0.15	0.0229	0.0876	0.1875	0.3162	0.4688
0.2	0.0228	0.0872	0.1862	0.3137	0.4645
0.25	0.0227	0.0867	0.1847	0.3106	0.4593
0.3	0.0226	0.086	0.1829	0.307	0.4533
0.35	0.0225	0.0854	0.181	0.3031	0.4467
0.4	0.0224	0.0846	0.1789	0.2989	0.4397
0.45	0.0223	0.0838	0.1767	0.2946	0.4324
0.5	0.0222	0.083	0.1745	0.2901	0.4249
0.55	0.0221	0.0822	0.1722	0.2855	0.4171
0.6	0.0219	0.0814	0.1698	0.2807	0.4092
0.65	0.0218	0.0805	0.1673	0.2757	0.401
0.7	0.0216	0.0795	0.1647	0.2705	0.3923
0.75	0.0215	0.0785	0.1618	0.2648	0.383
0.8	0.0213	0.0773	0.1585	0.2585	0.3725
0.85	0.0211	0.0758	0.1546	0.2508	0.36
0.9	0.0207	0.0739	0.1495	0.2409	0.3438

*V_f means V_{f-ring}

Table 8. Results from ring model
Normalized stress intensity
factors vs normalized
crack lengths (thermal loading)

Em/Ef=3 b/a=2

c/a	$\frac{kl(al)}{E_m(\alpha_m-\alpha_f)\Delta T}$				
	*Vf=0.2	Vf=0.4	Vf=0.6	Vf=0.8	Vf=1.0
0.05	0.0078	0.0307	0.0672	0.113	0.1585
0.1	0.0078	0.0308	0.0673	0.1134	0.1592
0.15	0.0078	0.0308	0.0676	0.1139	0.1603
0.2	0.0078	0.0309	0.0679	0.1147	0.1618
0.25	0.0078	0.031	0.0683	0.1157	0.1638
0.3	0.0078	0.0311	0.0687	0.1168	0.166
0.35	0.0078	0.0313	0.0692	0.118	0.1686
0.4	0.0079	0.0314	0.0697	0.1194	0.1715
0.45	0.0079	0.0316	0.0703	0.1209	0.1746
0.5	0.0079	0.0318	0.0709	0.1225	0.1779
0.55	0.0079	0.0319	0.0716	0.1241	0.1814
0.6	0.0079	0.0321	0.0722	0.1259	0.1851
0.65	0.008	0.0323	0.0729	0.1277	0.1891
0.7	0.008	0.0325	0.0737	0.1298	0.1935
0.75	0.008	0.0327	0.0746	0.132	0.1983
0.8	0.008	0.033	0.0755	0.1346	0.204
0.85	0.0081	0.0333	0.0768	0.1379	0.2112
0.9	0.0081	0.0338	0.0785	0.1425	0.2214

*V_f means V_{f-ring}

Table 9.
Results from ring model
Normalized stress intensity factors vs. normalized ring widths (thermal loading)
E_m/E_f= 3

b/a	c/a	Vf (RING)	$\frac{kl(al)}{E_m(\alpha_m-\alpha_f)\Delta T}$
2	0.9	1	0.2214
3	0.9	1	0.271
4	0.9	1	0.2898
5	0.9	1	0.2987
6	0.9	1	0.3036
7	0.9	1	0.3067
8	0.9	1	0.3086
9	0.9	1	0.31
10	0.9	1	0.3109
11	0.9	1	0.3117
12	0.9	1	0.3122
13	0.9	1	0.3126
14	0.9	1	0.313
15	0.9	1	0.3133
16	0.9	1	0.3135
17	0.9	1	0.3137
18	0.9	1	0.3138
19	0.9	1	0.314
20	0.9	1	0.3141
21	0.9	1	0.3142
22	0.9	1	0.3142
23	0.9	1	0.3143
24	0.9	1	0.3144
25	0.9	1	0.3144

Table 10. Results from ring model (thermal loading)
Normalized stress intensity
factors vs overall volume fractions
of fibers in the infinite demain

$E_m/E_f=3$ $V_{f-ring}=1.0$

Vf (OVERALL)	c/a	Vf (RING)	$\frac{kl(al)}{E_m(\alpha_m-\alpha_f)\Delta T}$
0	0.9	1	0.2214
0.1	0.9	1	0.1211
0.2	0.9	1	0.0316
0.3	0.9	1	-0.0487
0.4	0.9	1	-0.1212
0.5	0.9	1	-0.1869
0.6	0.9	1	-0.2468
0.7	0.9	1	-0.3016
0.8	0.9	1	-0.3519
0.9	0.9	1	-0.3983
1	0.9	1	-0.4412

Table 11. Results from ring model (uniform pressure on crack edges)
Normalized stress intensitys vs volume fractions of fibers in the ring

$E_m/E_f=3$ b/a=2.1 $V_{f\text{-}overall}=0$

Vf (RING)	$\frac{k1(a1)}{p\sqrt{c}}$					
	c/a=0.1	c/a=0.3	c/a=0.5	c/a=0.7	c/a=0.8	c/a=0.9
0.1	1.0004	1.0031	1.0076	1.013	1.0165	1.022
0.2	1.0008	1.0065	1.0158	1.0272	1.0346	1.0462
0.3	1.0012	1.0102	1.0248	1.0428	1.0545	1.0729
0.4	1.0017	1.0142	1.0346	1.0601	1.0767	1.1028
0.5	1.0022	1.0186	1.0456	1.0793	1.1015	1.1366
0.6	1.0028	1.0235	1.0578	1.1011	1.1296	1.1751
0.7	1.0035	1.029	1.0716	1.126	1.162	1.2197
0.8	1.0042	1.0352	1.0875	1.1548	1.1998	1.2722
0.9	1.005	1.0423	1.1059	1.189	1.2448	1.3355
1	1.006	1.0506	1.1278	1.2304	1.3001	1.4141

Table 12. Results from ring model (constant pressure on crack edges) Normalized stress intensity factors vs volume fractions of fibers in the ring for various crack lengths

$E_m/E_f=0.3$ b/a=2.1 $V_{f\text{-overall}}=0$

Vf (RING)	$\frac{k1(a1)}{p\sqrt{c}}$					
	c/a=0.1	c/a=0.3	c/a=0.5	c/a=0.7	c/a=0.8	c/a=0.9
0.1	0.999	0.9918	0.9804	0.9666	0.9578	0.9444
0.2	0.9982	0.985	0.9643	0.9396	0.9239	0.9002
0.3	0.9975	0.9793	0.9508	0.9169	0.8957	0.8639
0.4	0.9968	0.9742	0.9391	0.8976	0.8718	0.8334
0.5	0.9963	0.9698	0.9288	0.8809	0.8512	0.8075
0.6	0.9958	0.9659	0.9198	0.8662	0.8332	0.785
0.7	0.9953	0.9623	0.9117	0.8532	0.8173	0.7653
0.8	0.9949	0.9591	0.9044	0.8415	0.8032	0.7478
0.9	0.9946	0.9562	0.8978	0.831	0.7905	0.7323
1	0.9942	0.9535	0.8917	0.8214	0.779	0.7183

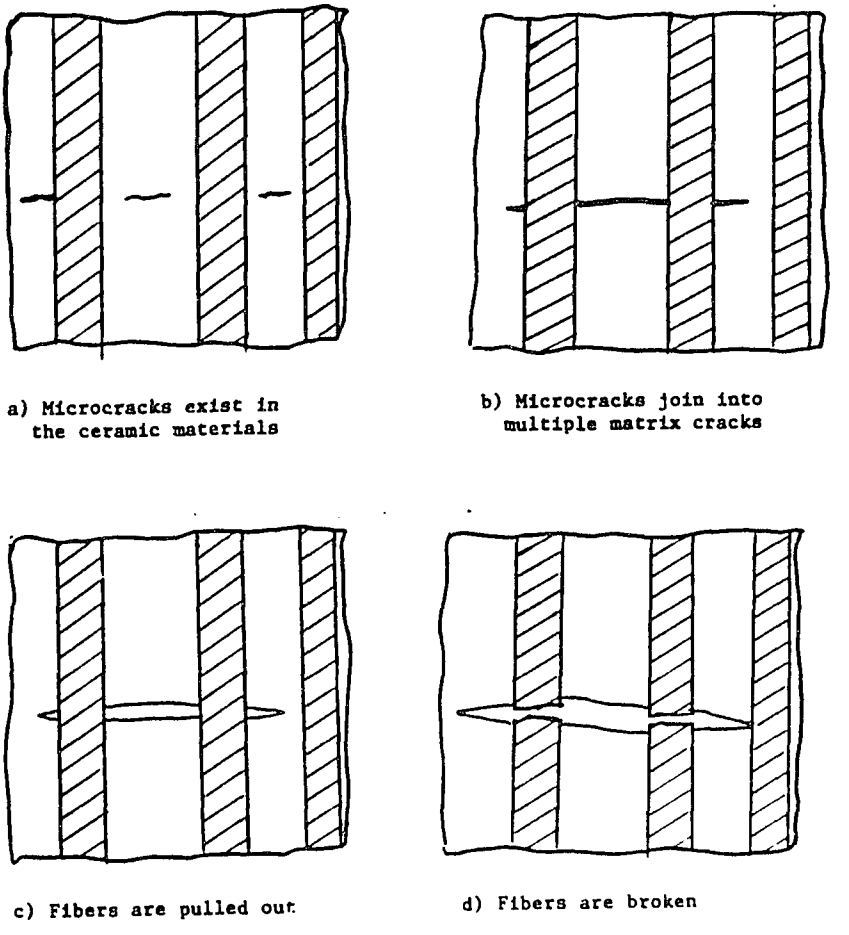

Fig. 1 Failure process of ceramic-fiber/ceramic-matrix composite materials

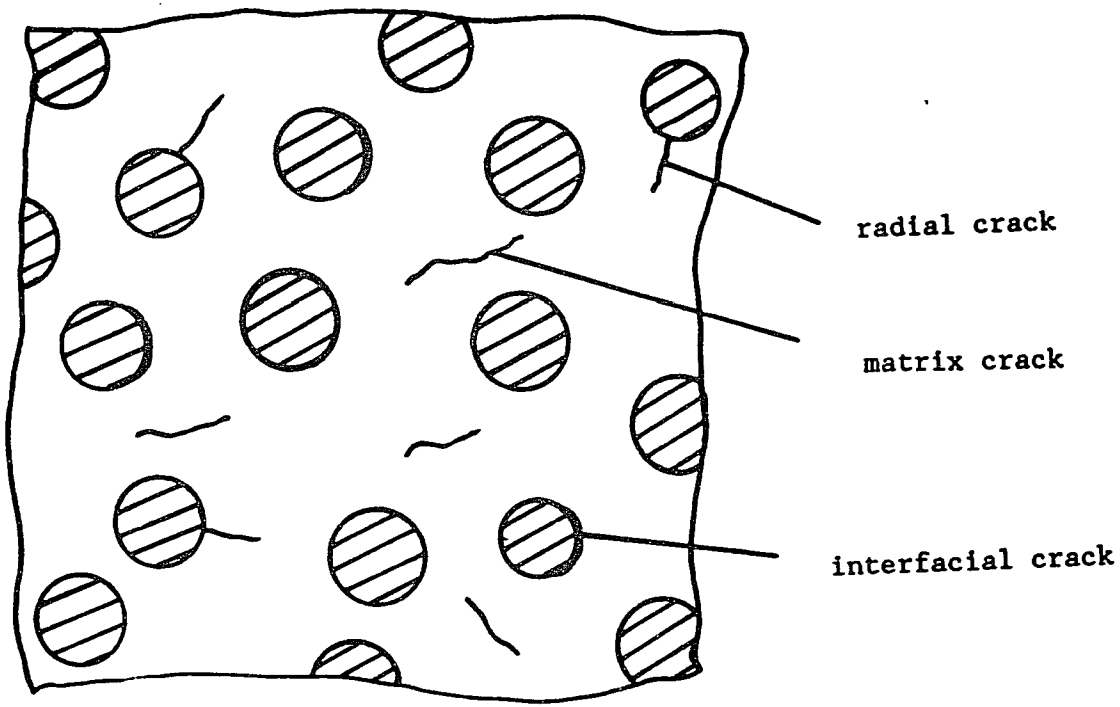

Fig.2 Cracks in composites

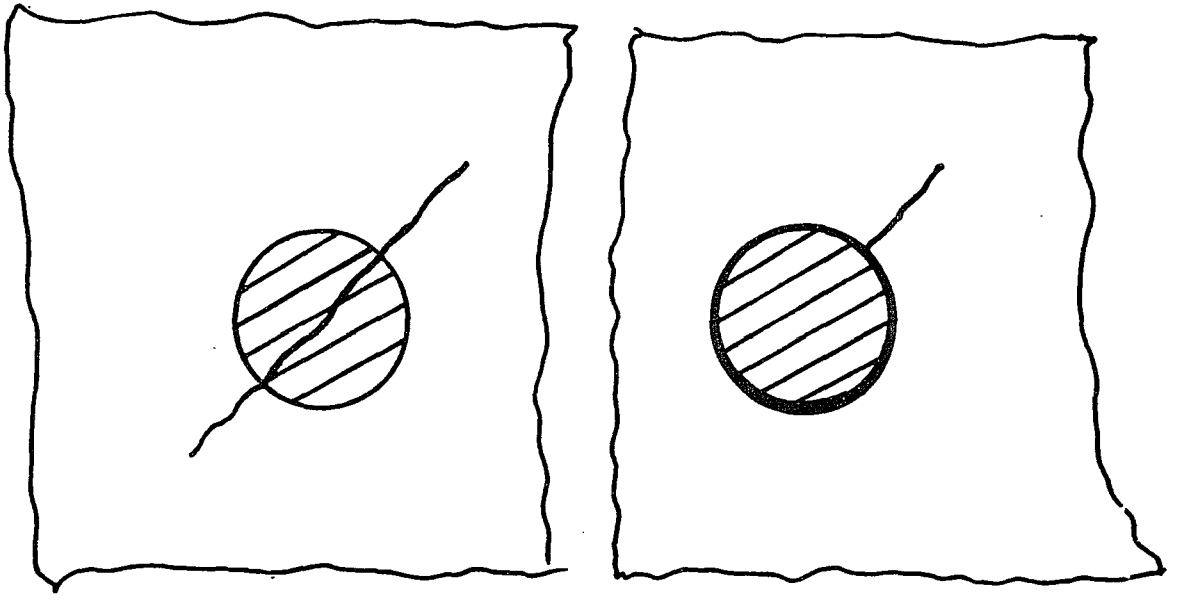

a) when bonding is strong crack propagates through fiber and propagates ahead

b) when bonding is not very strong crack is deflected and stops there

Fig. 3 Crack deflection

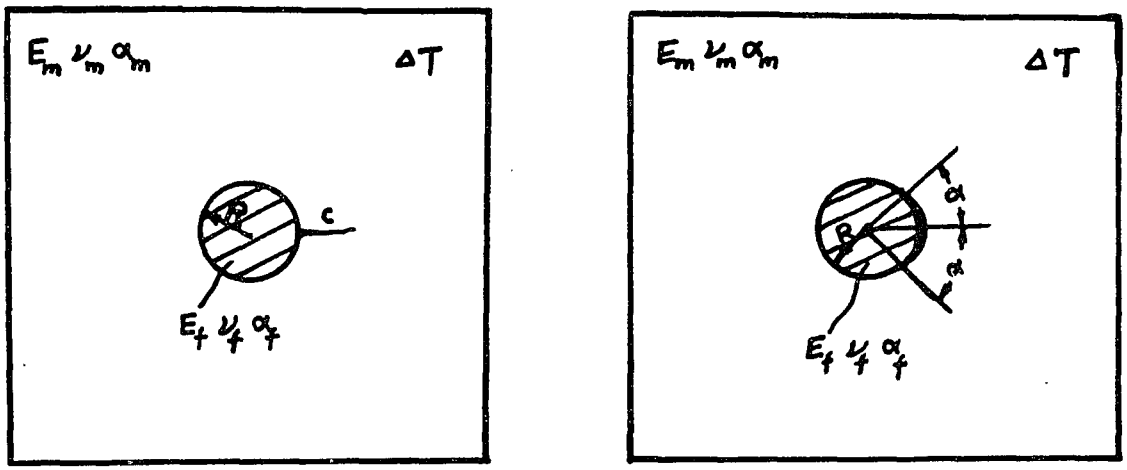

a) radial crack

b) interfacial crack

Fig. 4 Delale's solution to microcracking due to residual stresses

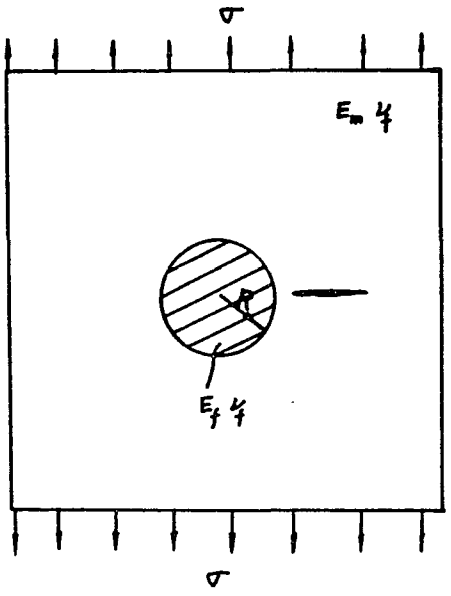

Fig. 5 C.Atkinson's solution to inclusion-radial crack problem

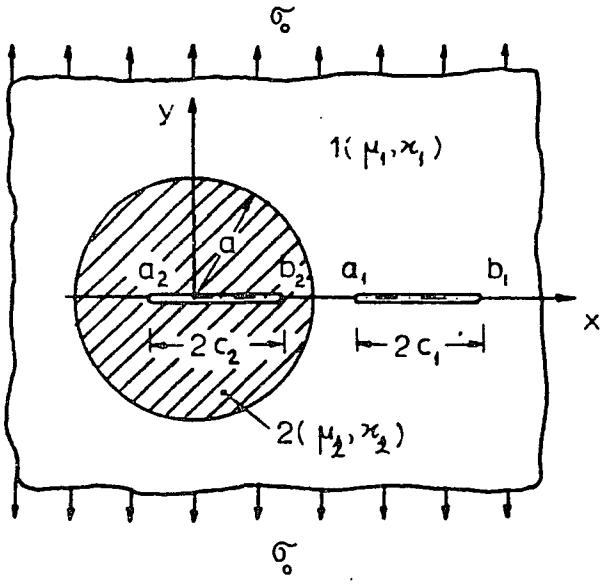

Fig. 6 Erdogen and G.D.Gupta's solution to inclusion-radial crack problem

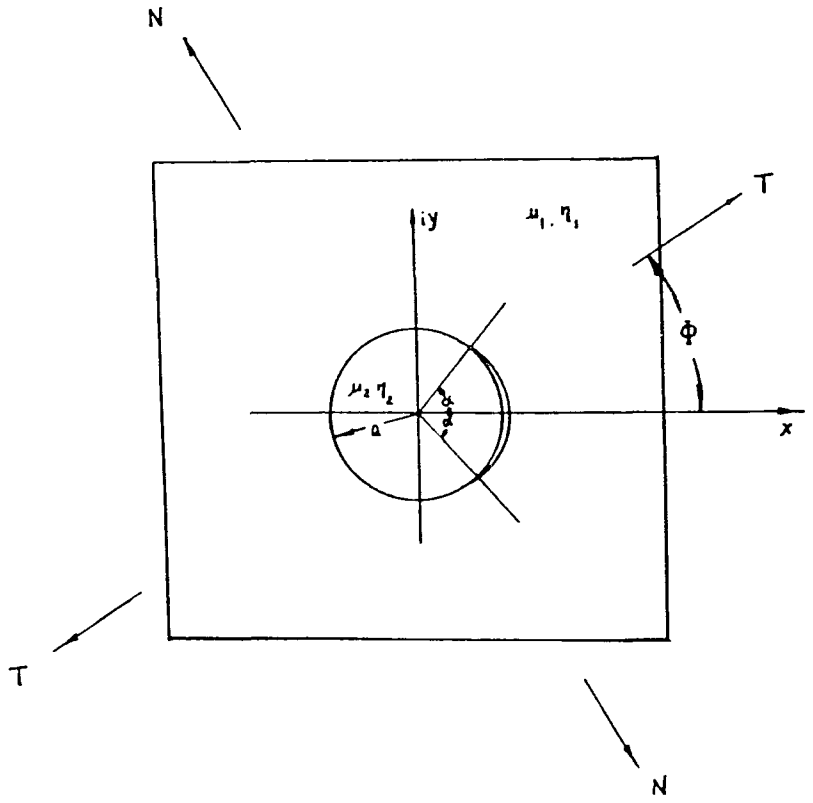

Fig. 7 M.Toya's solution to inclution-interfacial crack problem

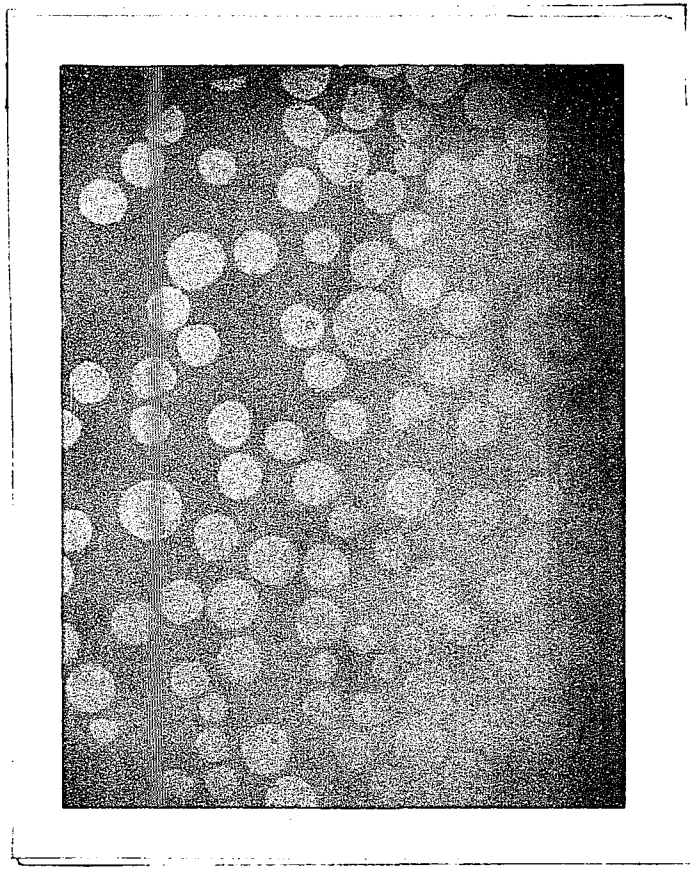

Fig. 8 Fiber distribution in ceramic composites

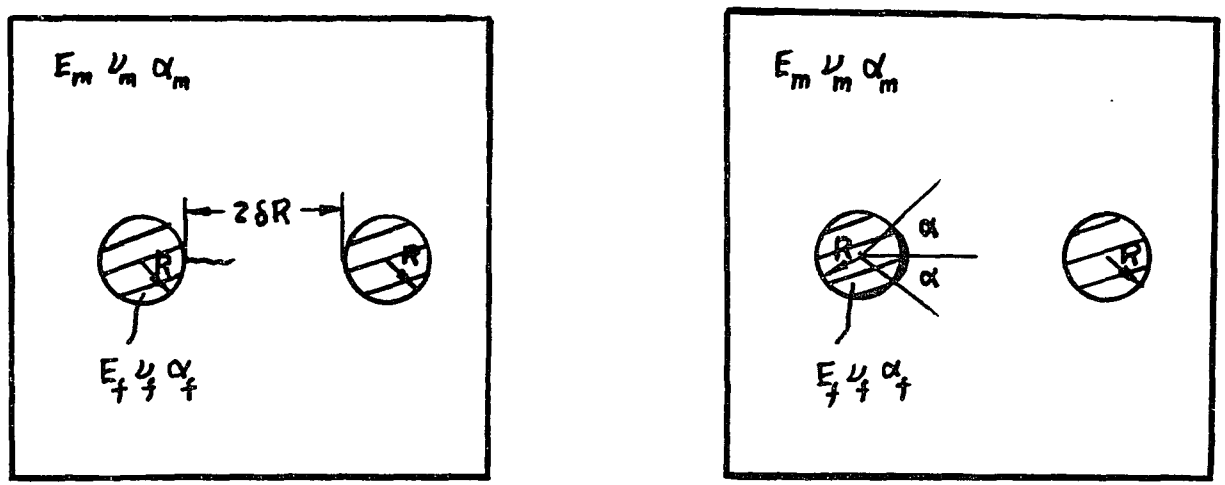

(a) Radial crack in matrix

(b) Interfacial crack

Fig. 9 Two-fiber model

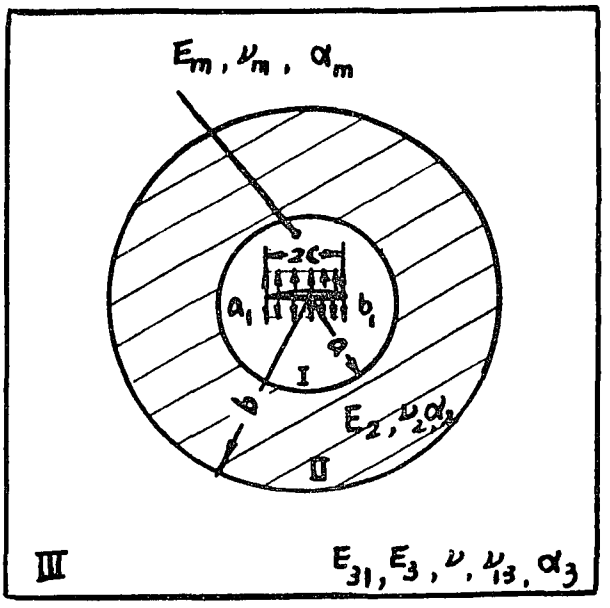

Fig. 10a Ring model

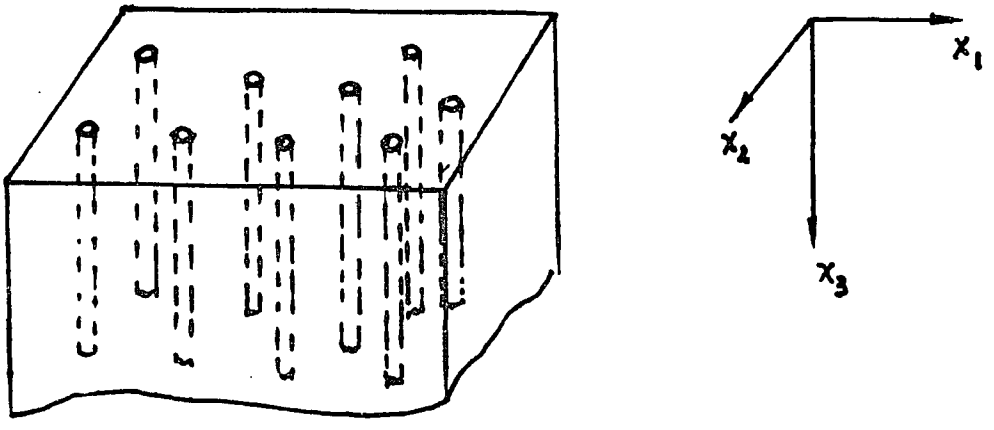

10b) Coordinate system for calculation of elastic parameters

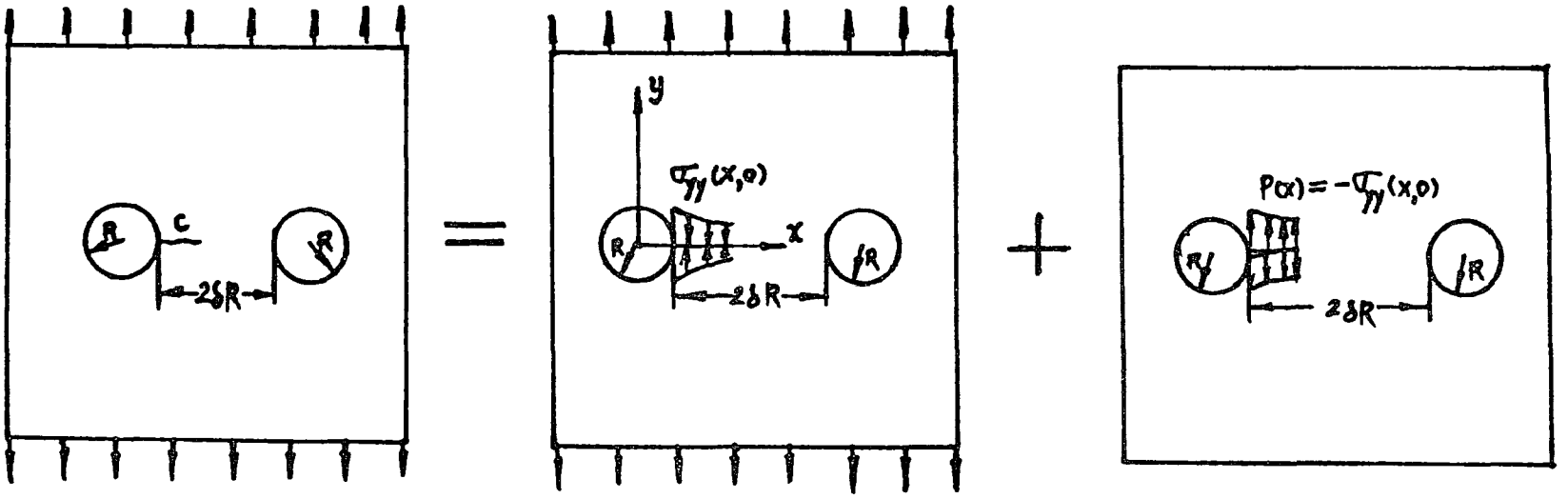

a) Original problem

b) corresponding uncracked problem

c) Translated crack problem

Fig.11 Superposition of the crack problem

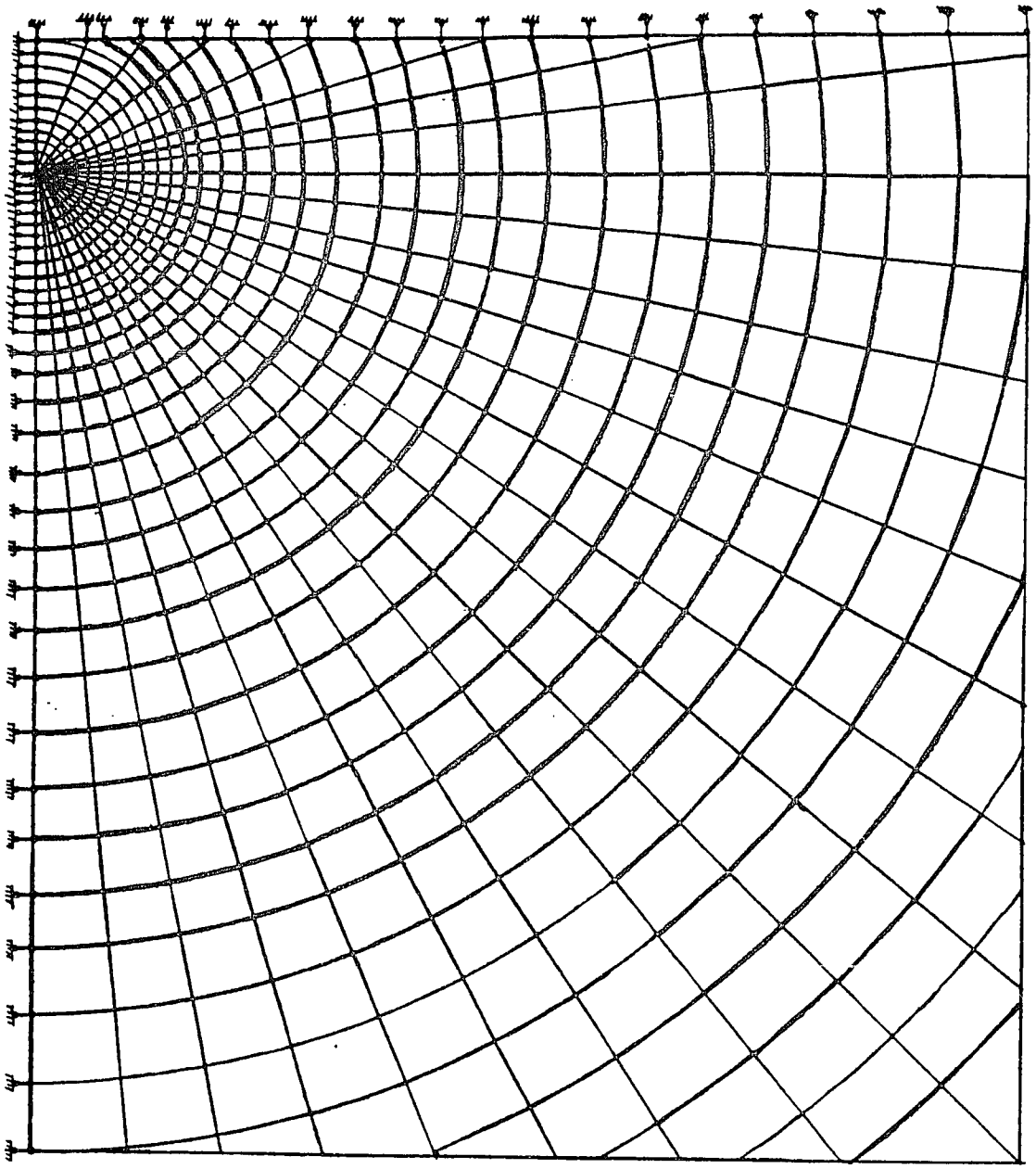

Fig. 12 Finite element model for two fiber case

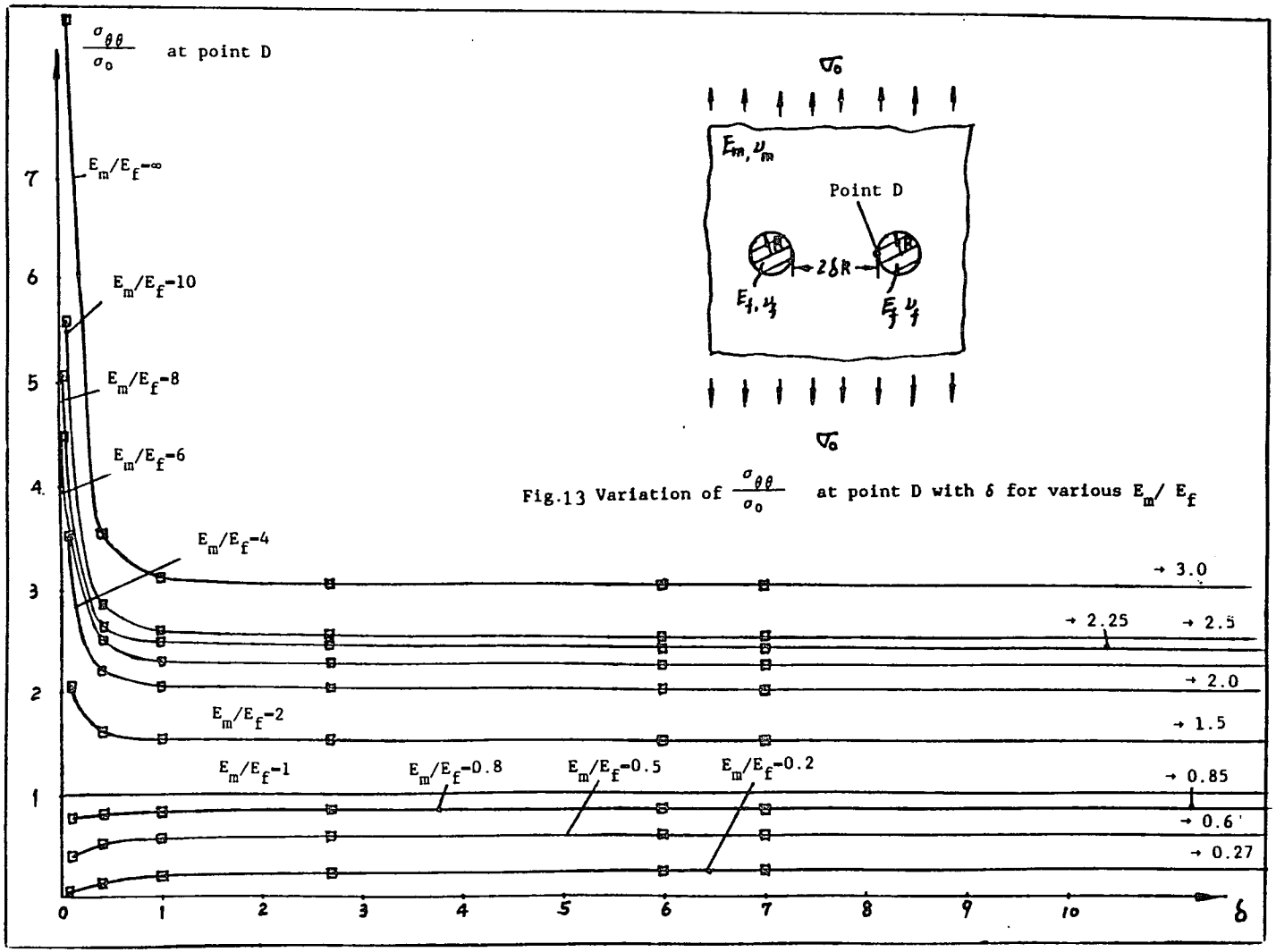

Fig.13 Variation of $\frac{\sigma_{\theta\theta}}{\sigma_0}$ at point D with δ for various E_m/E_f

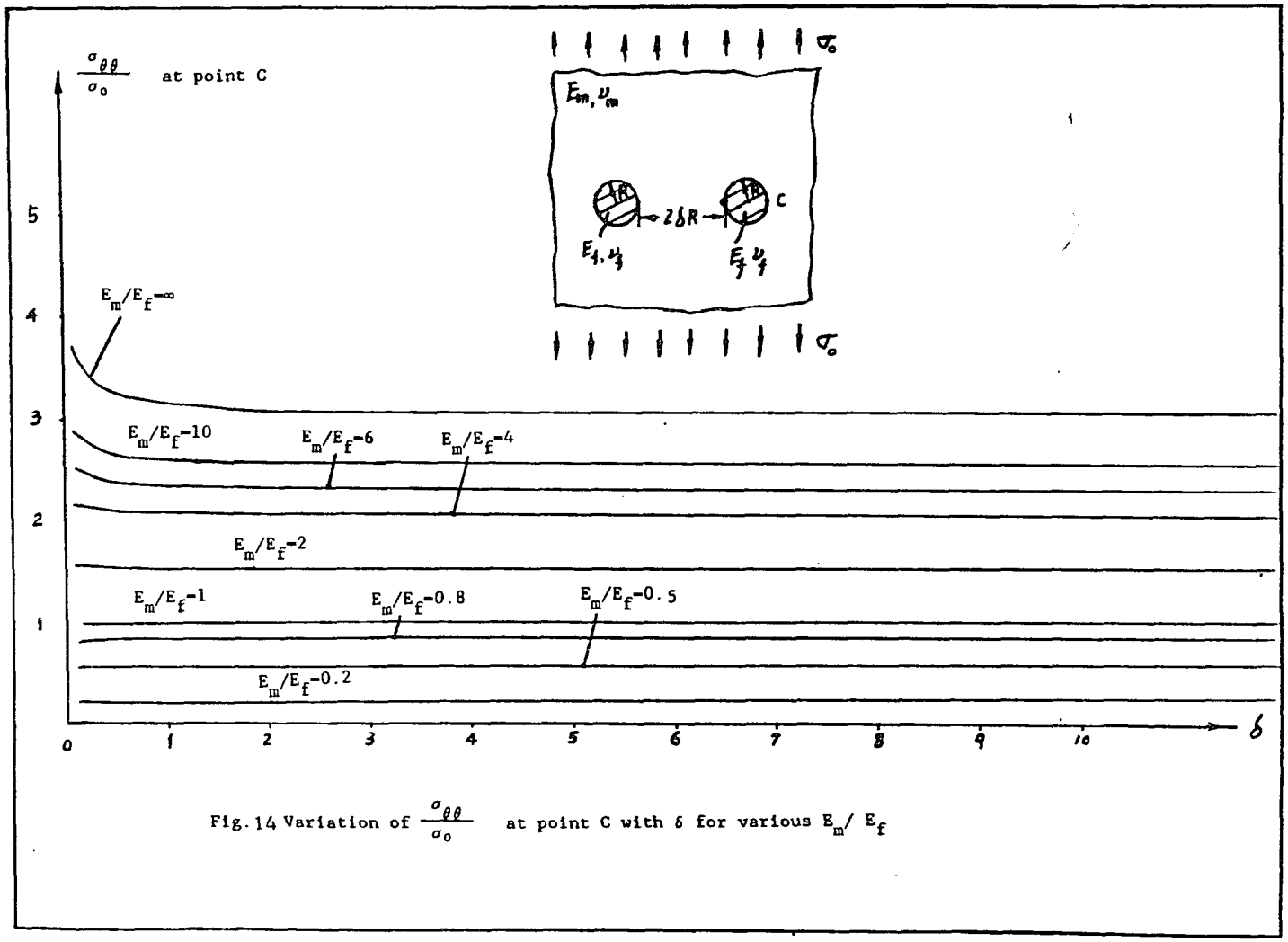

Fig. 14 Variation of $\frac{\sigma_{\theta\theta}}{\sigma_0}$ at point C with δ for various E_m/E_f

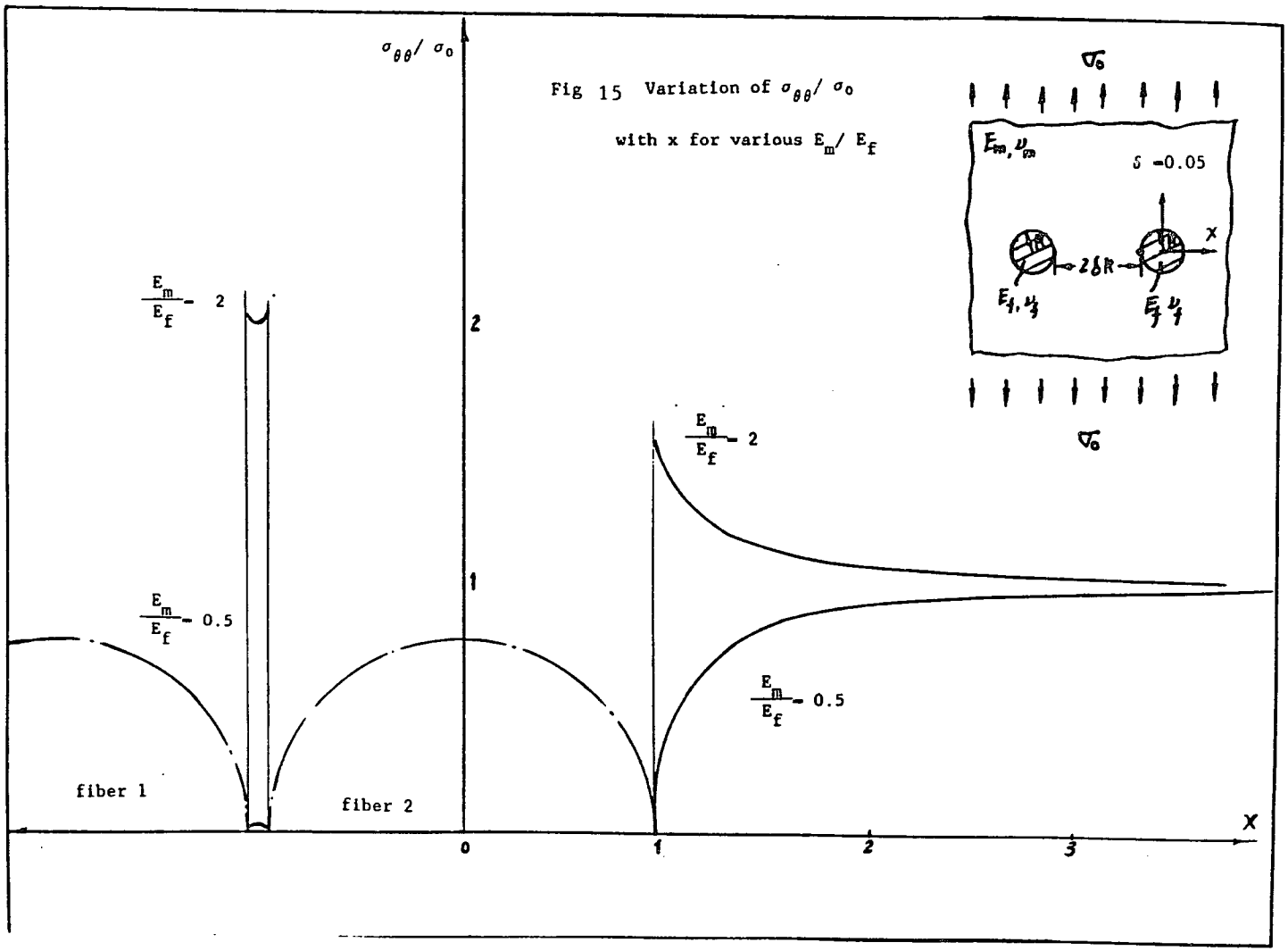

Fig 15 Variation of $\sigma_{\theta\theta}/\sigma_0$ with x for various E_m/E_f

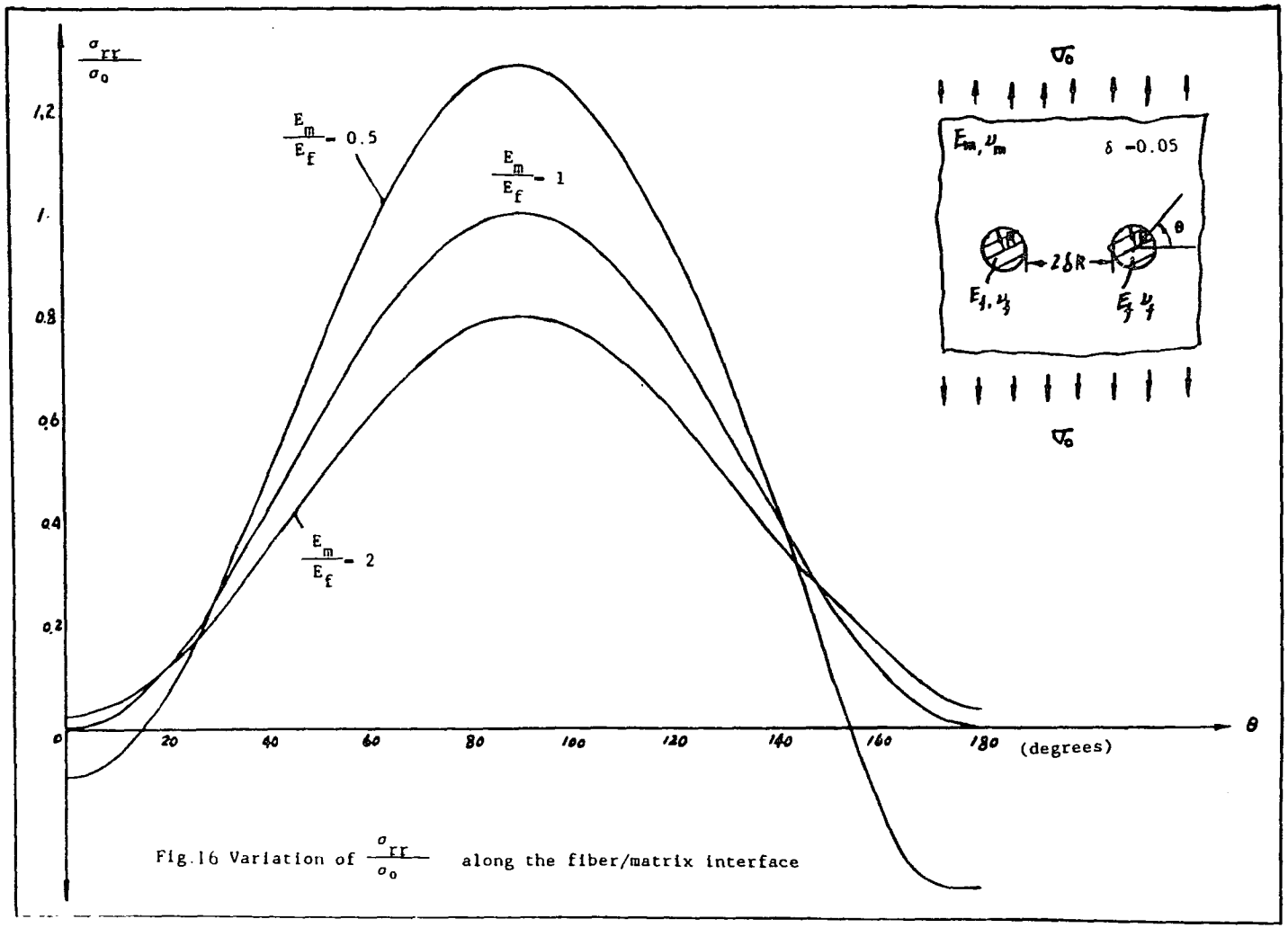

Fig.16 Variation of $\frac{\sigma_{rr}}{\sigma_0}$ along the fiber/matrix interface

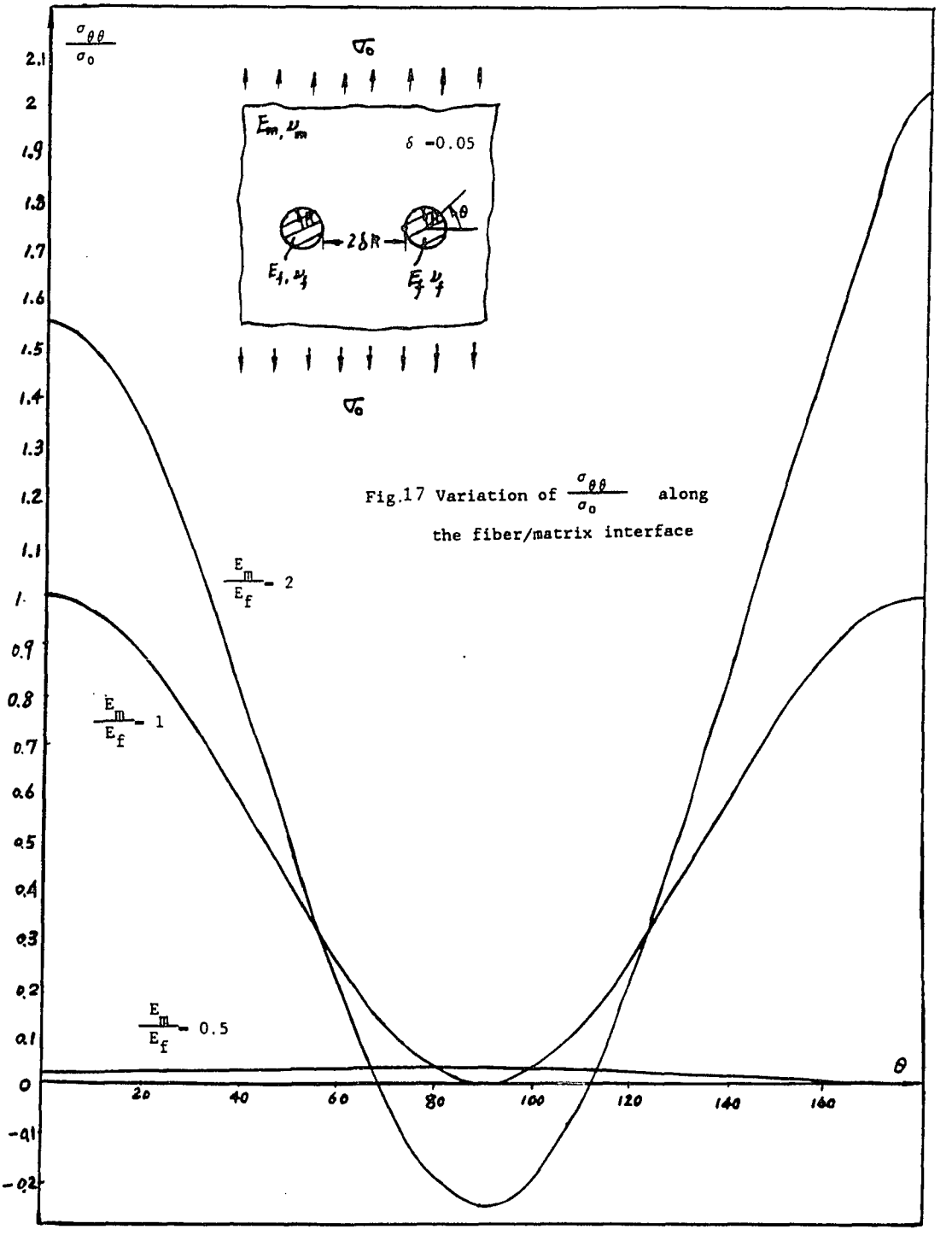

Fig.17 Variation of $\frac{\sigma_{\theta\theta}}{\sigma_0}$ along the fiber/matrix interface

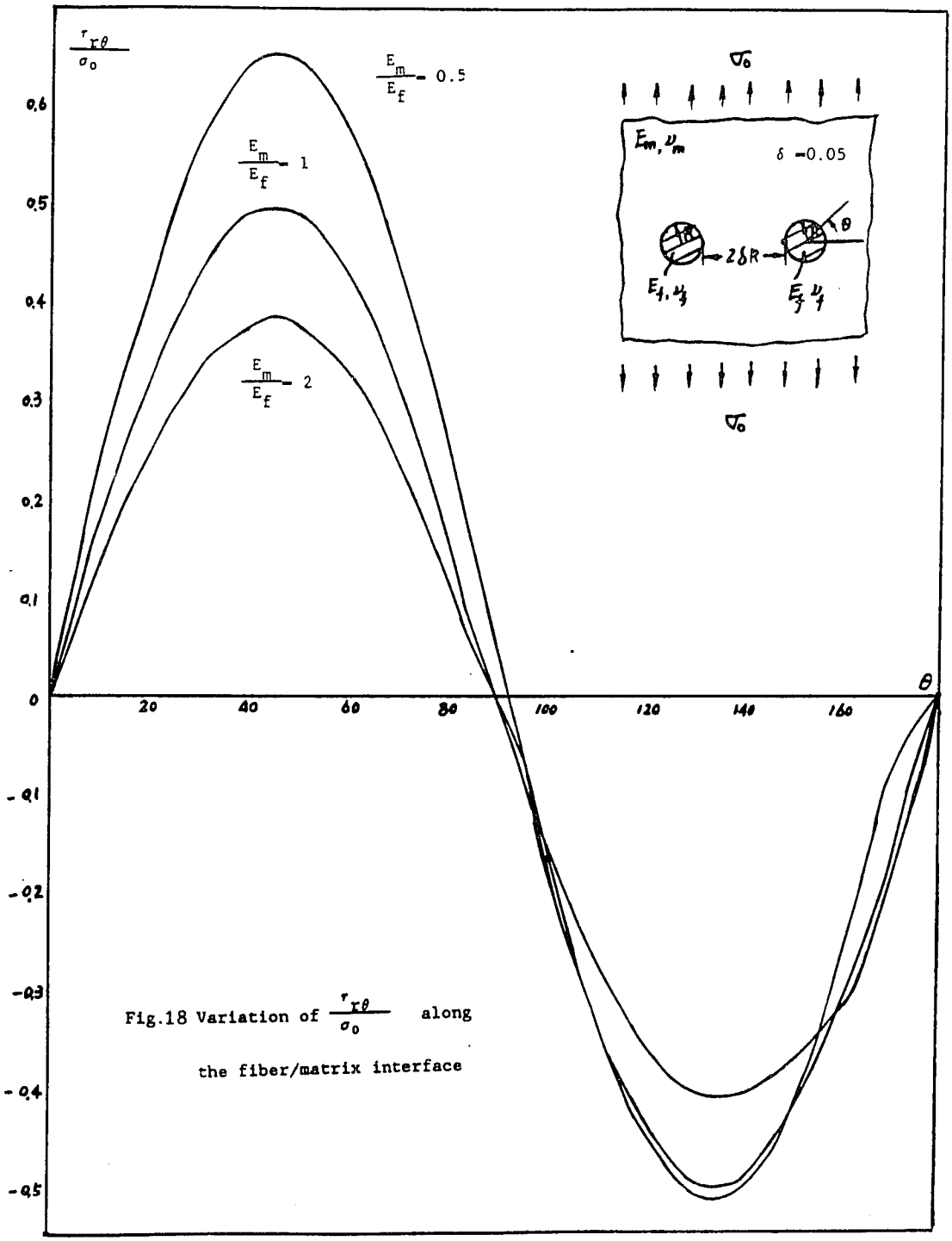

Fig.18 Variation of $\frac{\tau_{r\theta}}{\sigma_0}$ along the fiber/matrix interface

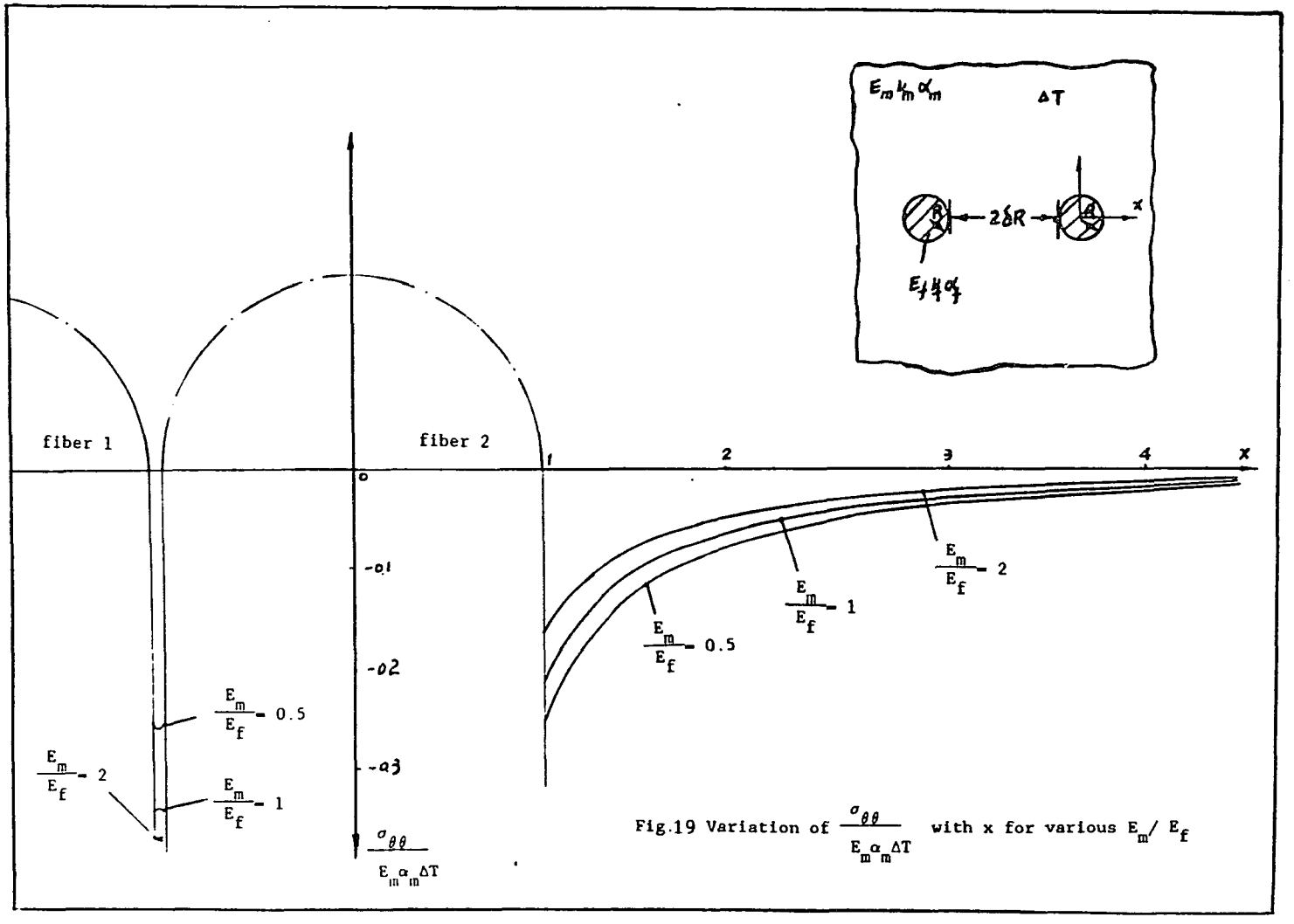

Fig.19 Variation of $\frac{\sigma_{\theta\theta}}{E_m \alpha_m \Delta T}$ with x for various E_m / E_f

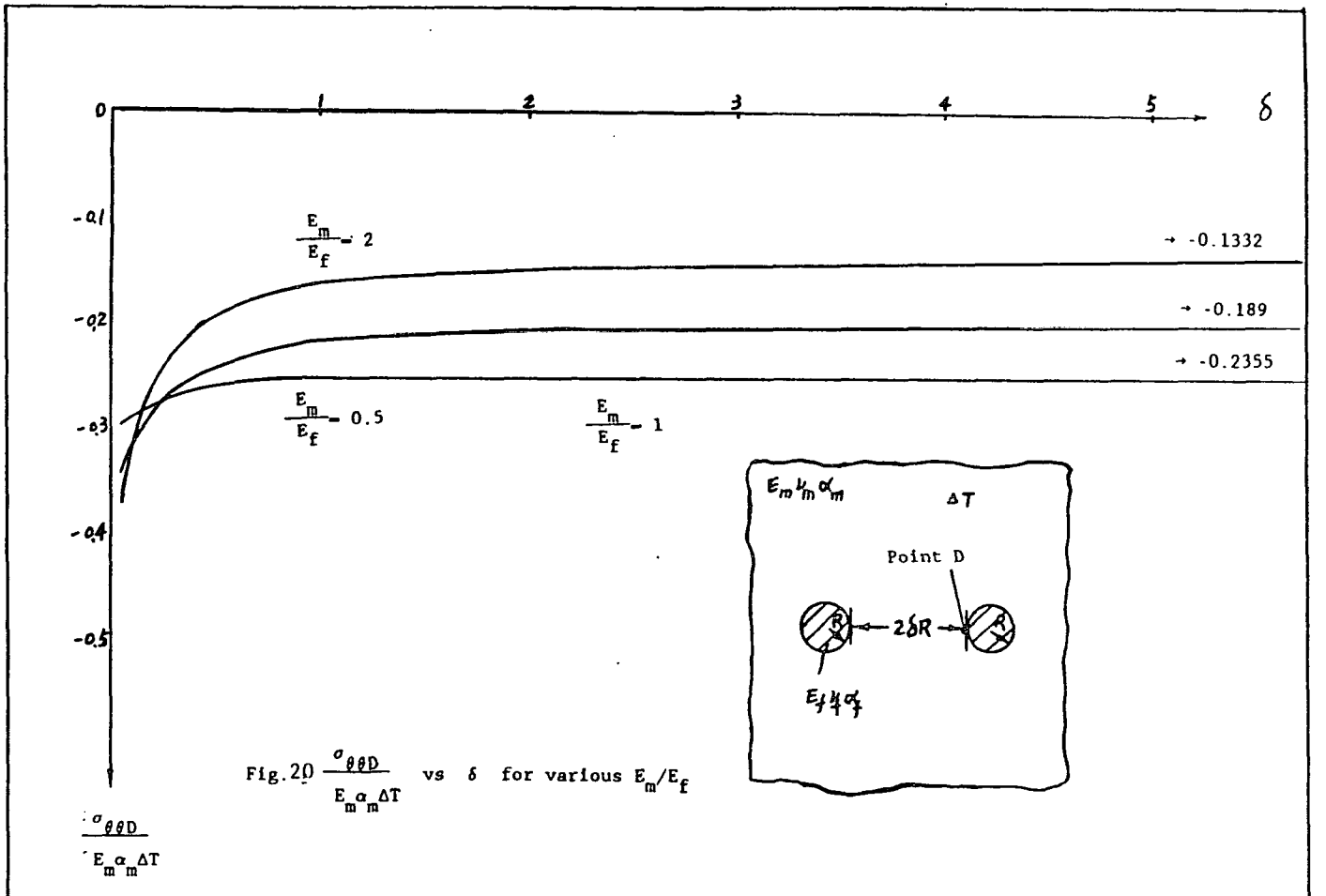

Fig. 20 $\frac{\sigma_{\theta\theta D}}{E_m \alpha_m \Delta T}$ vs δ for various E_m/E_f

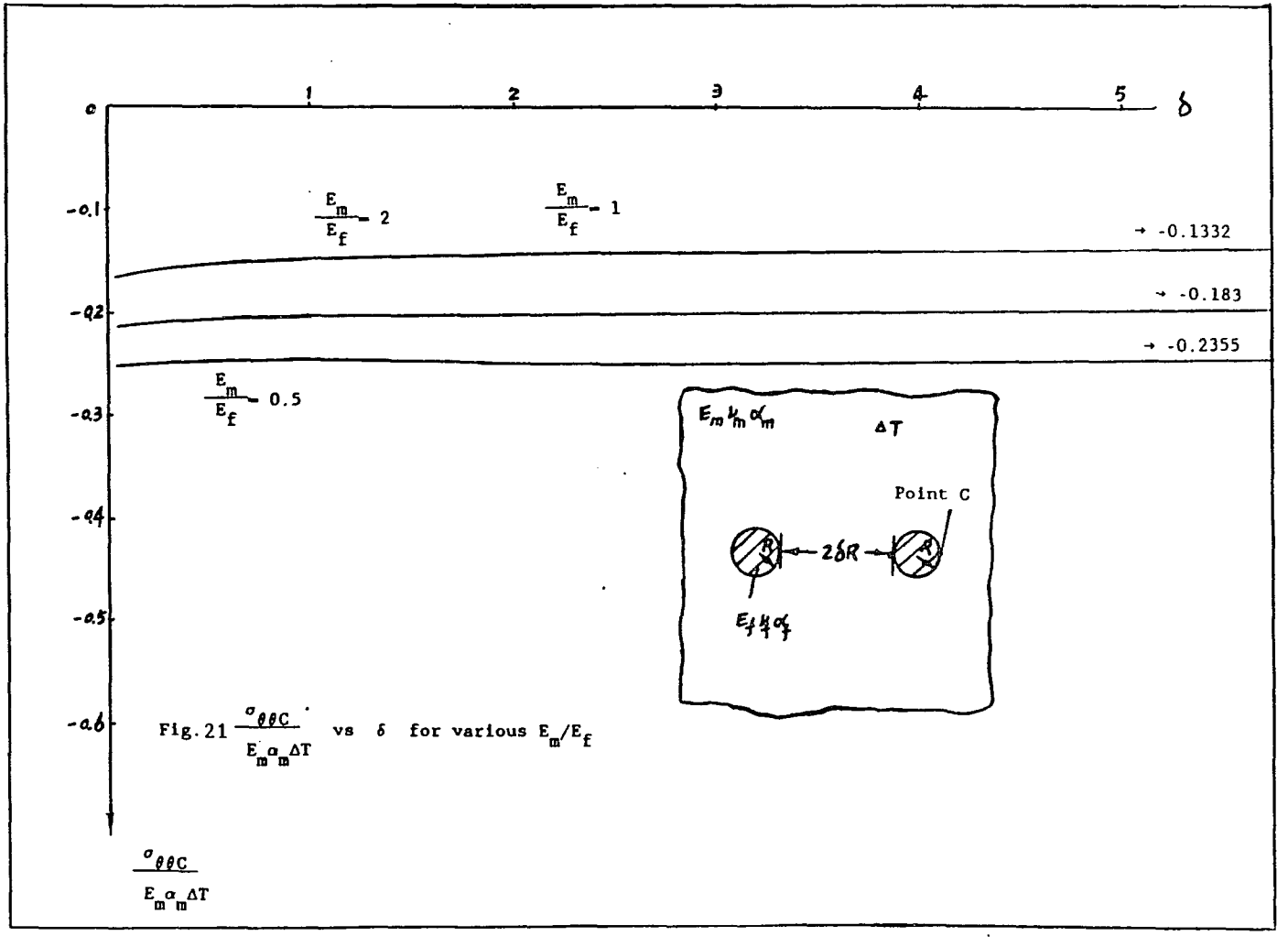

Fig. 21 $\frac{\sigma_{\theta\theta C}}{E_m \alpha_m \Delta T}$ vs δ for various E_m/E_f

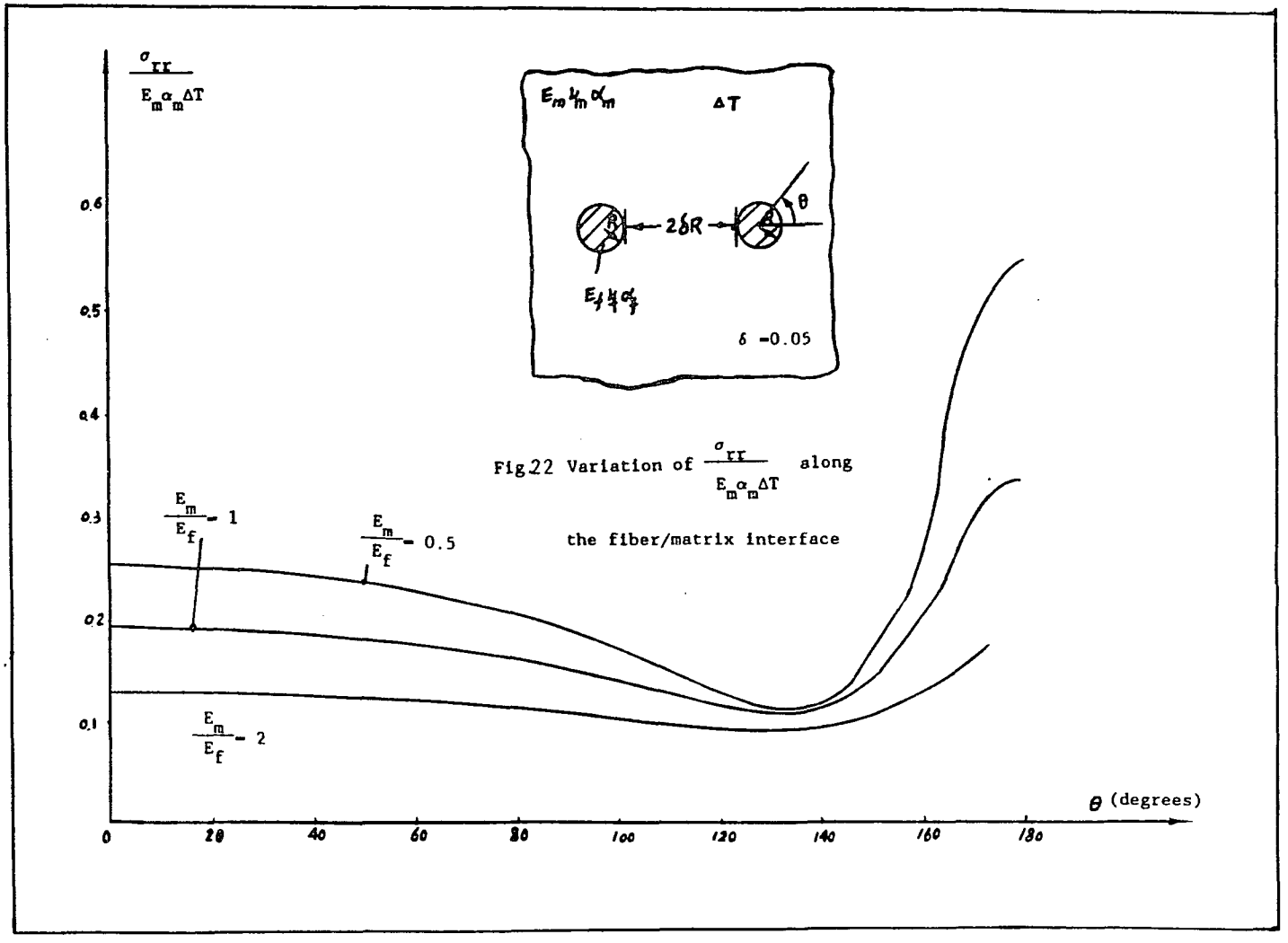

Fig.22 Variation of $\frac{\sigma_{rr}}{E_m \alpha_m \Delta T}$ along the fiber/matrix interface

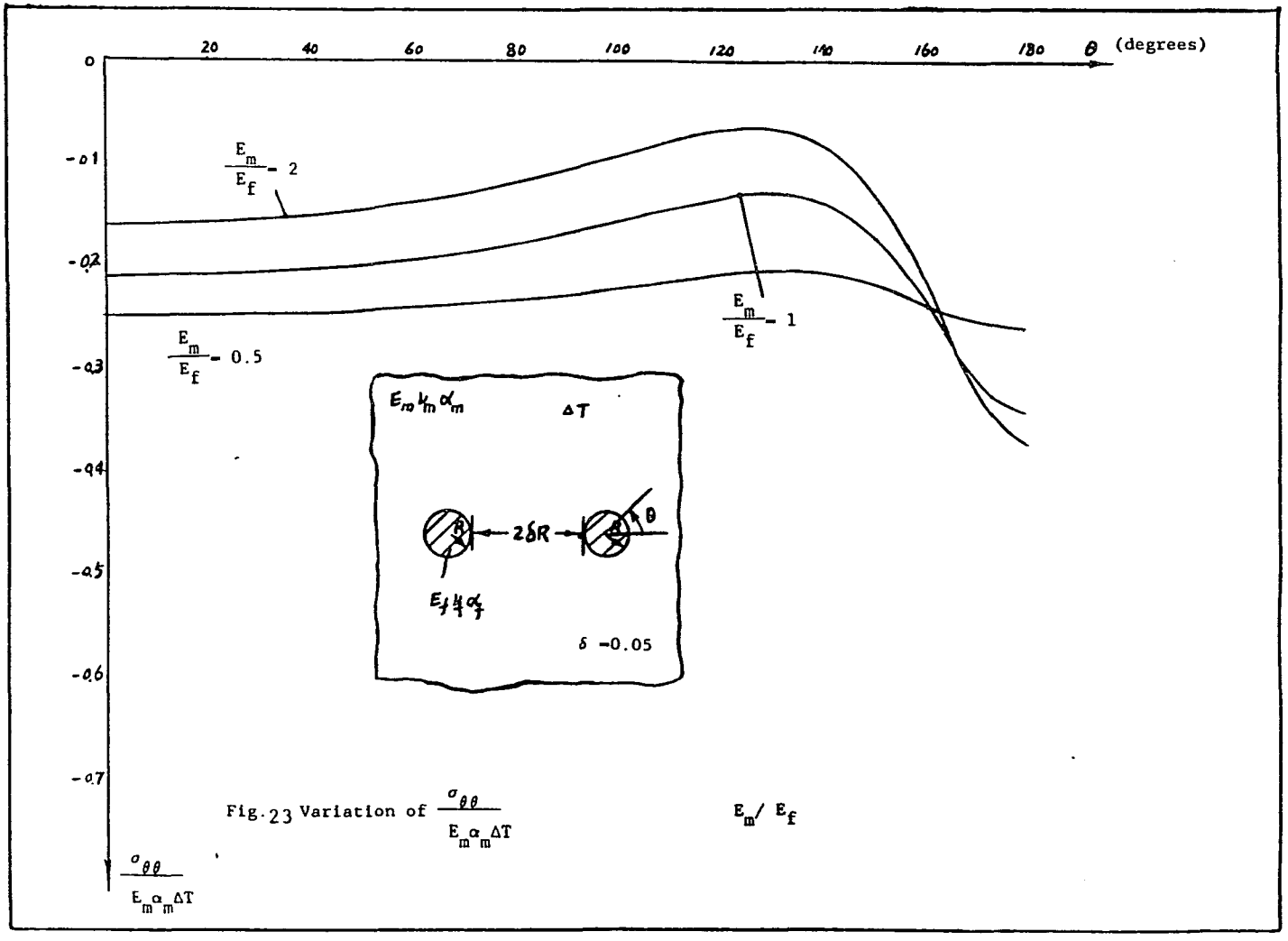

Fig.23 Variation of $\frac{\sigma_{\theta\theta}}{E_m \alpha_m \Delta T}$ E_m / E_f

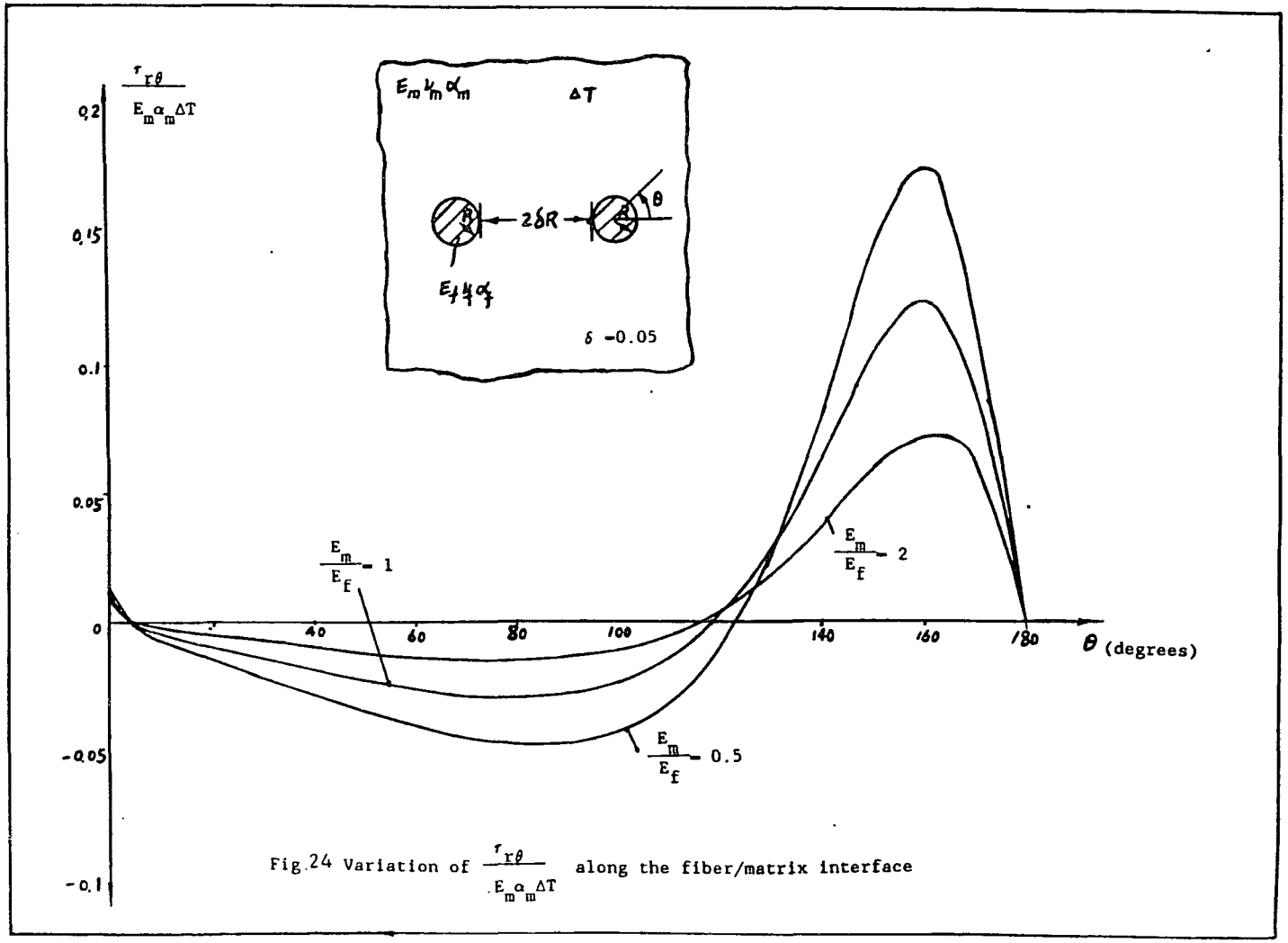

Fig.24 Variation of $\frac{\tau_{r\theta}}{E_m \alpha_m \Delta T}$ along the fiber/matrix interface

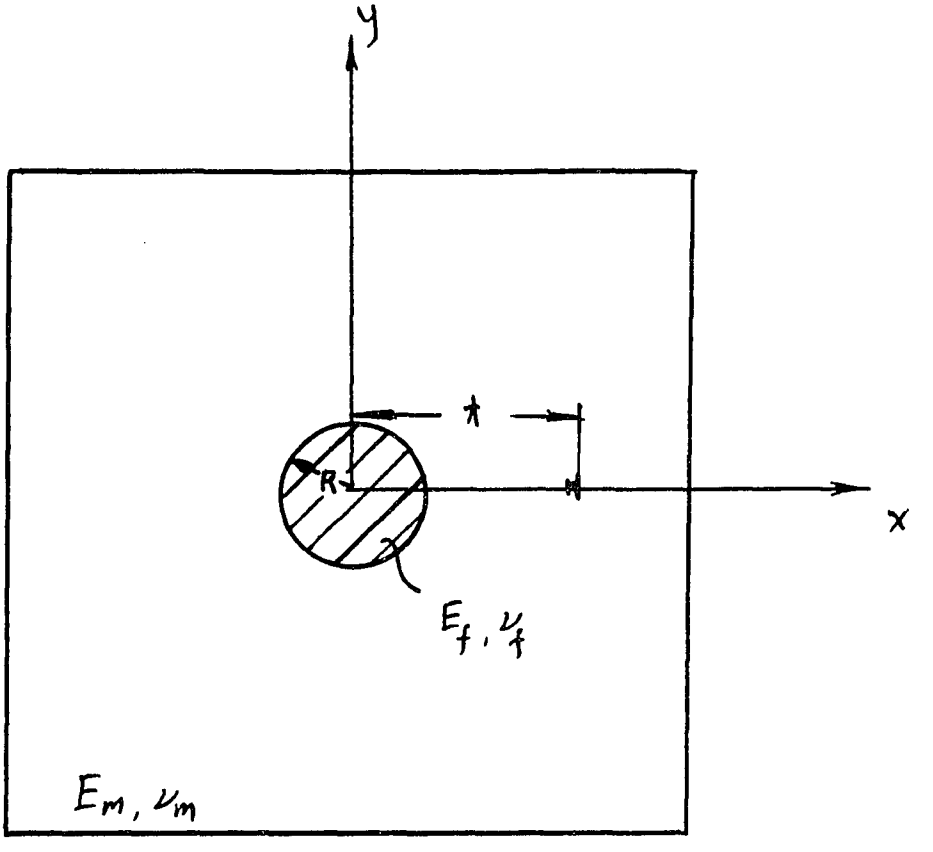

Fig.25 Dundurs and Mura's dislocation solution

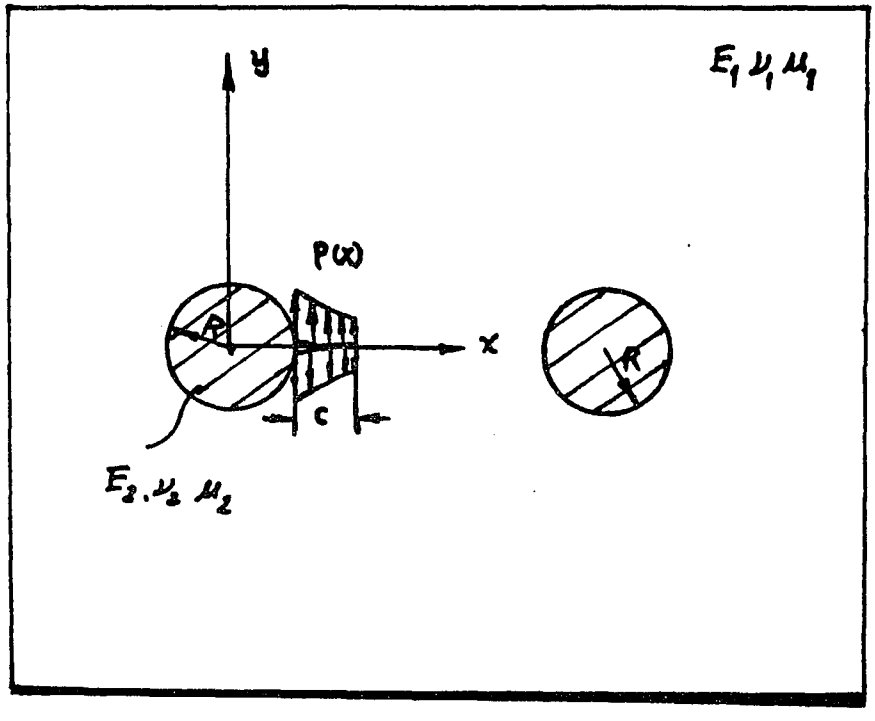

Fig26 Singular integral equation approach for radial crack case

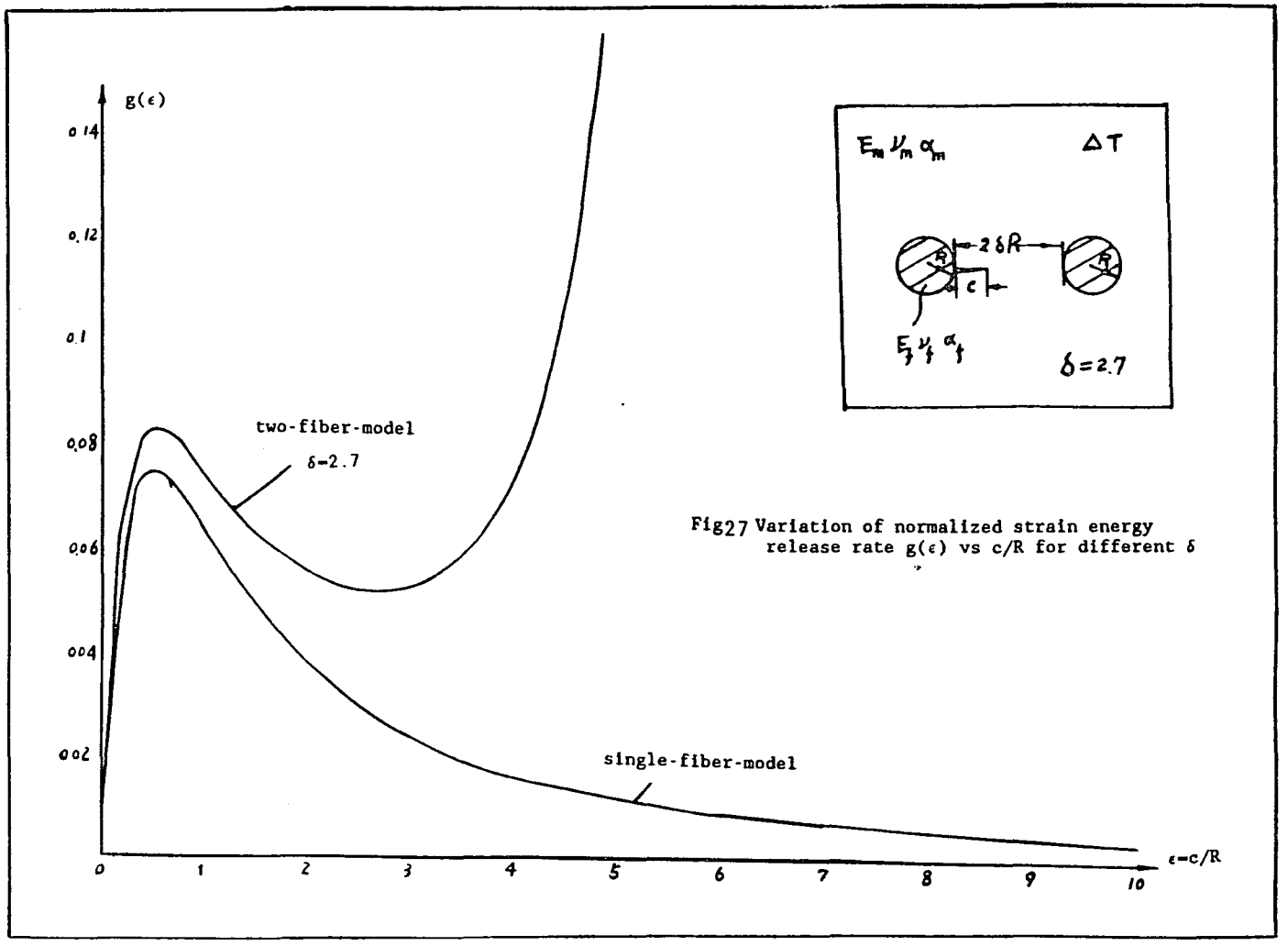

Fig27 Variation of normalized strain energy release rate $g(\epsilon)$ vs c/R for different δ

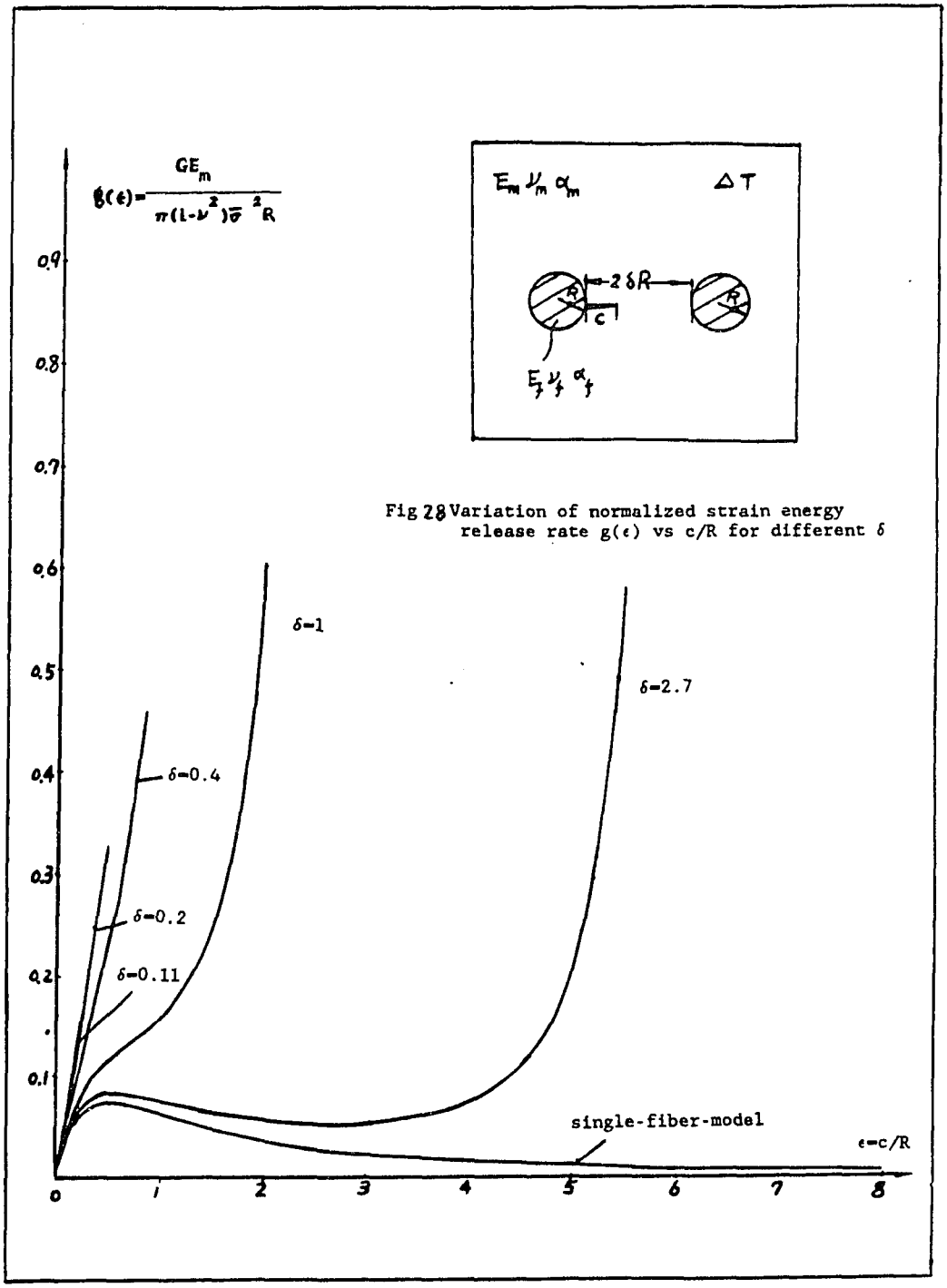

Fig 28 Variation of normalized strain energy release rate $g(\epsilon)$ vs c/R for different δ

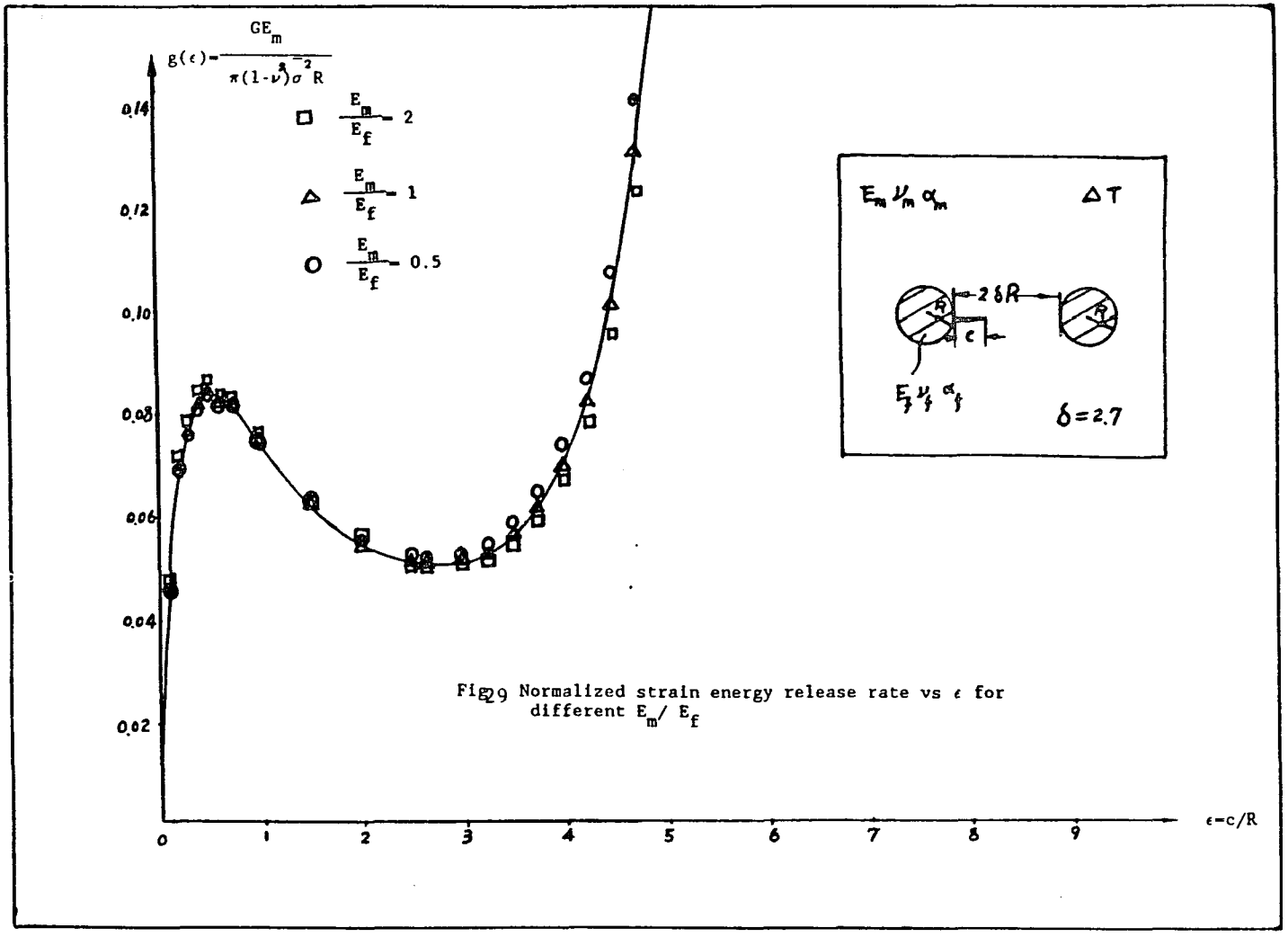

Fig 29 Normalized strain energy release rate vs ϵ for different E_m/E_f

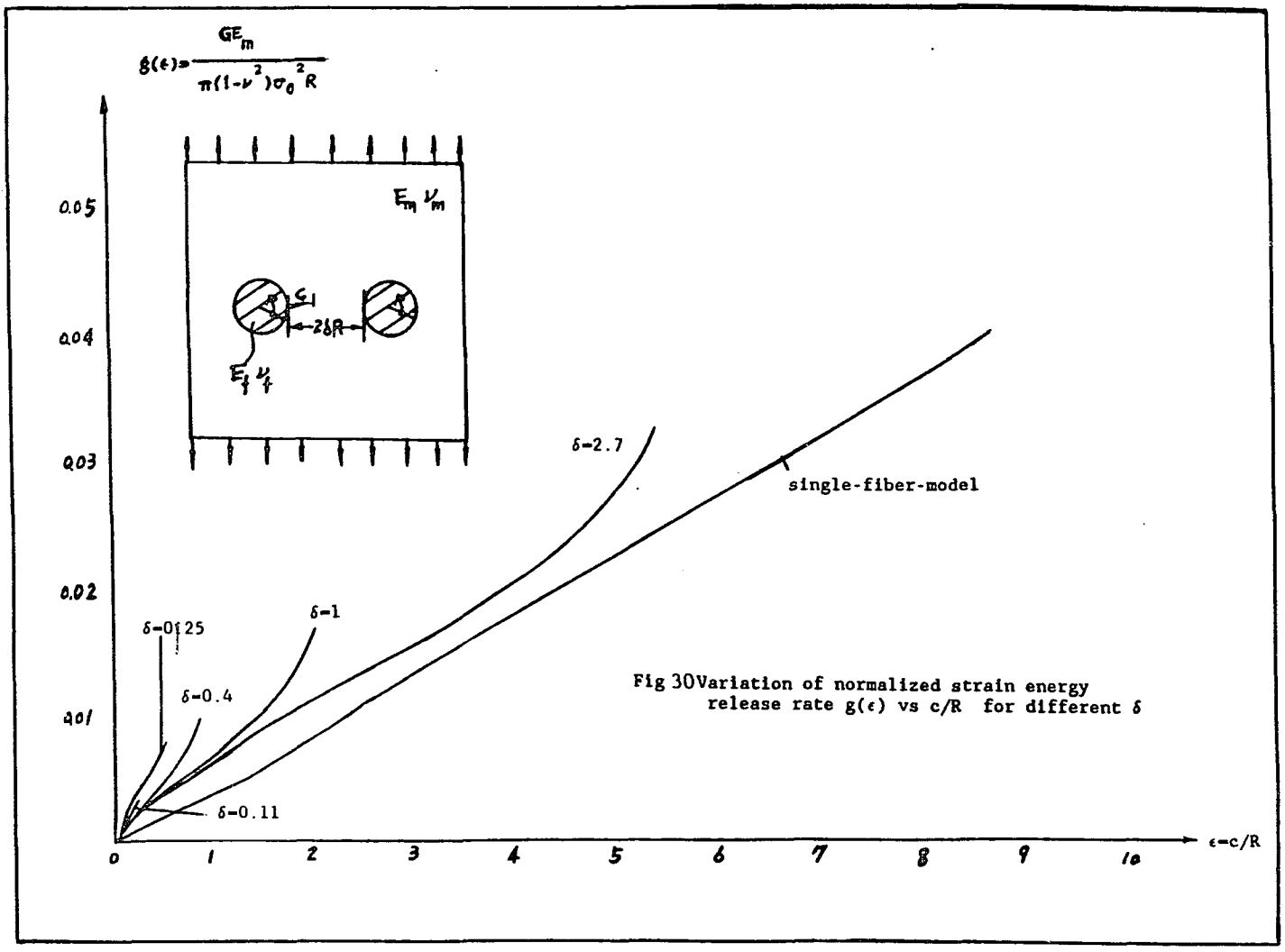

Fig 30 Variation of normalized strain energy release rate $g(\epsilon)$ vs c/R for different δ

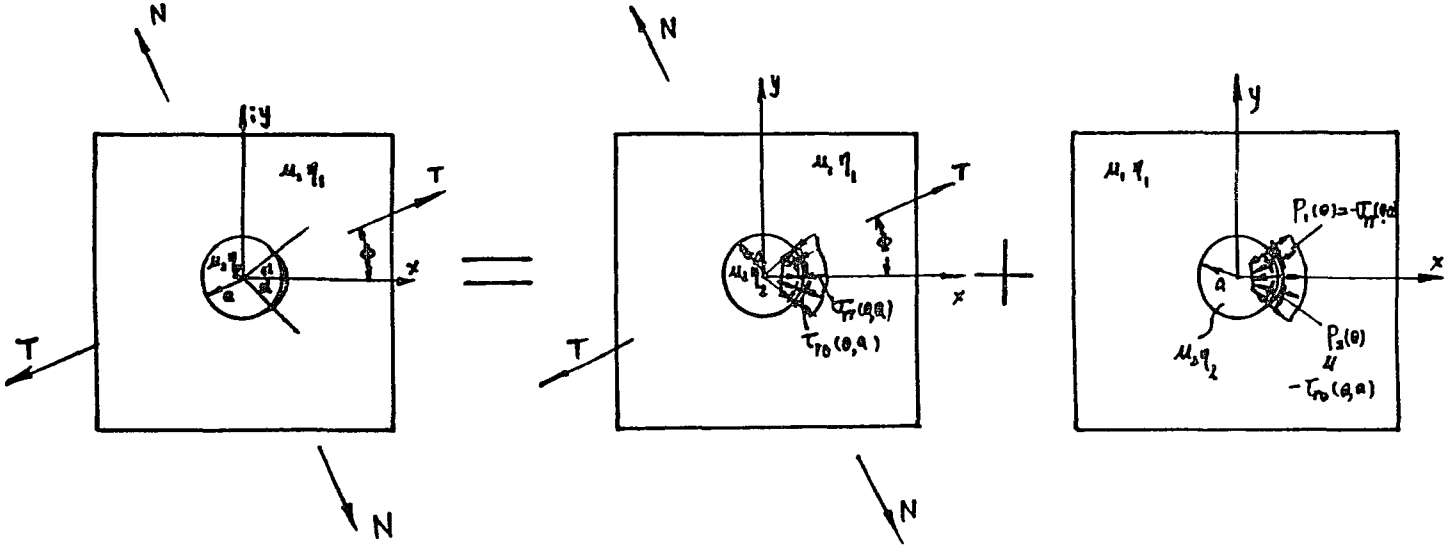

a) Original problem

b) uncracked Toya's problem

c) Translated Toya's problem

Fig.31 Decomposition of Toya's solution

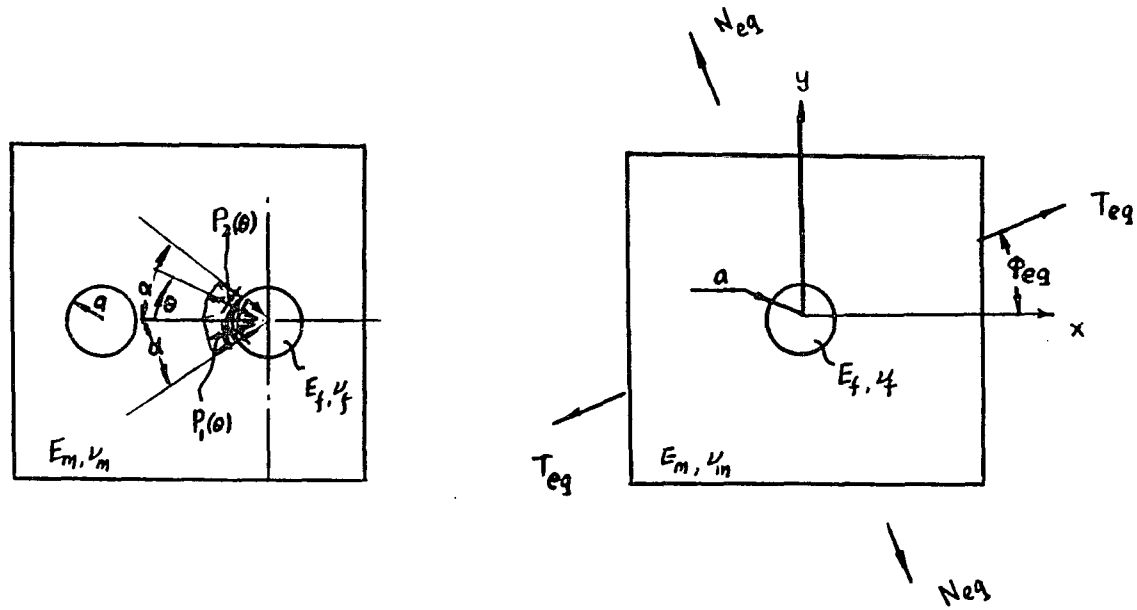

Fig.32 using least square method find

T_{eq}, N_{eq}

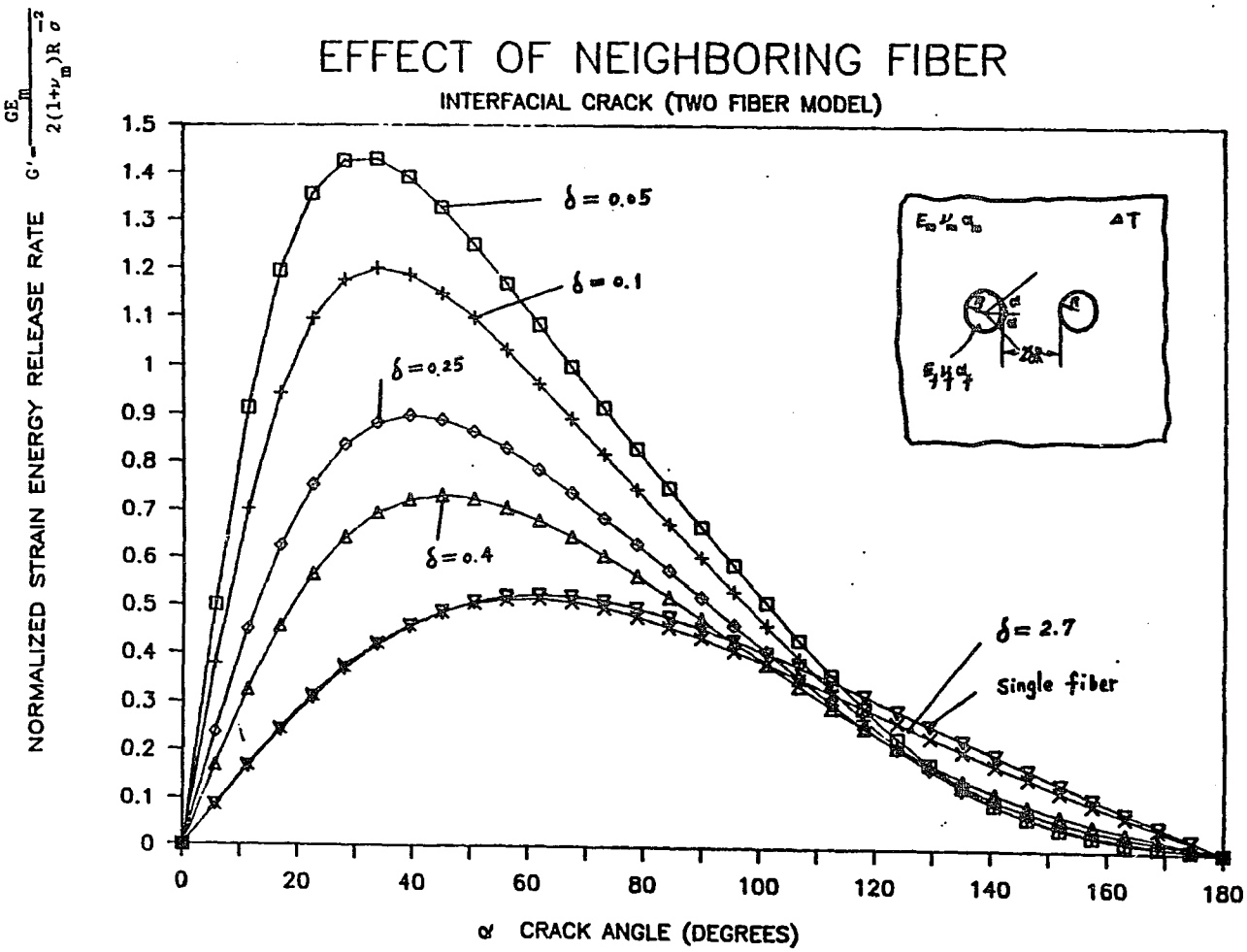
EFFECT OF NEIGHBORING FIBER
INTERFACIAL CRACK (TWO FIBER MODEL)
NORMALIZED STRAIN ENERGY RELEASE RATE $G' = \frac{GE_m}{2(1+\nu_m)R\sigma^2}$
δ = 0.5
δ = 0.1
δ = 0.25
δ = 0.4
δ = 2.7
Single fiber
ΔT
α CRACK ANGLE (DEGREES)
0
0.1
0.2
0.3
0.4
0.5
0.6
0.7
0.8
0.9
1
1.1
1.2
1.3
1.4
1.5
0
20
40
60
80
100
120
140
160
180

Fig.33

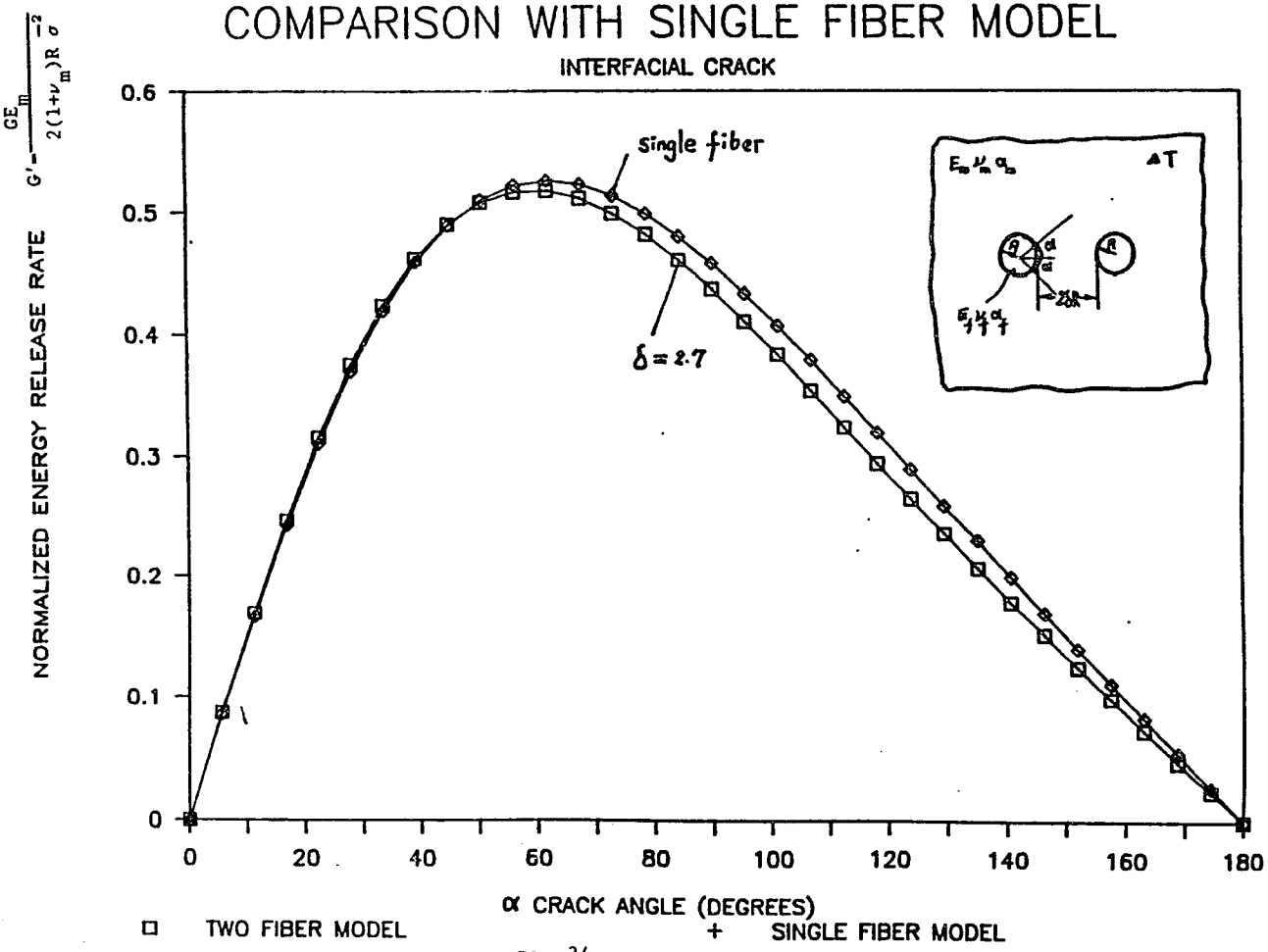
COMPARISON WITH SINGLE FIBER MODEL
INTERFACIAL CRACK
NORMALIZED ENERGY RELEASE RATE $G' = \frac{GE_m}{2(1+\nu_m)R\sigma^2}$
single fiber
$\delta = 2.7$
$E_m \nu_m \alpha_m$
ΔT
$E_f \nu_f \alpha_f$
0.6
0.5
0.4
0.3
0.2
0.1
0
0
20
40
60
80
100
120
140
160
180
α CRACK ANGLE (DEGREES)
□ TWO FIBER MODEL
+ SINGLE FIBER MODEL

Fig. 34

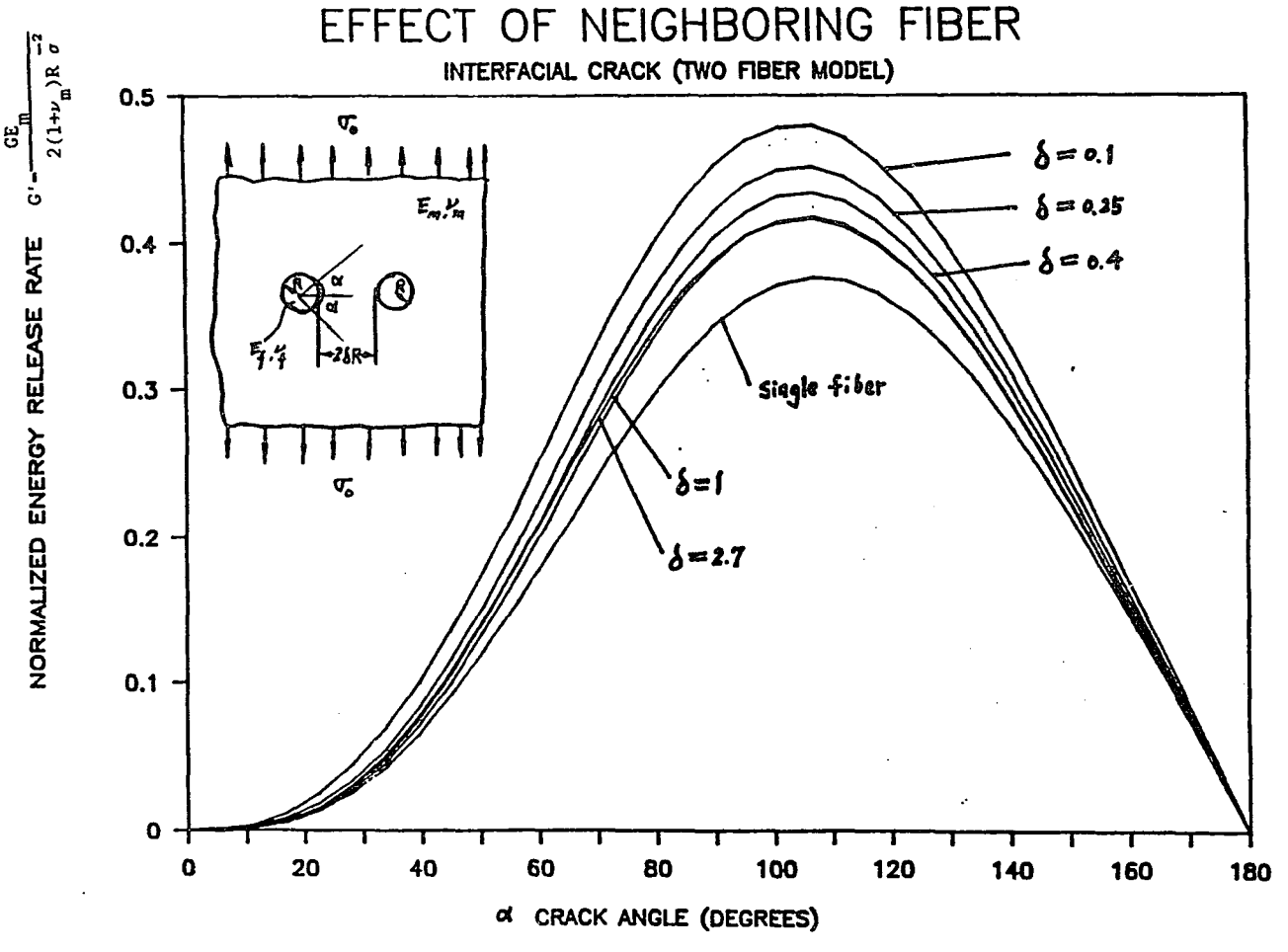
EFFECT OF NEIGHBORING FIBER
INTERFACIAL CRACK (TWO FIBER MODEL)
NORMALIZED ENERGY RELEASE RATE $G' = \frac{GE_m}{2(1+\nu_m)R\sigma^2}$
σ_∞
E_m, ν_m
E_f, ν_f
$2\delta R$
α
$\delta = 0.1$
$\delta = 0.25$
$\delta = 0.4$
Single fiber
$\delta = 1$
$\delta = 2.7$
0
0.1
0.2
0.3
0.4
0.5
0
20
40
60
80
100
120
140
160
180
α CRACK ANGLE (DEGREES)

Fig. 35

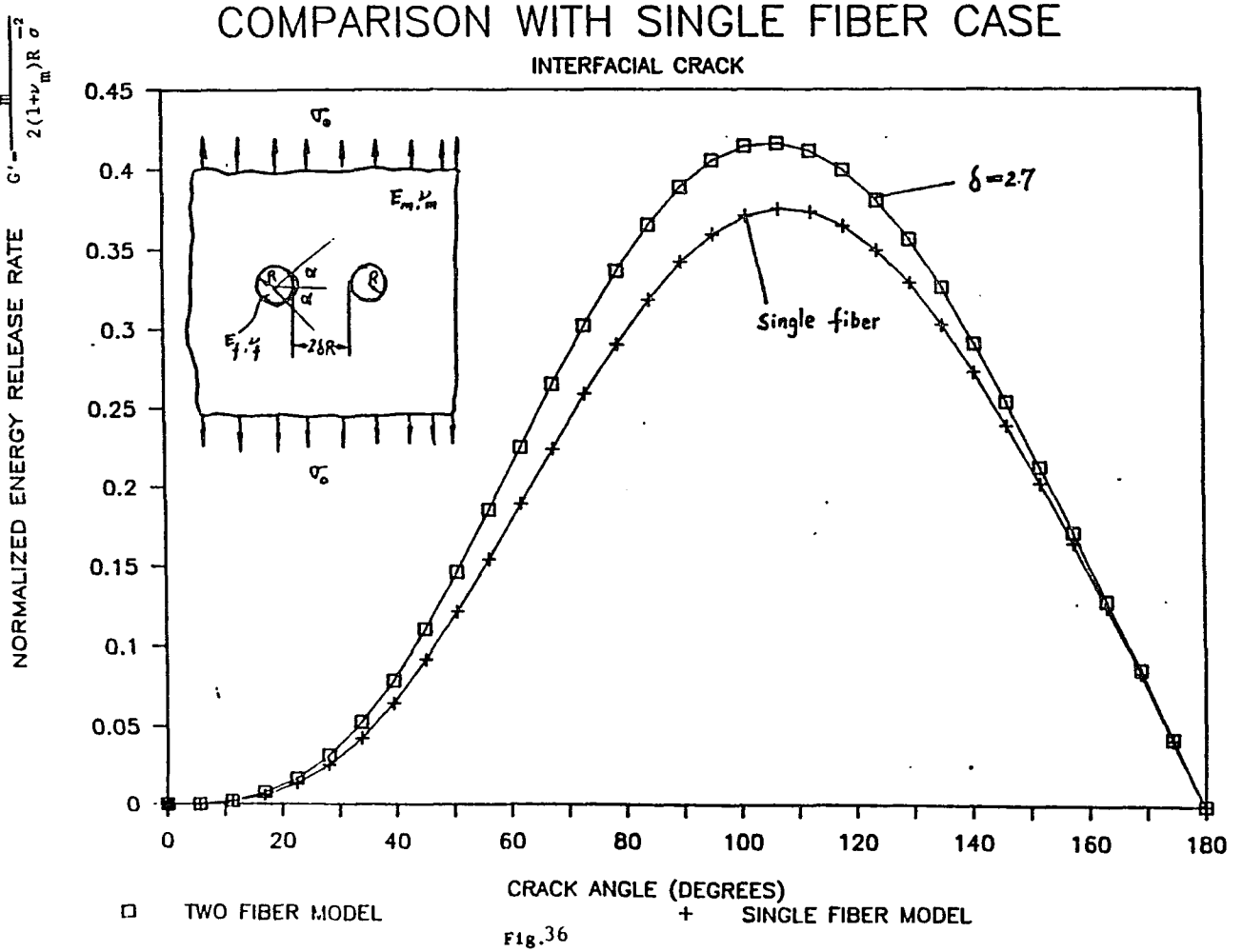
COMPARISON WITH SINGLE FIBER CASE
INTERFACIAL CRACK
NORMALIZED ENERGY RELEASE RATE $G' = \frac{GE_m}{2(1+\nu_m)R\,\bar{\sigma}^2}$
0.45
0.4
0.35
0.3
0.25
0.2
0.15
0.1
0.05
0
0
20
40
60
80
100
120
140
160
180
CRACK ANGLE (DEGREES)
σ_0
E_m, ν_m
E_f, ν_f
$2\delta R$
α
R
$\delta = 2.7$
Single fiber
TWO FIBER MODEL
SINGLE FIBER MODEL

Fig.36

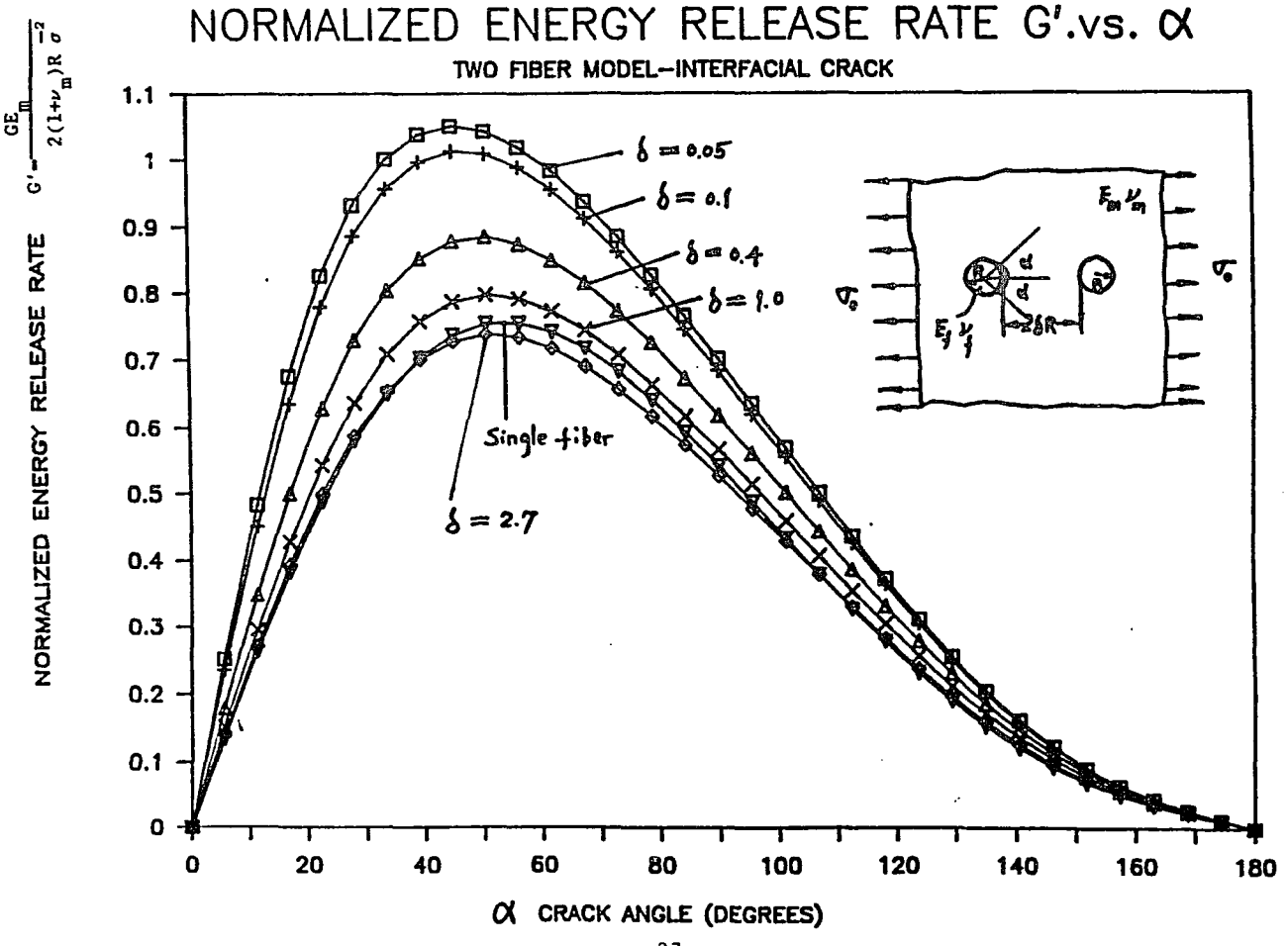
NORMALIZED ENERGY RELEASE RATE G'.vs. α
TWO FIBER MODEL--INTERFACIAL CRACK
NORMALIZED ENERGY RELEASE RATE $G'=\frac{GE_m}{2(1+\nu_m)R\sigma^2}$
δ = 0.05
δ = 0.1
δ = 0.4
δ = 1.0
Single fiber
δ = 2.7
α CRACK ANGLE (DEGREES)
0
0.1
0.2
0.3
0.4
0.5
0.6
0.7
0.8
0.9
1
1.1
0
20
40
60
80
100
120
140
160
180

Fig. 37

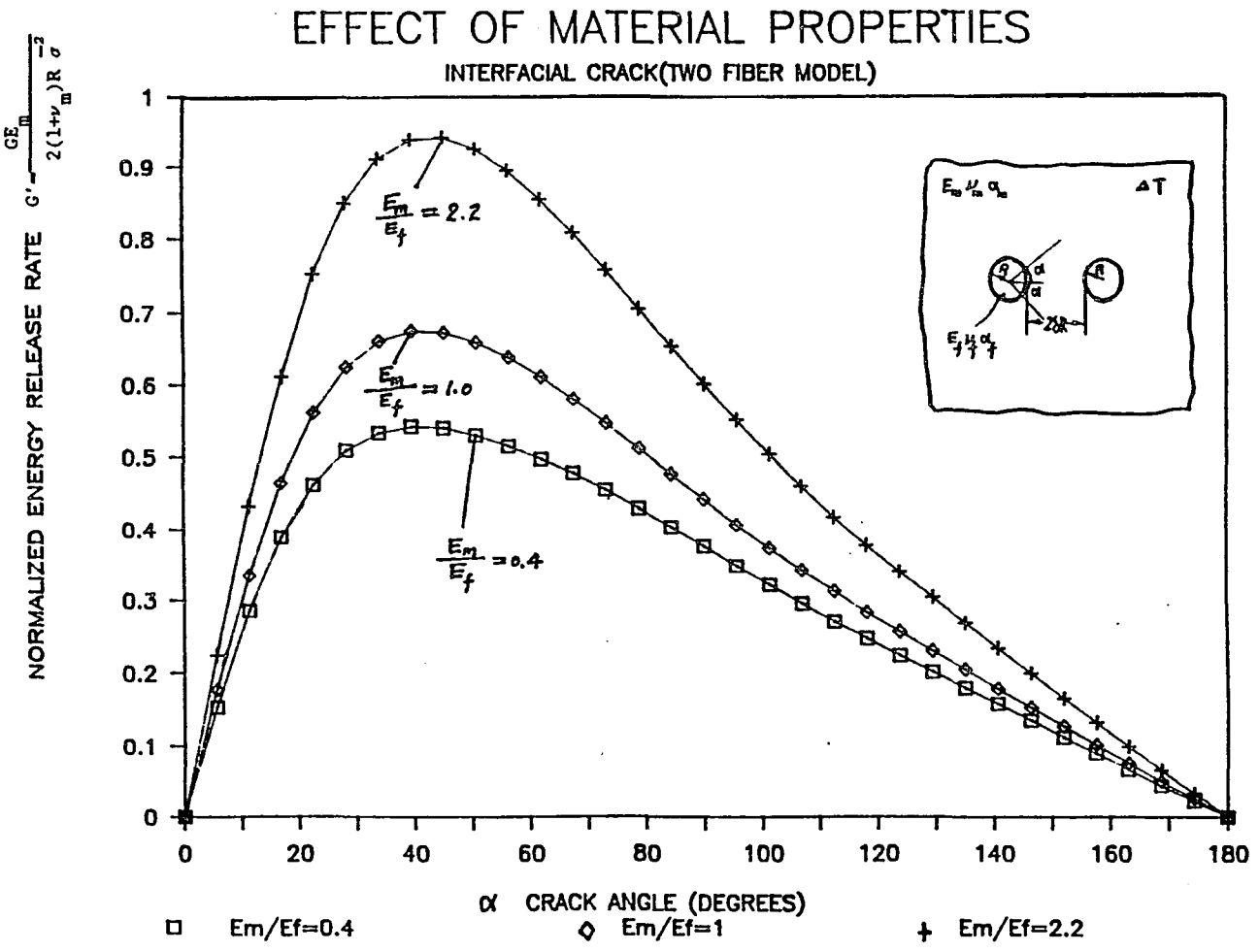
EFFECT OF MATERIAL PROPERTIES
INTERFACIAL CRACK(TWO FIBER MODEL)
NORMALIZED ENERGY RELEASE RATE $G' = \frac{GE_m}{2(1+\nu_m)R\sigma^2}$
$\frac{E_m}{E_f} = 2.2$
$\frac{E_m}{E_f} = 1.0$
$\frac{E_m}{E_f} = 0.4$
ΔT
α CRACK ANGLE (DEGREES)
Em/Ef=0.4
Em/Ef=1
Em/Ef=2.2

Fig. 38

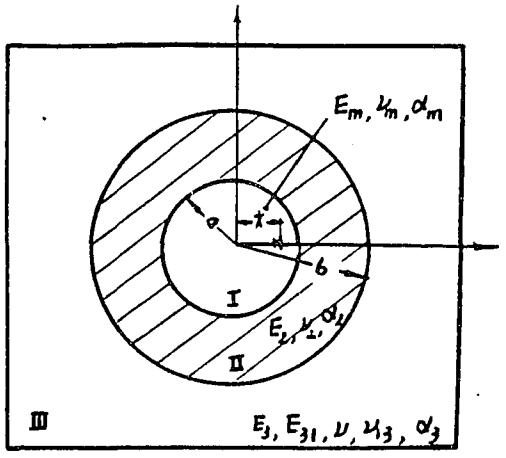

Fig39. Dislocation solution

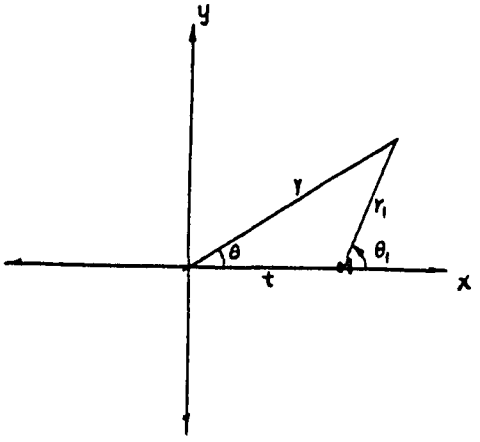

Fig. 40 Edge dislocation embedded in infinite media

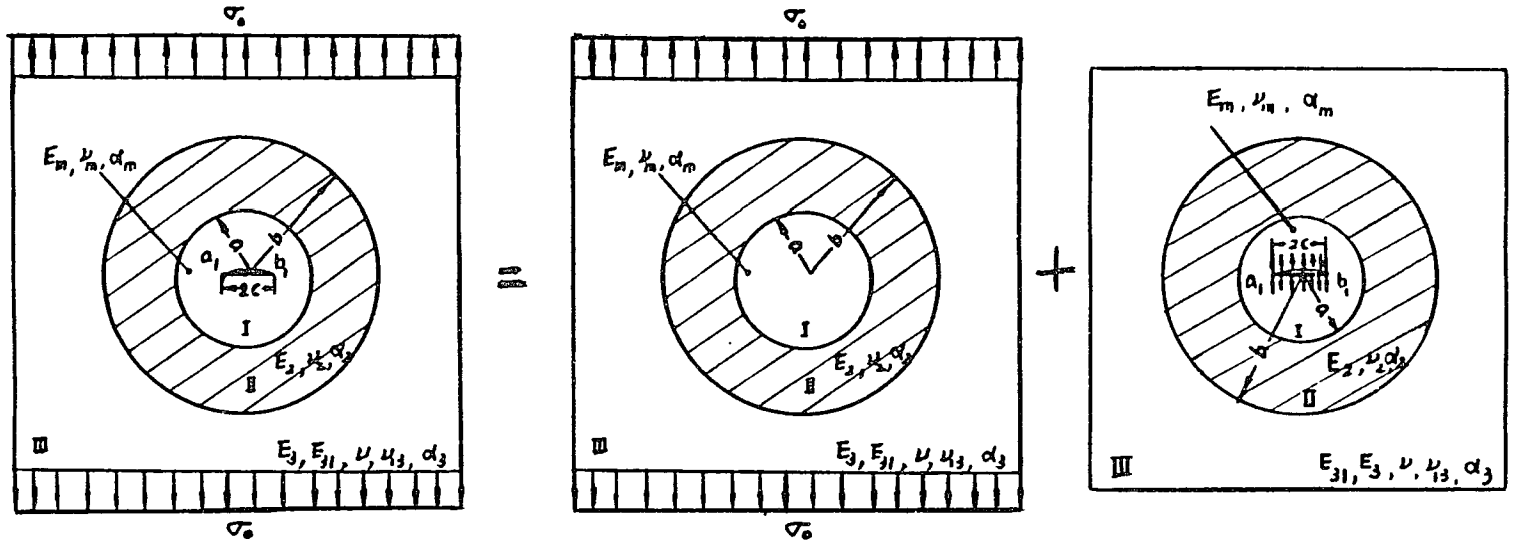

a) original problem

b) uncracked geometry

c) perturbation problem

Fig. 41 superposition of ring model crack problem

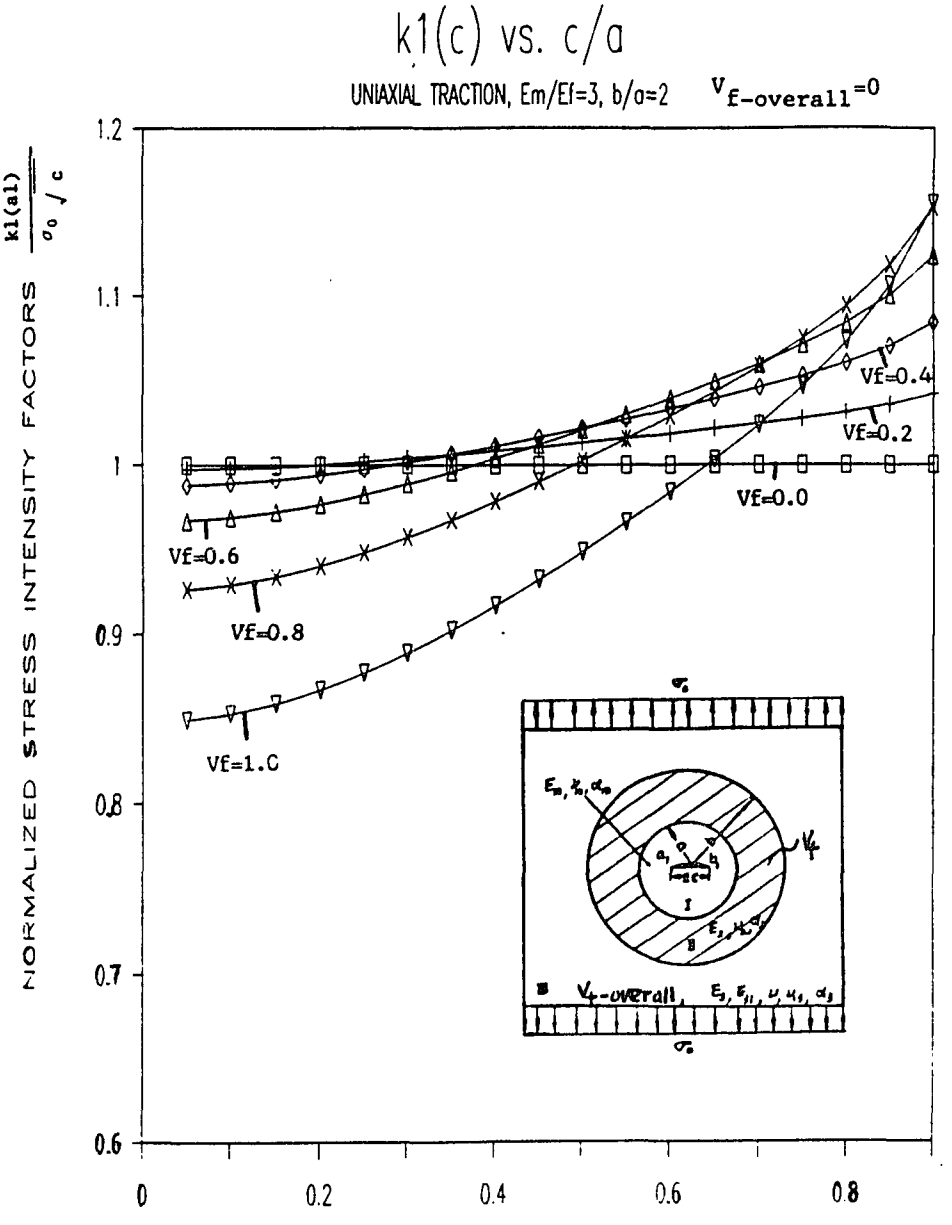

Fig. 42 NORMALIZED CRACK LENGTHS c/a

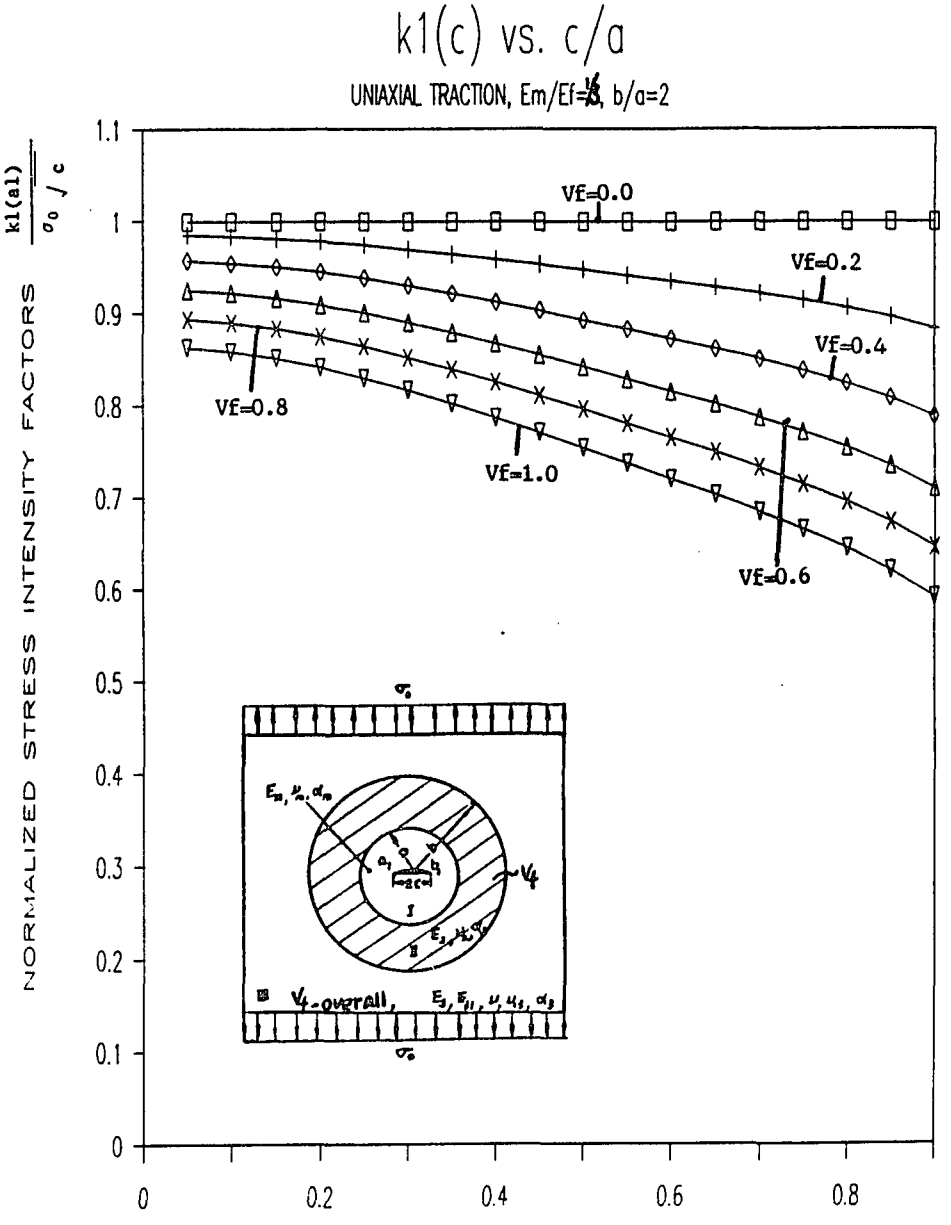

Fig.43 NORMALIZED CRACK LENGTH c/a

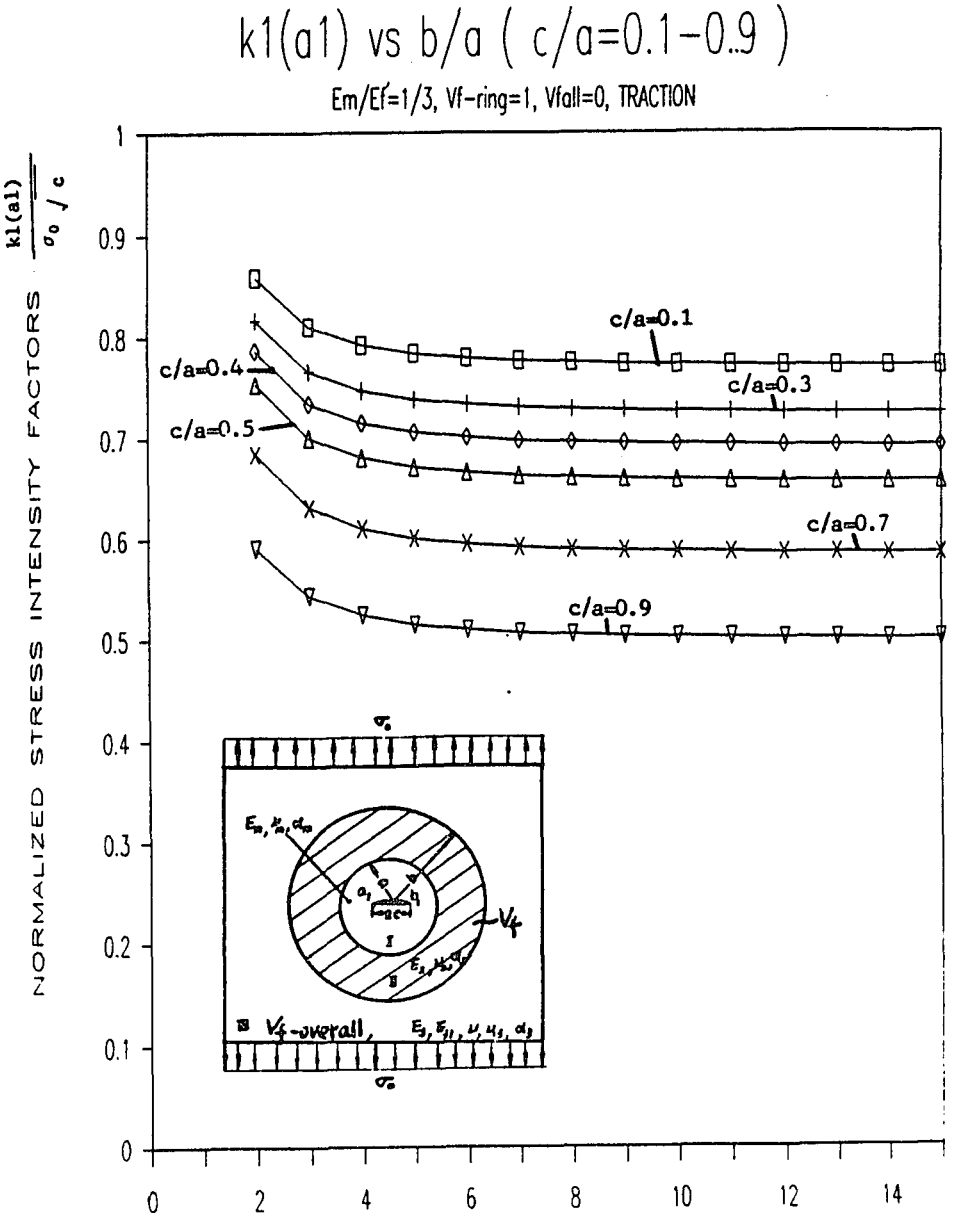

Fig.44 NORMALIZED RING WIDTHS (b/a)

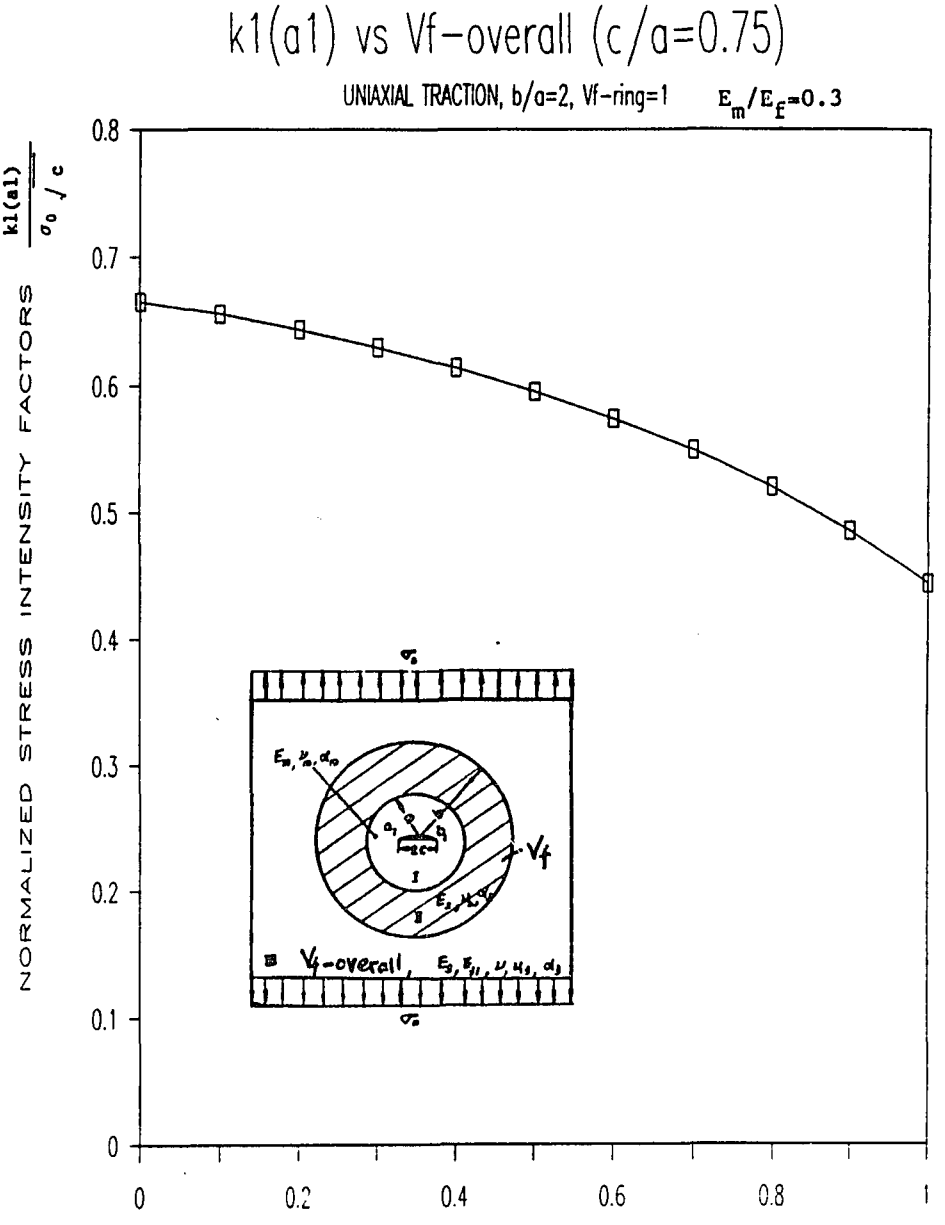

Fig.45 OVERALL VOLUME FRACTIONS OF FIBERS

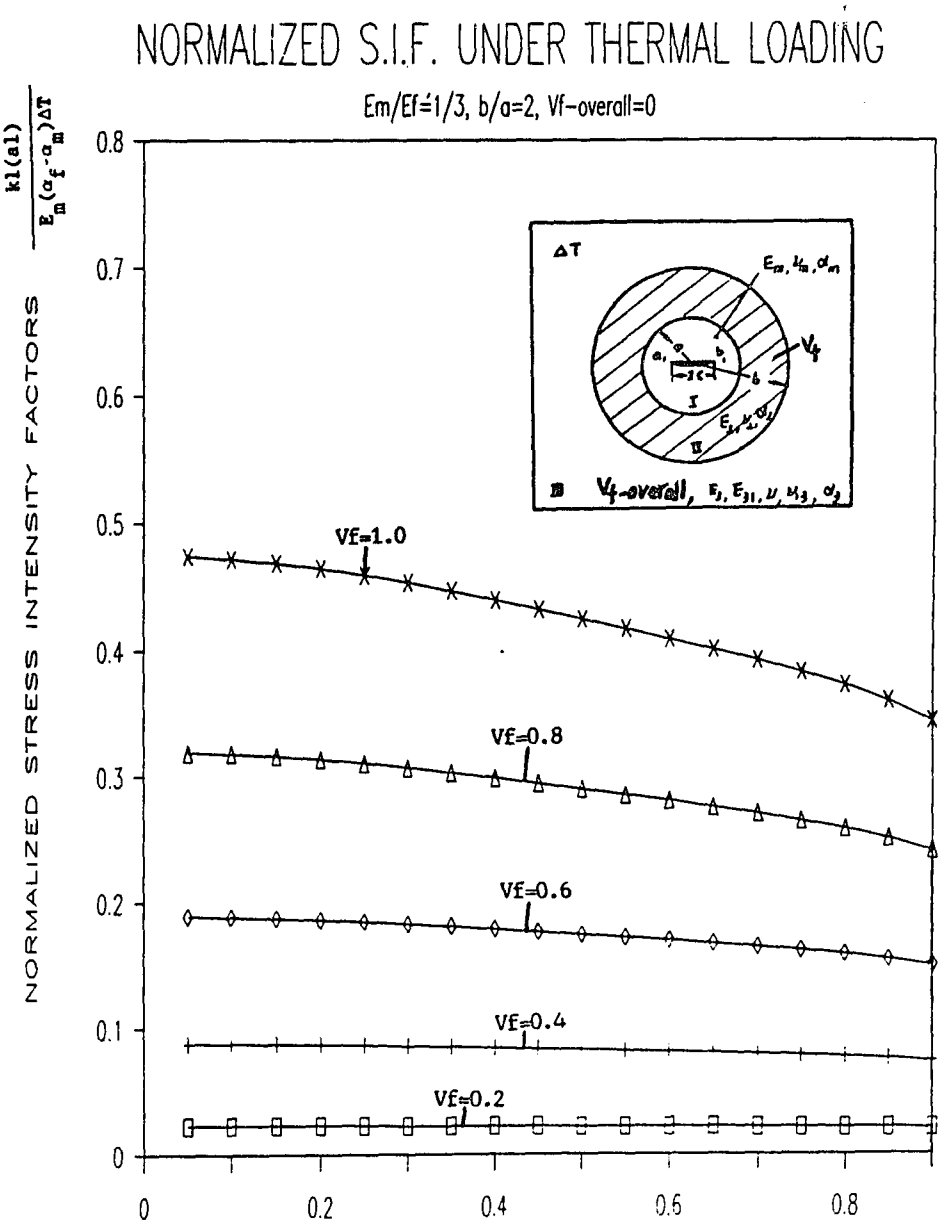

Fig. 46 NORMALIZED CRACK LENGTHS (c/a)

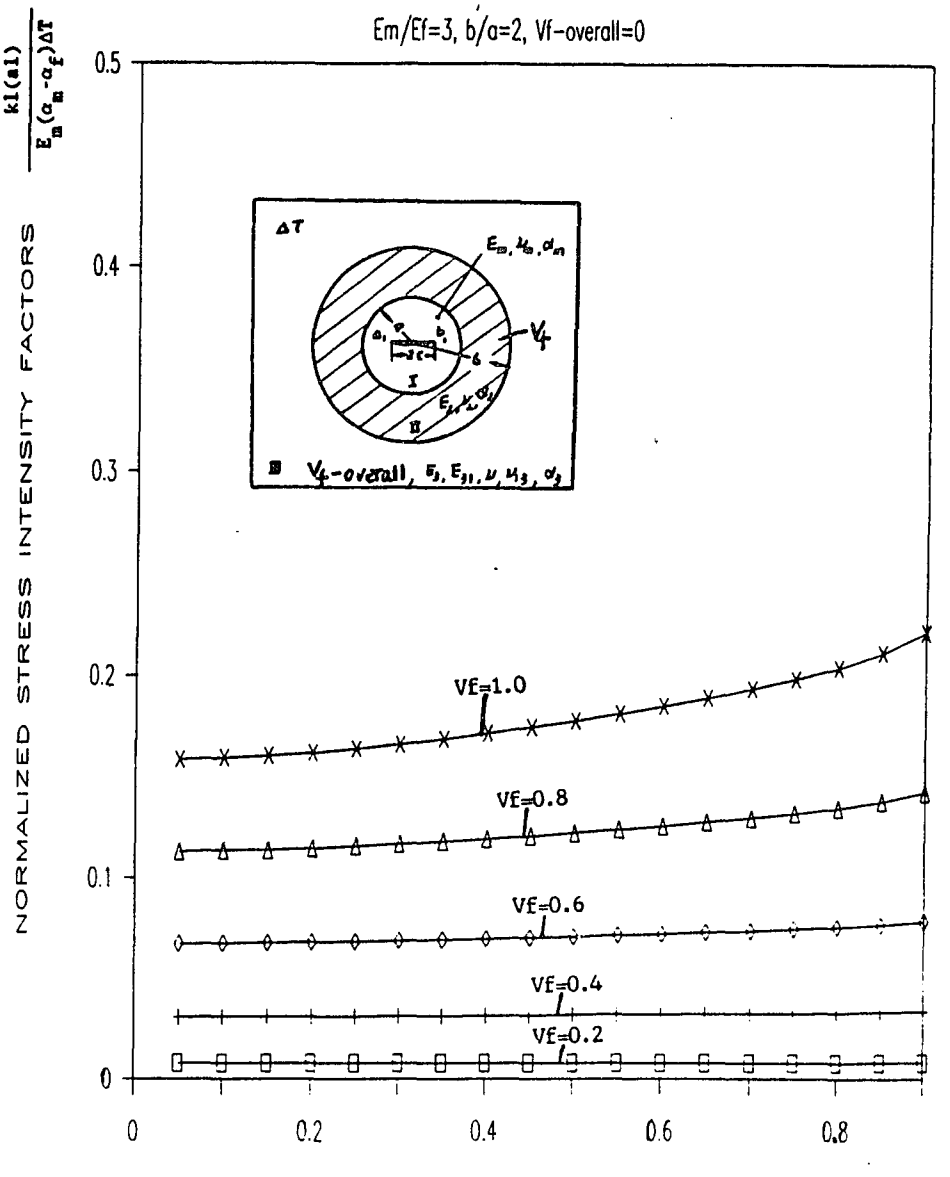
NORMALIZED S.I.F. UNDER THERMAL LOADING
Em/Ef=3, b/a=2, Vf-overall=0
NORMALIZED STRESS INTENSITY FACTORS
k1(a1) / Em(αm-αf)ΔT
NORMALIZED CRACK LENGTHS (c/a)
ΔT
Vf=1.0
Vf=0.8
Vf=0.6
Vf=0.4
Vf=0.2
0
0.1
0.2
0.3
0.4
0.5
0.2
0.4
0.6
0.8

Fig. 47

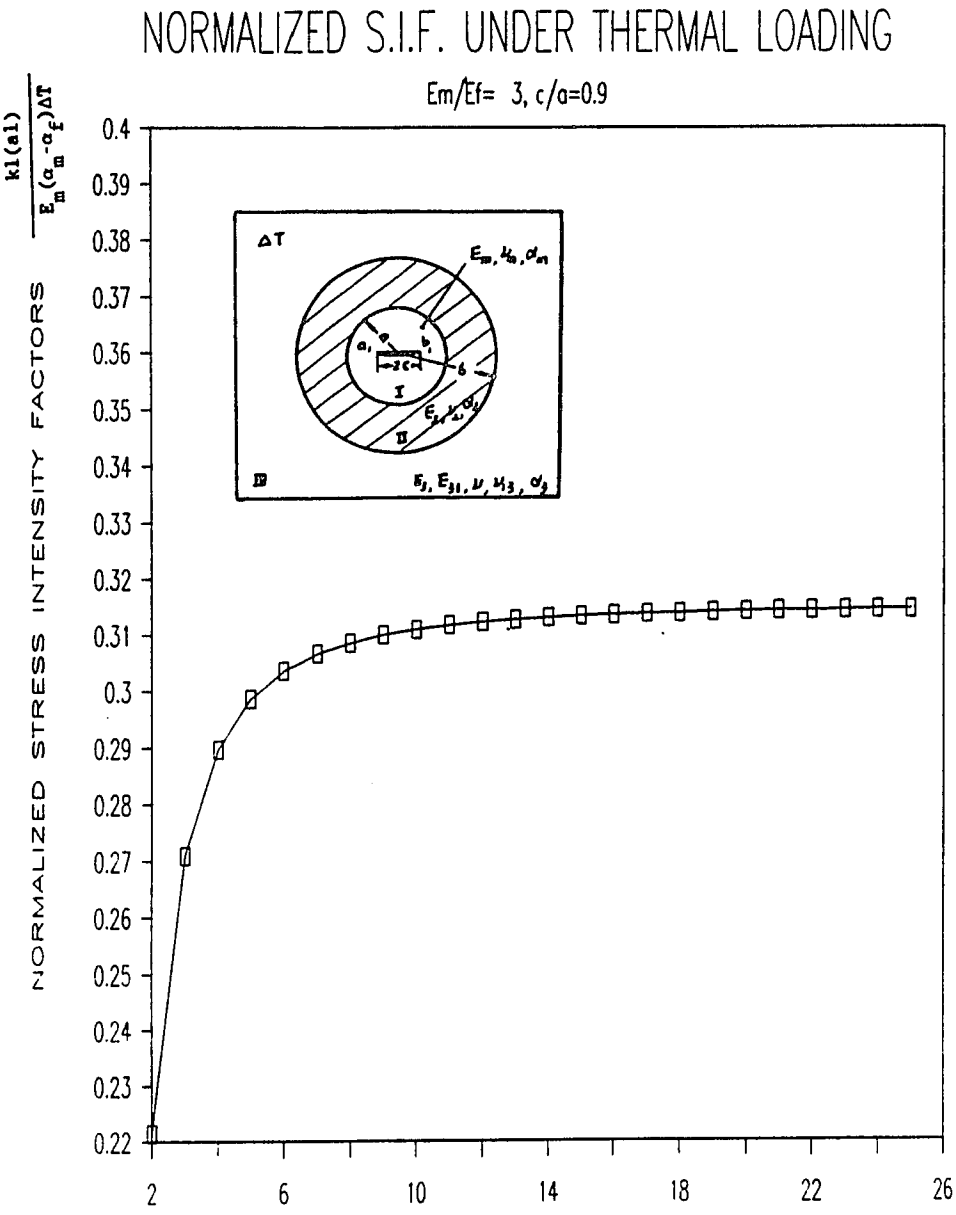
NORMALIZED S.I.F. UNDER THERMAL LOADING
Em/Ef= 3, c/a=0.9
NORMALIZED STRESS INTENSITY FACTORS
k1(a1) / Em(αm-αf)ΔT
0.4
0.39
0.38
0.37
0.36
0.35
0.34
0.33
0.32
0.31
0.3
0.29
0.28
0.27
0.26
0.25
0.24
0.23
0.22
2
6
10
14
18
22
26
ΔT
I
II
III
NORMALIZED RING WIDTHS (b/a)

Fig.48

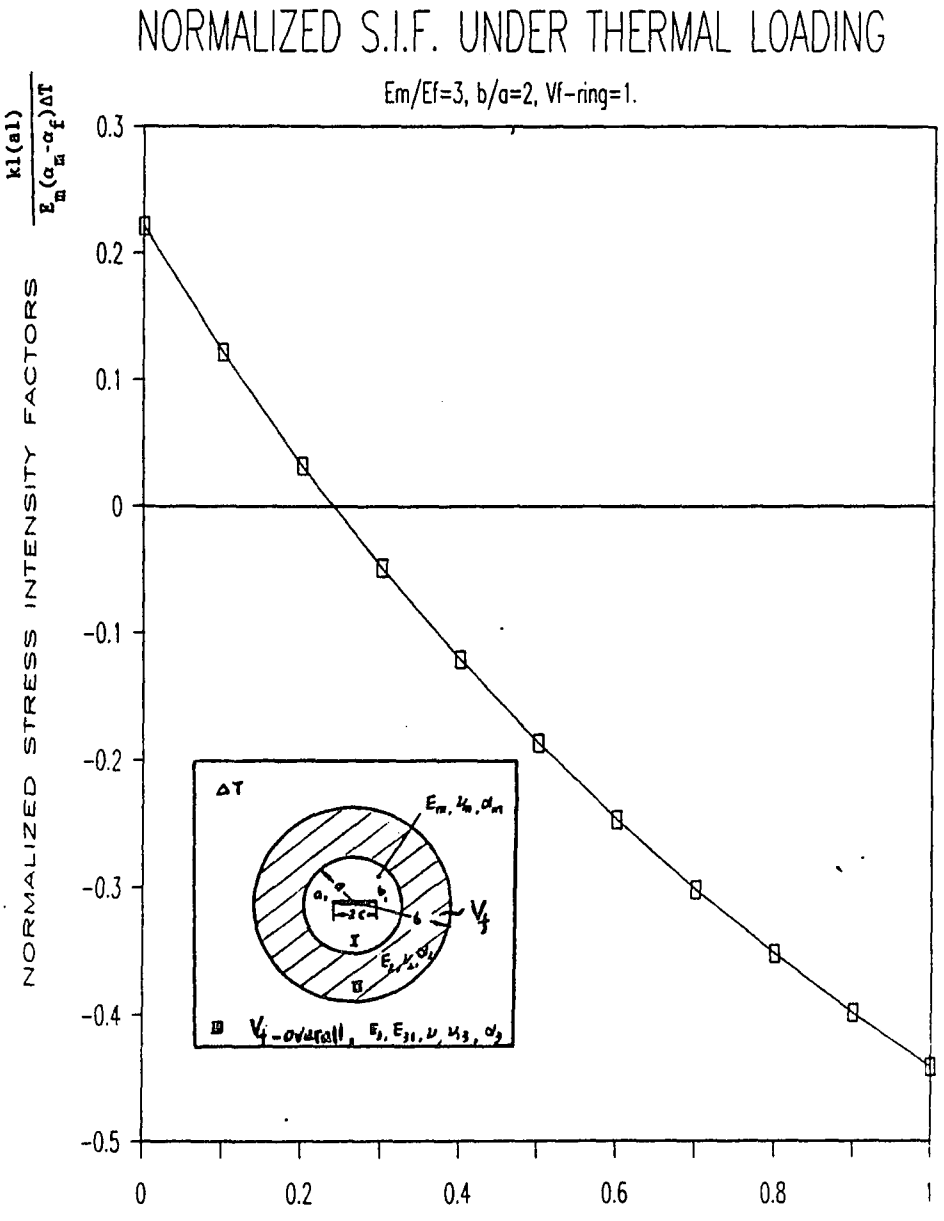

Fig.49 OVERALL VOLUME FRACTION OF FIBERS

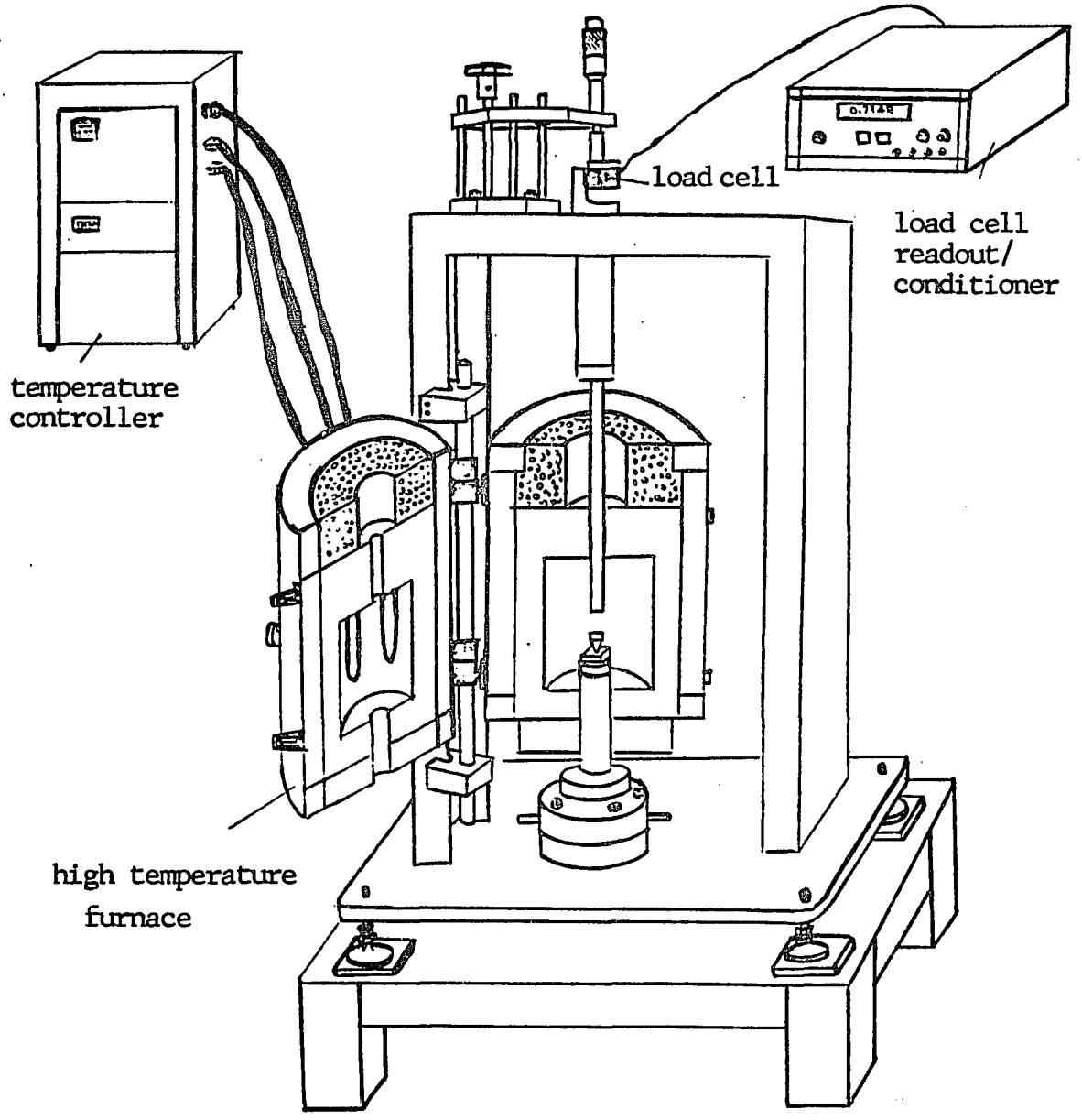

Fig.50 Configuration of series 3320 split-tube laboratory furnace

a) monolithic SiC coating by CVD technology on graphite base

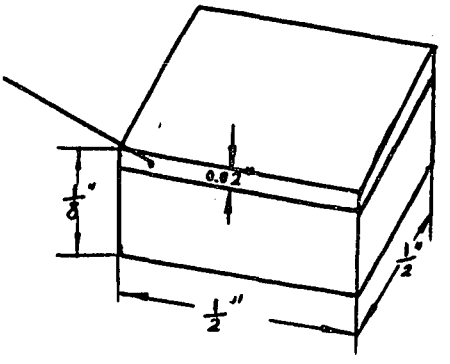

b) Nicalon/SiC composite

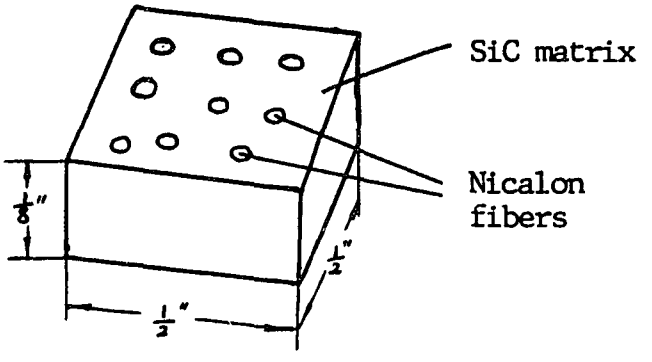

Fig. 51 Specimens

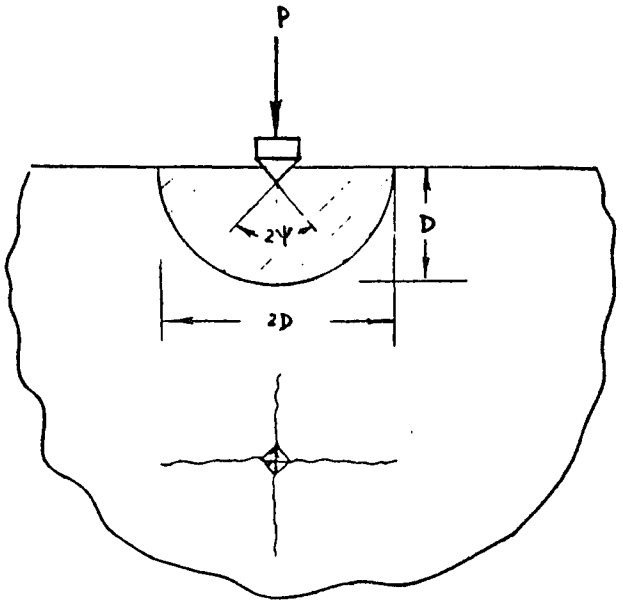

Fig. 52 Indentation test to determine K_{1C} of ceramic matrix materials

Effect of Temperature on the Fracture Toughness of the Two Matrix Materials Used in the Composites

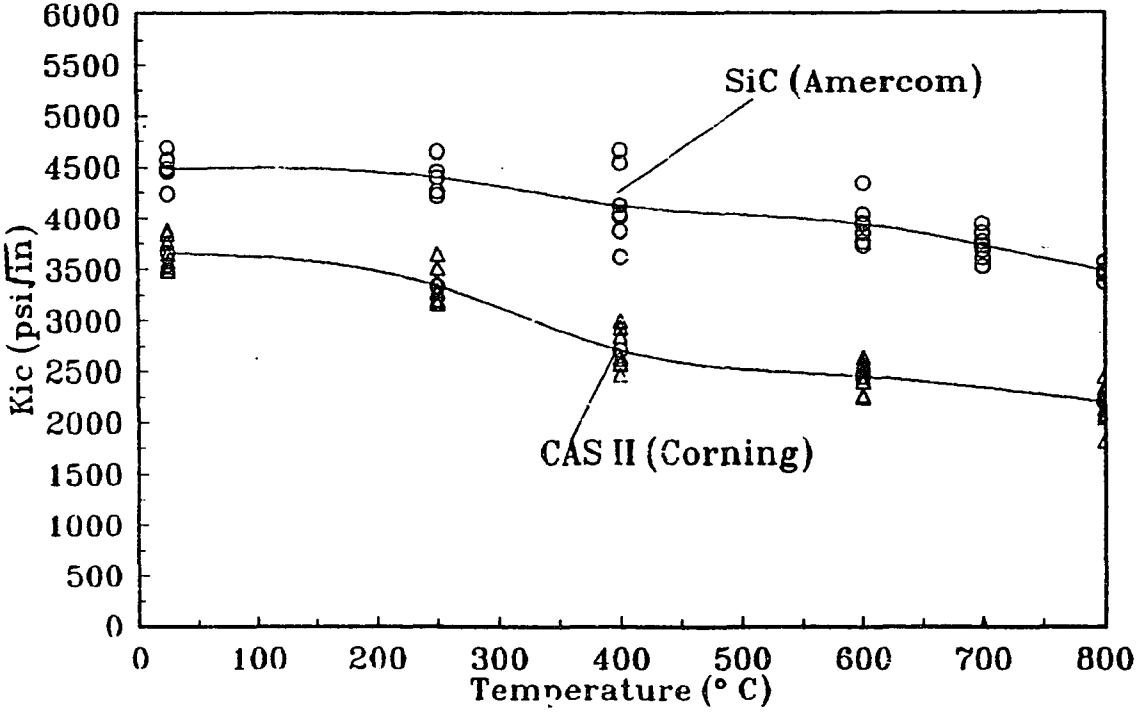

Fig. 53

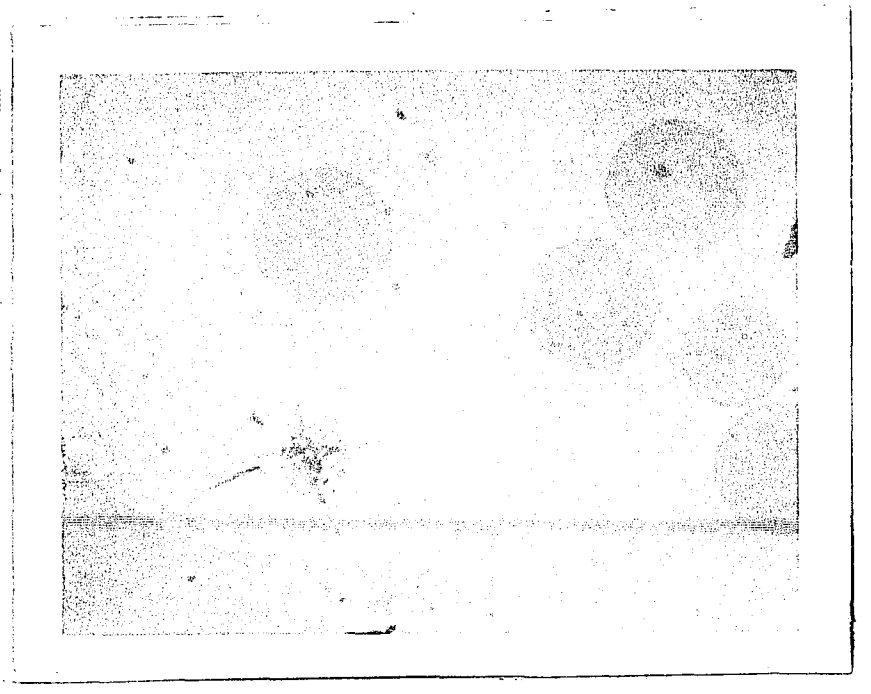

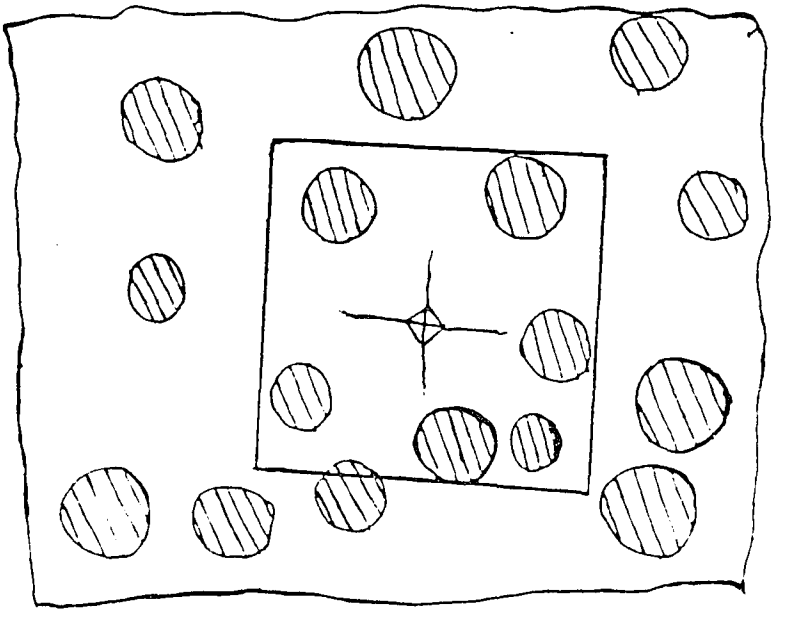

Fig. 54 sample cell for calculation of local volume fraction of fibers

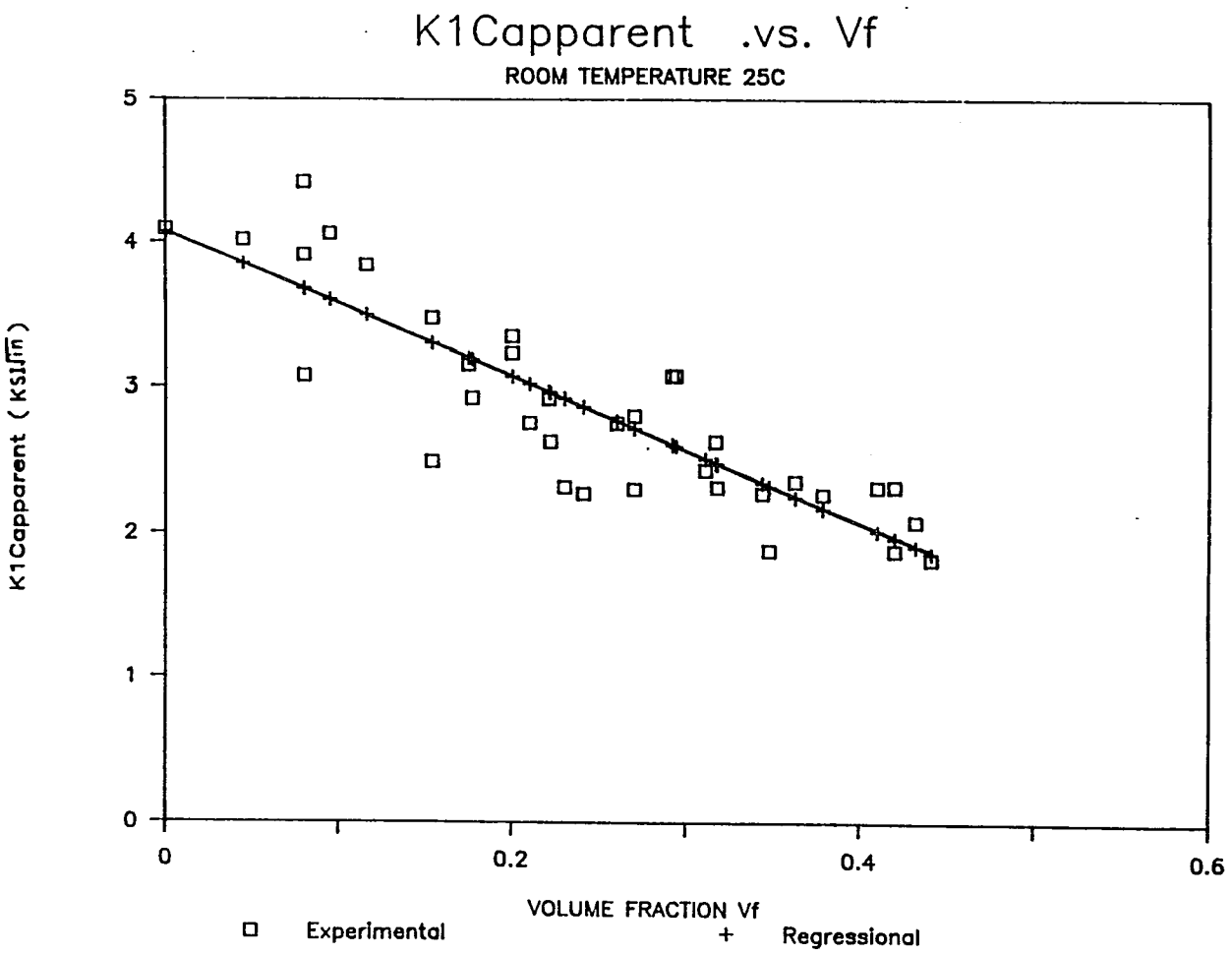
K1Capparent .vs. Vf
ROOM TEMPERATURE 25C
K1Capparent (KSI√in)
5
4
3
2
1
0
0
0.2
0.4
0.6
VOLUME FRACTION Vf
Experimental
Regressional

Fig. 55

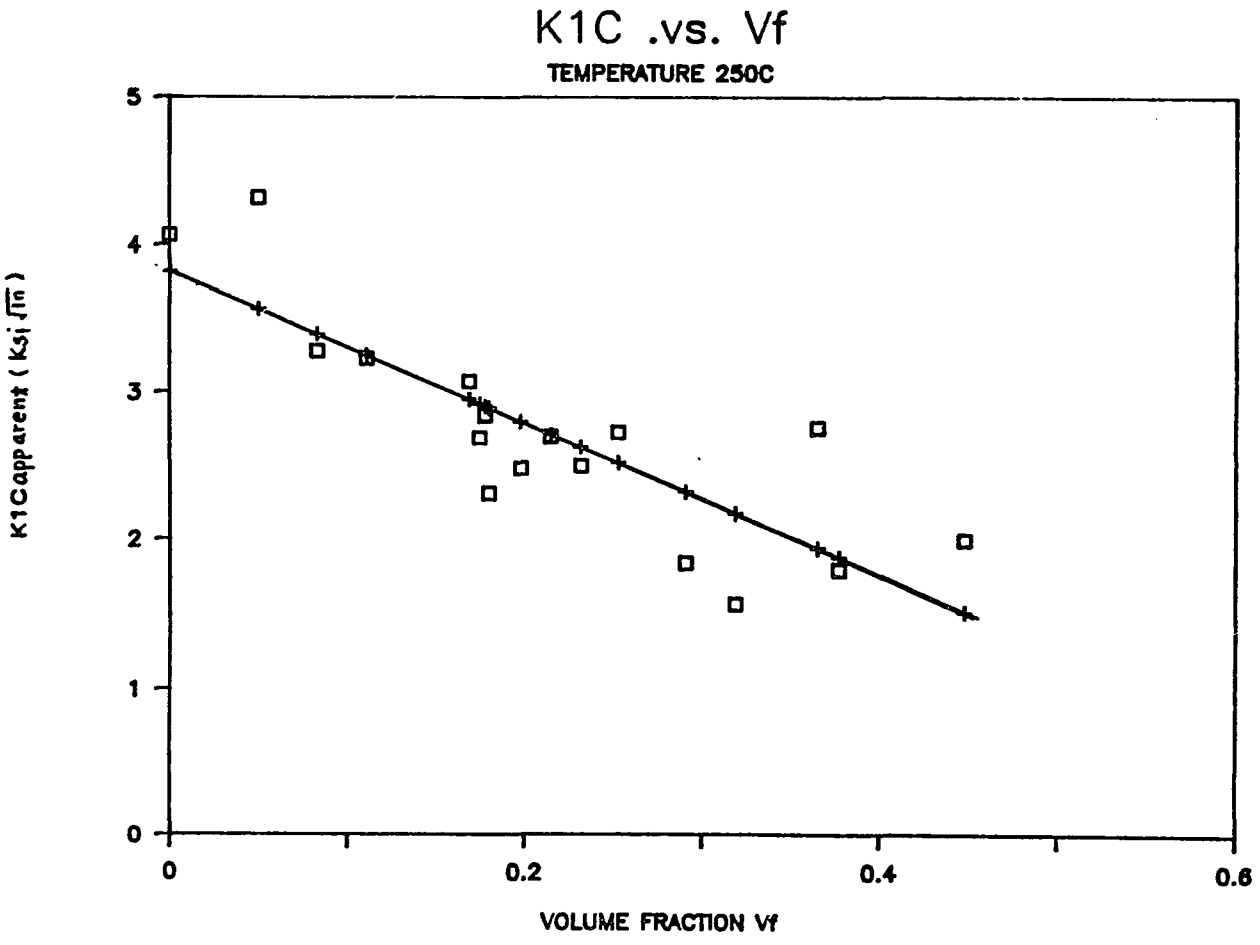
K1C .vs. Vf
TEMPERATURE 250C
K1Capparent (Ksi √in)
VOLUME FRACTION Vf
0
1
2
3
4
5
0
0.2
0.4
0.6

Fig. 56

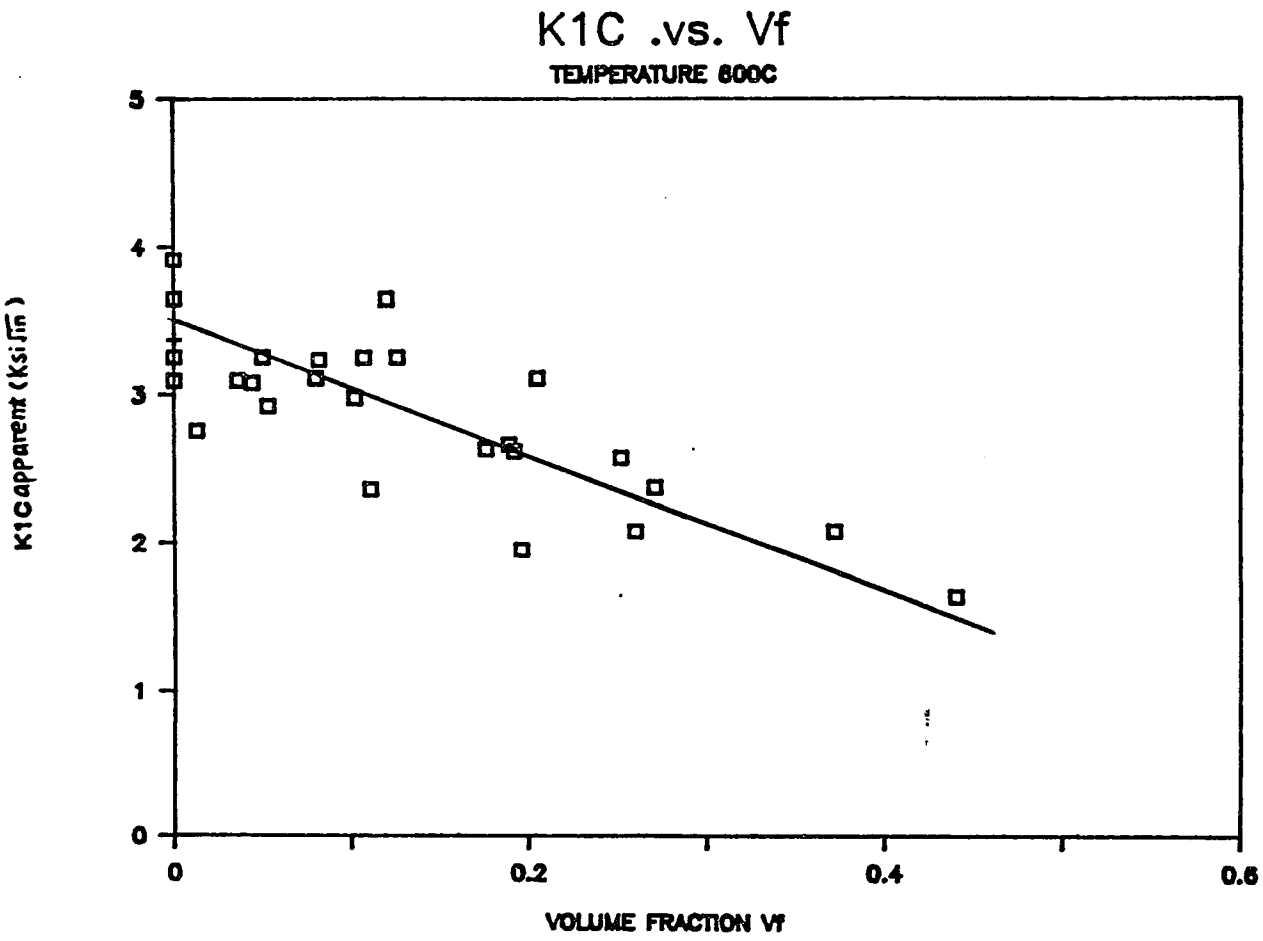
K1C .vs. Vf
TEMPERATURE 600C
K1Capparent (Ksi√in)
VOLUME FRACTION Vf
0
1
2
3
4
5
0
0.2
0.4
0.6

Fig. 57

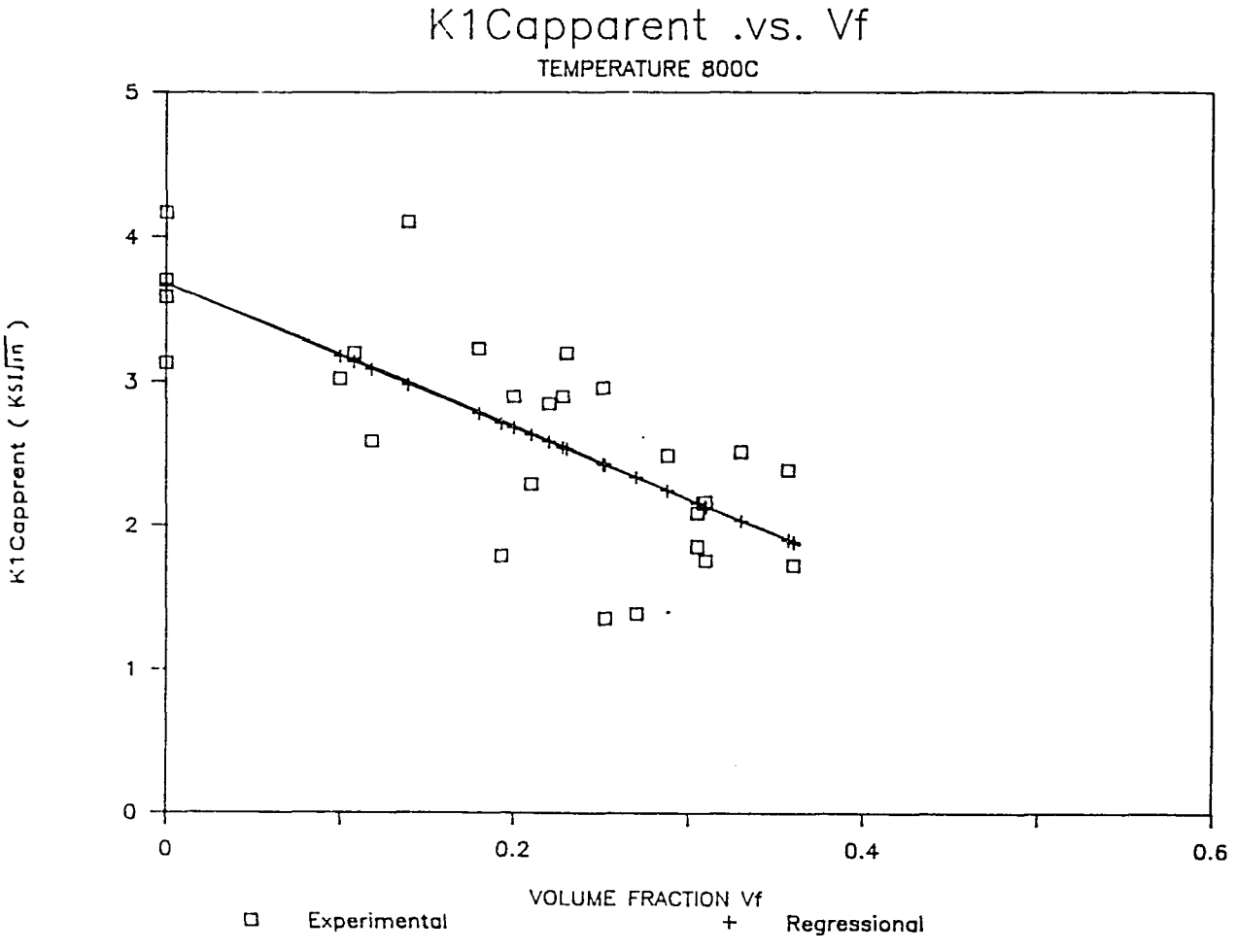
K1Capparent .vs. Vf
TEMPERATURE 800C
K1Capprent (KSI√in)
5
4
3
2
1
0
0
0.2
0.4
0.6
VOLUME FRACTION Vf
Experimental
Regressional

Fig. 58

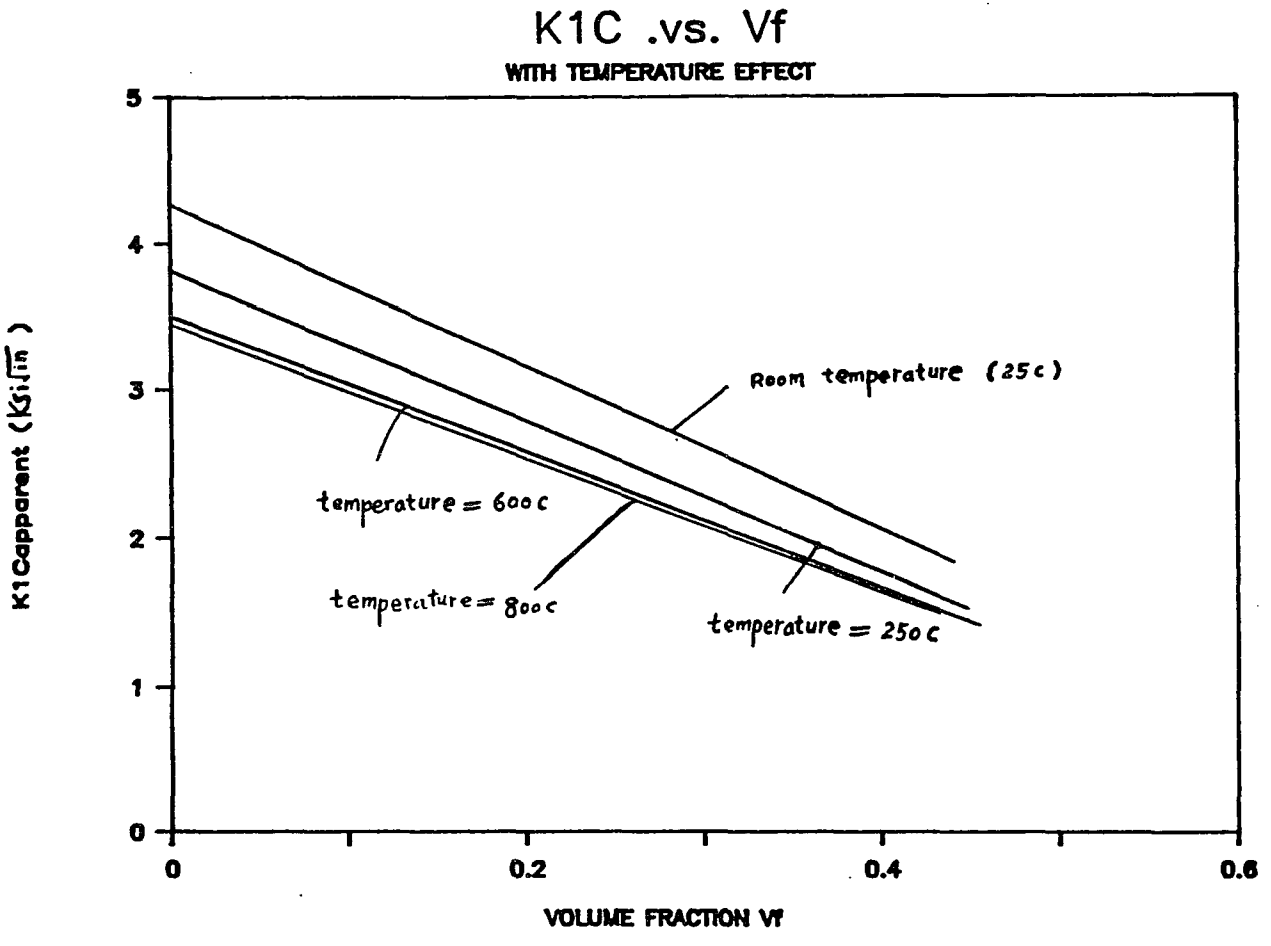
K1C .vs. Vf
WITH TEMPERATURE EFFECT
K1Capparent (Ksi√in)
VOLUME FRACTION Vf
Room temperature (25c)
temperature = 600c
temperature = 800c
temperature = 250c
0
1
2
3
4
5
0
0.2
0.4
0.6

Fig. 59

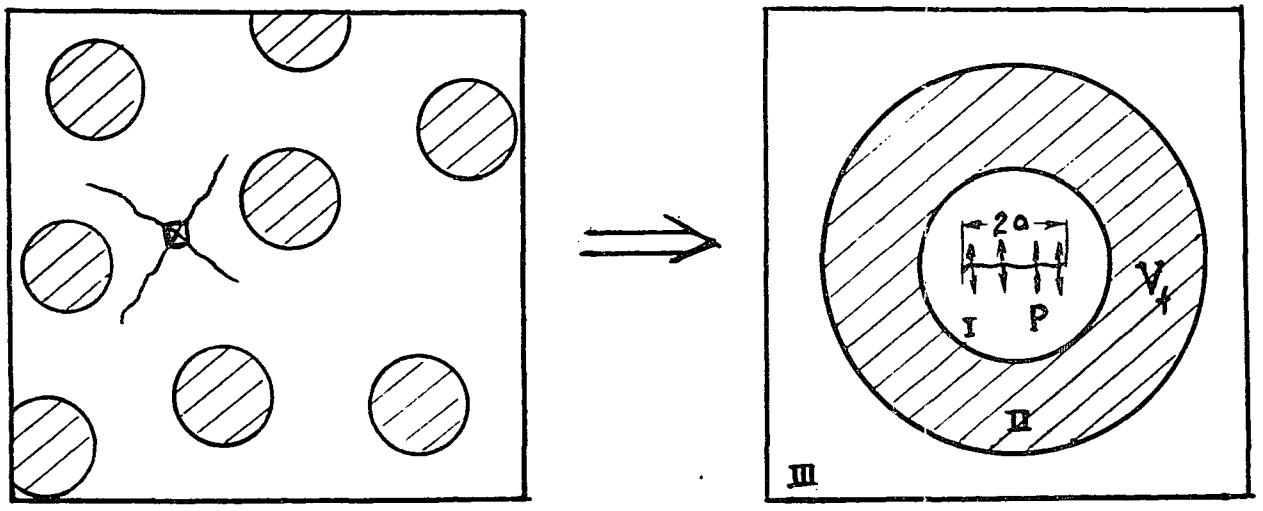

a) indentation crack in composite

b) theoretical model for anticipation

Fig. 60 Theoretical model

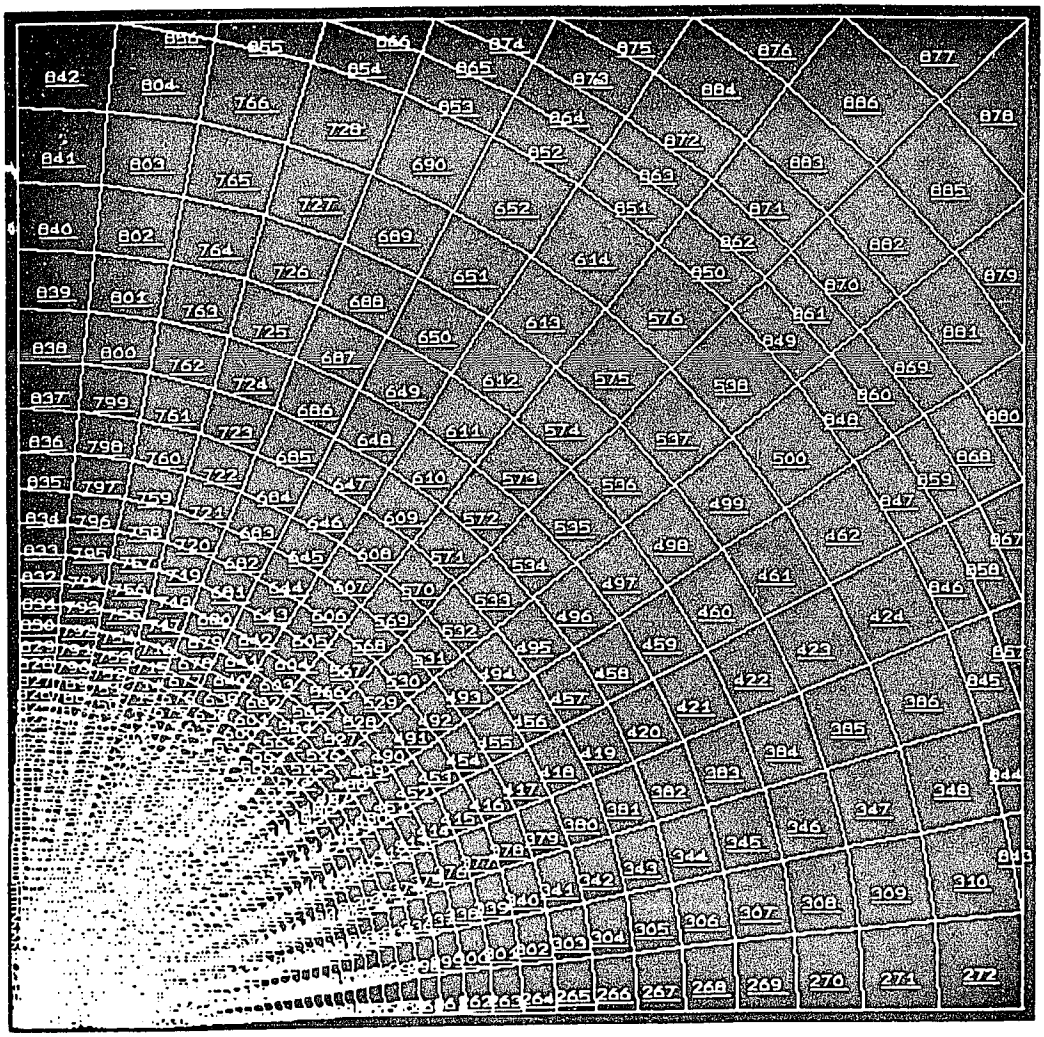

Finite Element Model for Theoretical Prediction

Fig. 61

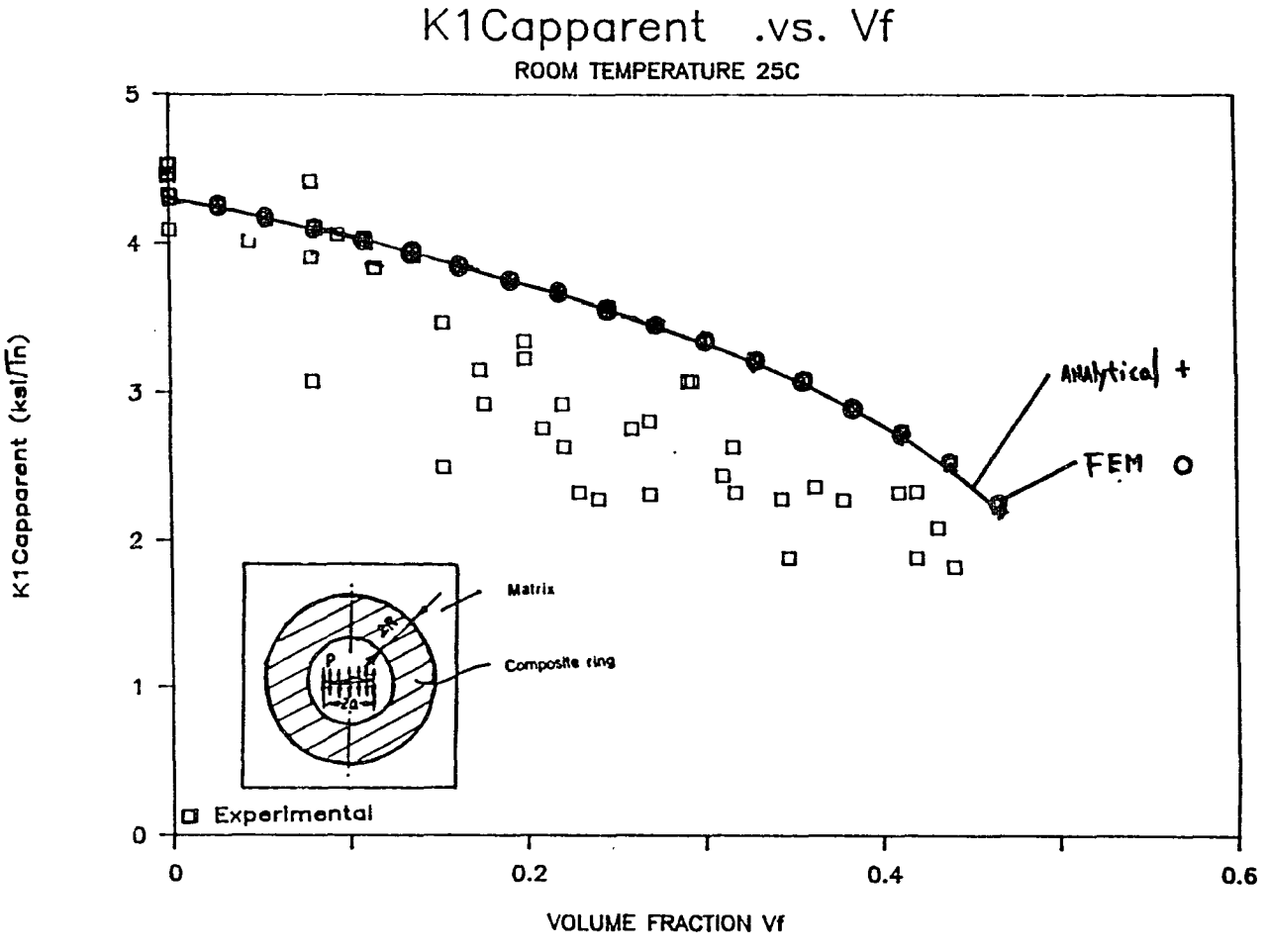
K1Capparent .vs. Vf
ROOM TEMPERATURE 25C
K1Capparent (ksi√in)
VOLUME FRACTION Vf
Analytical +
FEM O
Experimental
Matrix
Composite ring
0
1
2
3
4
5
0
0.2
0.4
0.6

Fig. 62

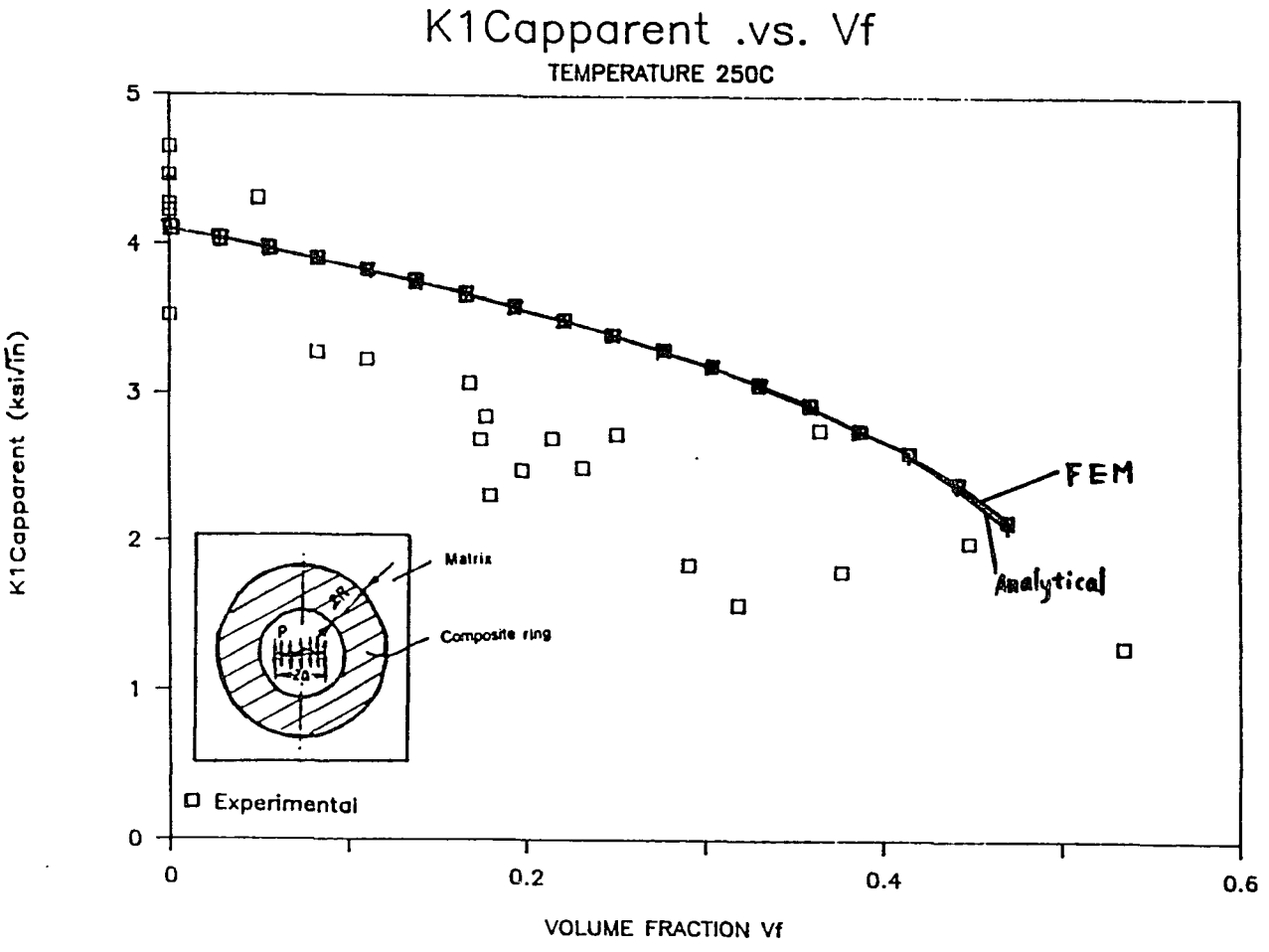
K1Capparent .vs. Vf
TEMPERATURE 250C
K1Capparent (ksi√in)
VOLUME FRACTION Vf
0
1
2
3
4
5
0
0.2
0.4
0.6
FEM
Analytical
Matrix
Composite ring
Experimental

Fig. 63

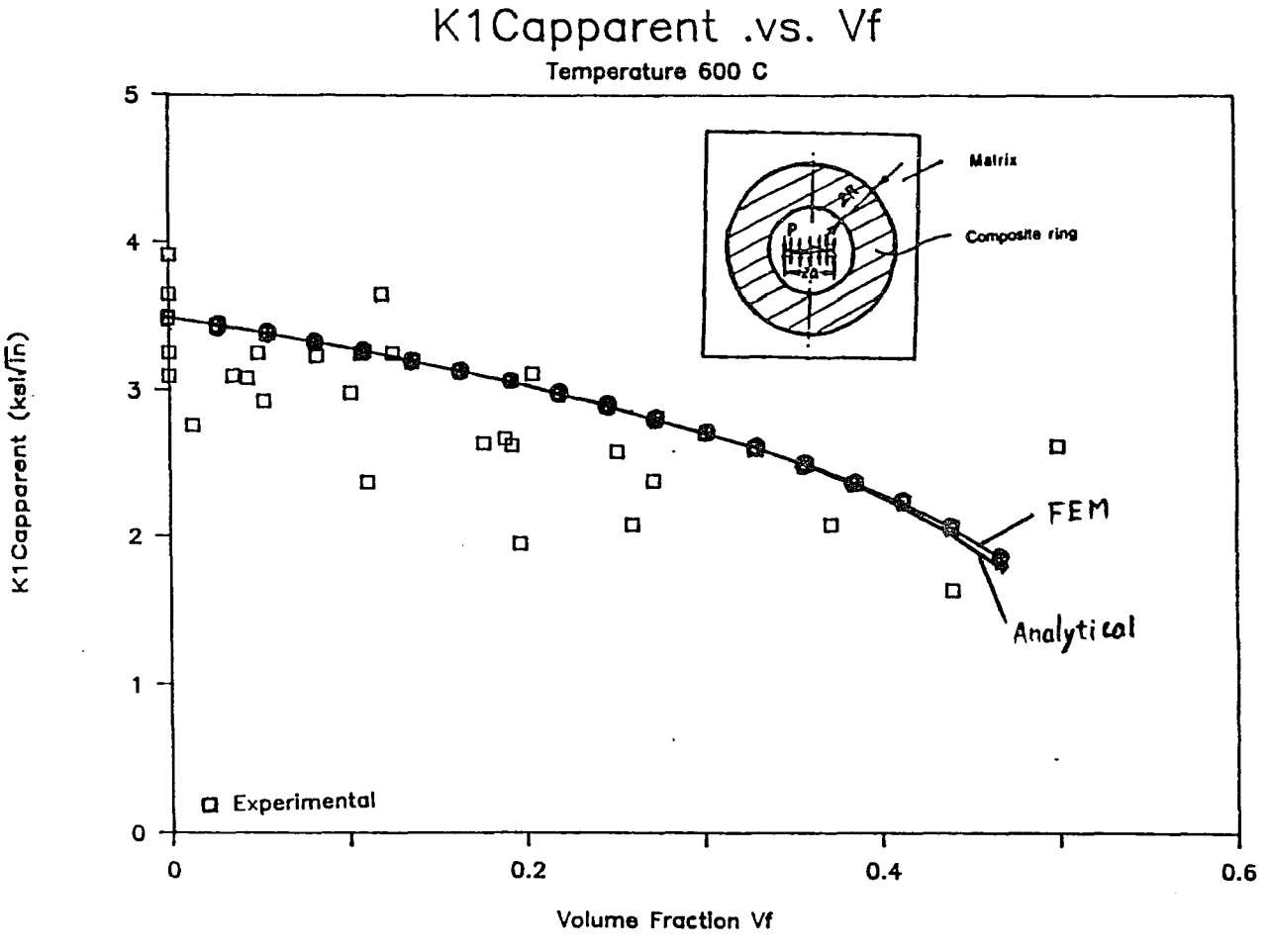
K1Capparent .vs. Vf
Temperature 600 C
K1Capparent (ksi/in)
Volume Fraction Vf
Matrix
Composite ring
FEM
Analytical
Experimental
0
1
2
3
4
5
0.2
0.4
0.6

Fig. 64

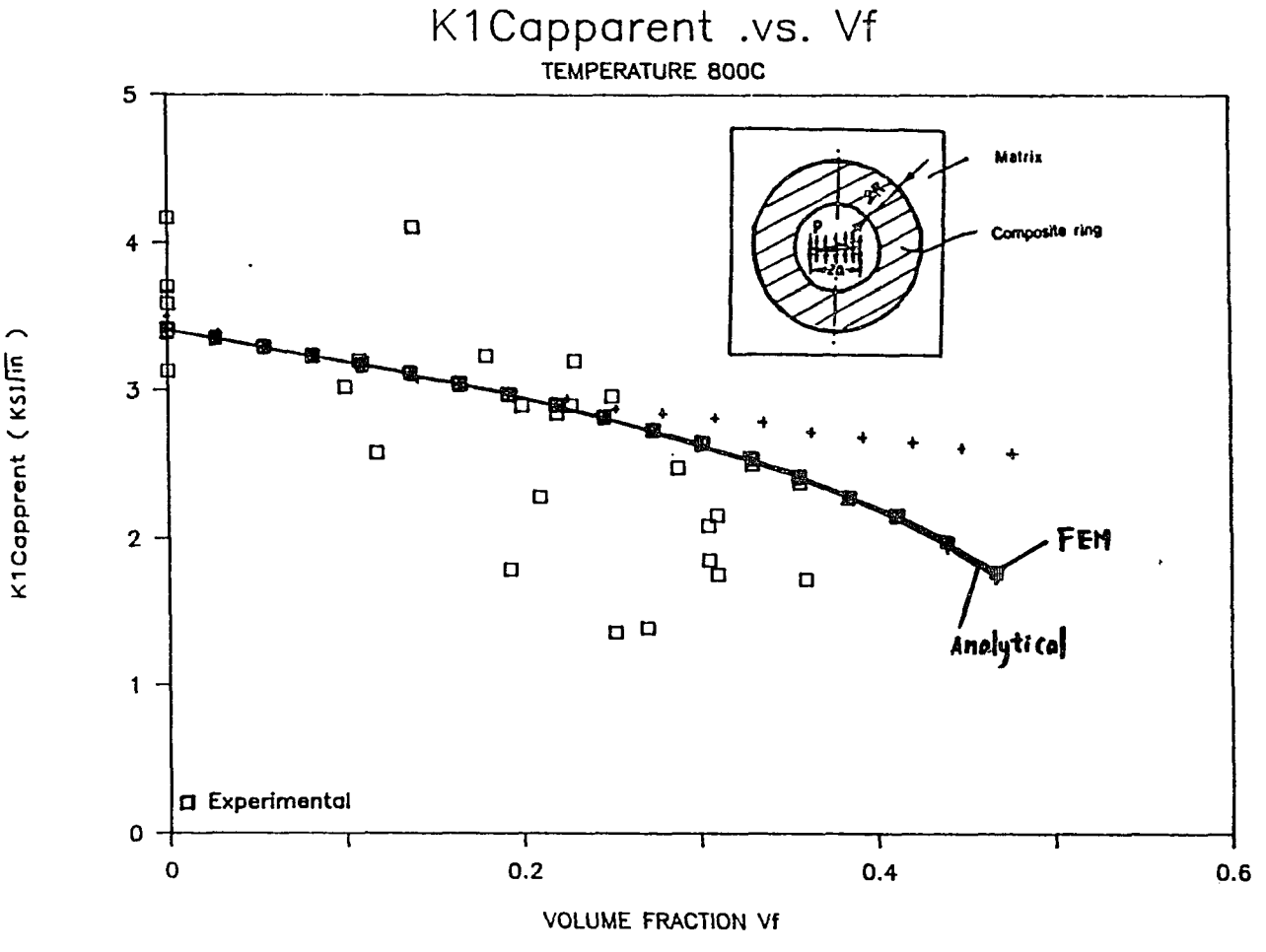
K1Capparent .vs. Vf
TEMPERATURE 800C
K1Capprent (KSI√in)
VOLUME FRACTION Vf
Matrix
Composite ring
FEM
Analytical
Experimental
0
1
2
3
4
5
0
0.2
0.4
0.6

Fig. 65

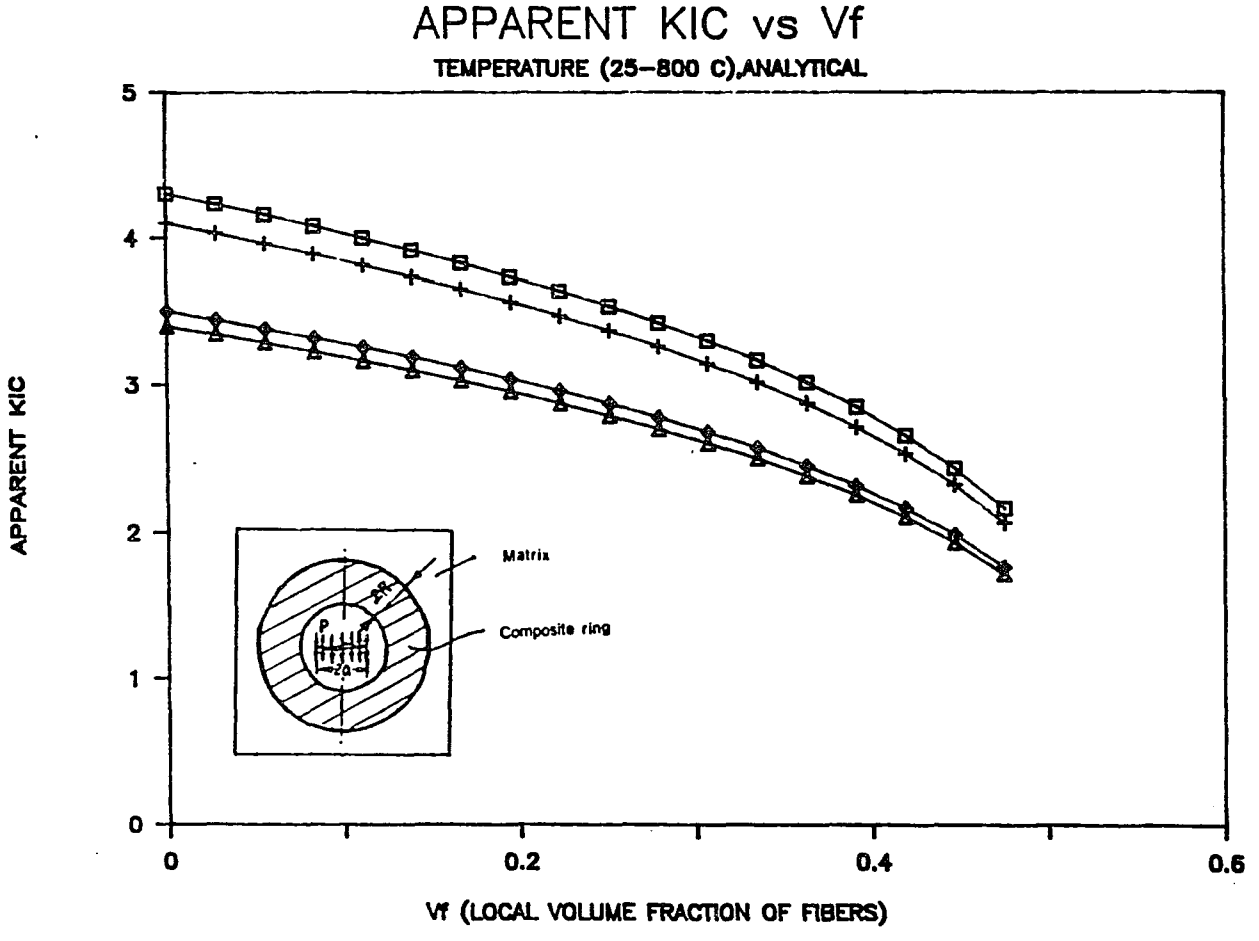
APPARENT KIC vs Vf
TEMPERATURE (25–800 C),ANALYTICAL
APPARENT KIC
Vf (LOCAL VOLUME FRACTION OF FIBERS)
0
1
2
3
4
5
0
0.2
0.4
0.6
Matrix
Composite ring
P
2R
2a

Fig. 66

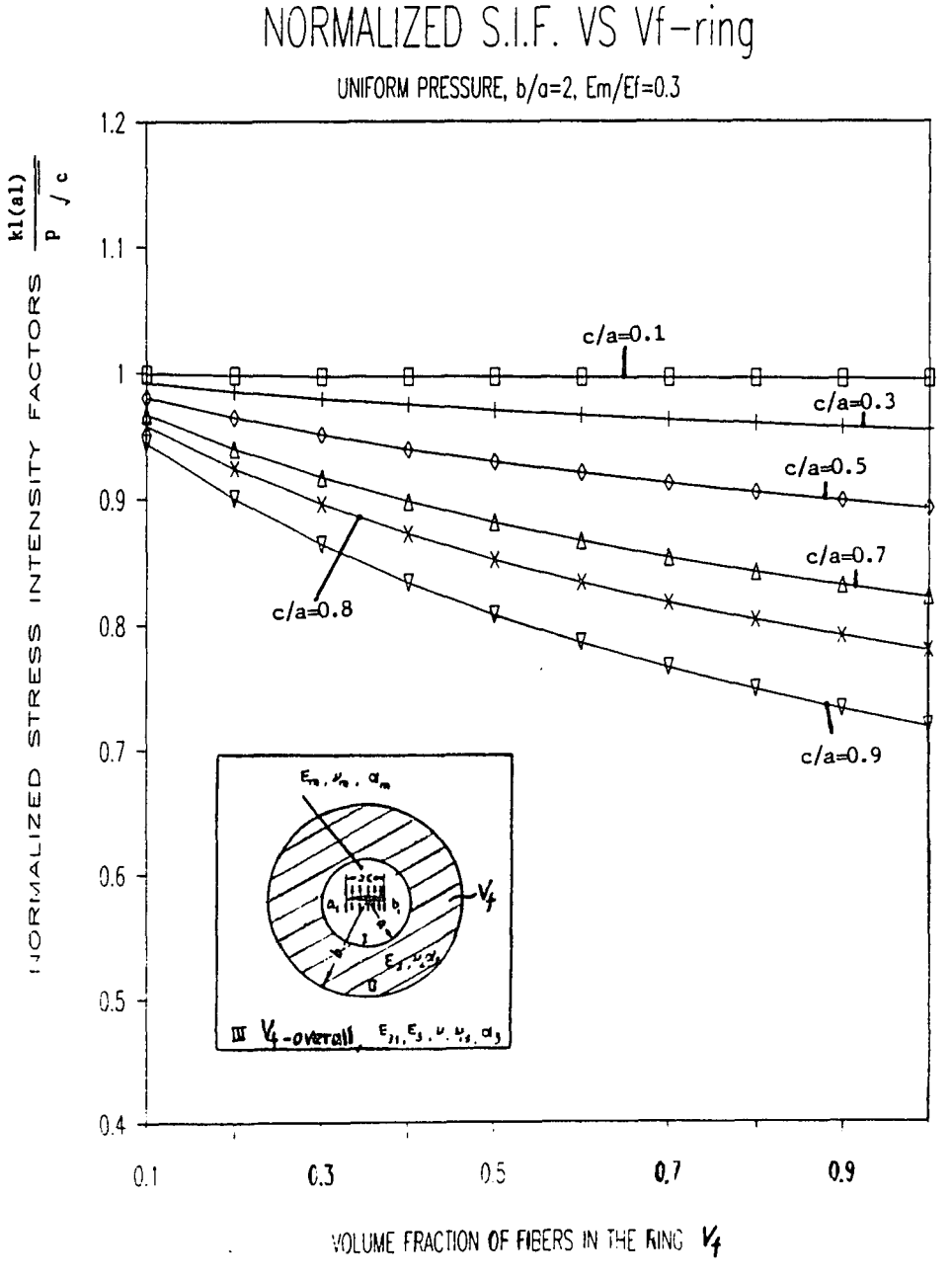
NORMALIZED S.I.F. VS Vf-ring
UNIFORM PRESSURE, b/a=2, Em/Ef=0.3
NORMALIZED STRESS INTENSITY FACTORS k1(a1) / p √c
1.2
1.1
1
0.9
0.8
0.7
0.6
0.5
0.4
c/a=0.1
c/a=0.3
c/a=0.5
c/a=0.7
c/a=0.8
c/a=0.9
0.1
0.3
0.5
0.7
0.9
VOLUME FRACTION OF FIBERS IN THE RING Vf

Fig. 67

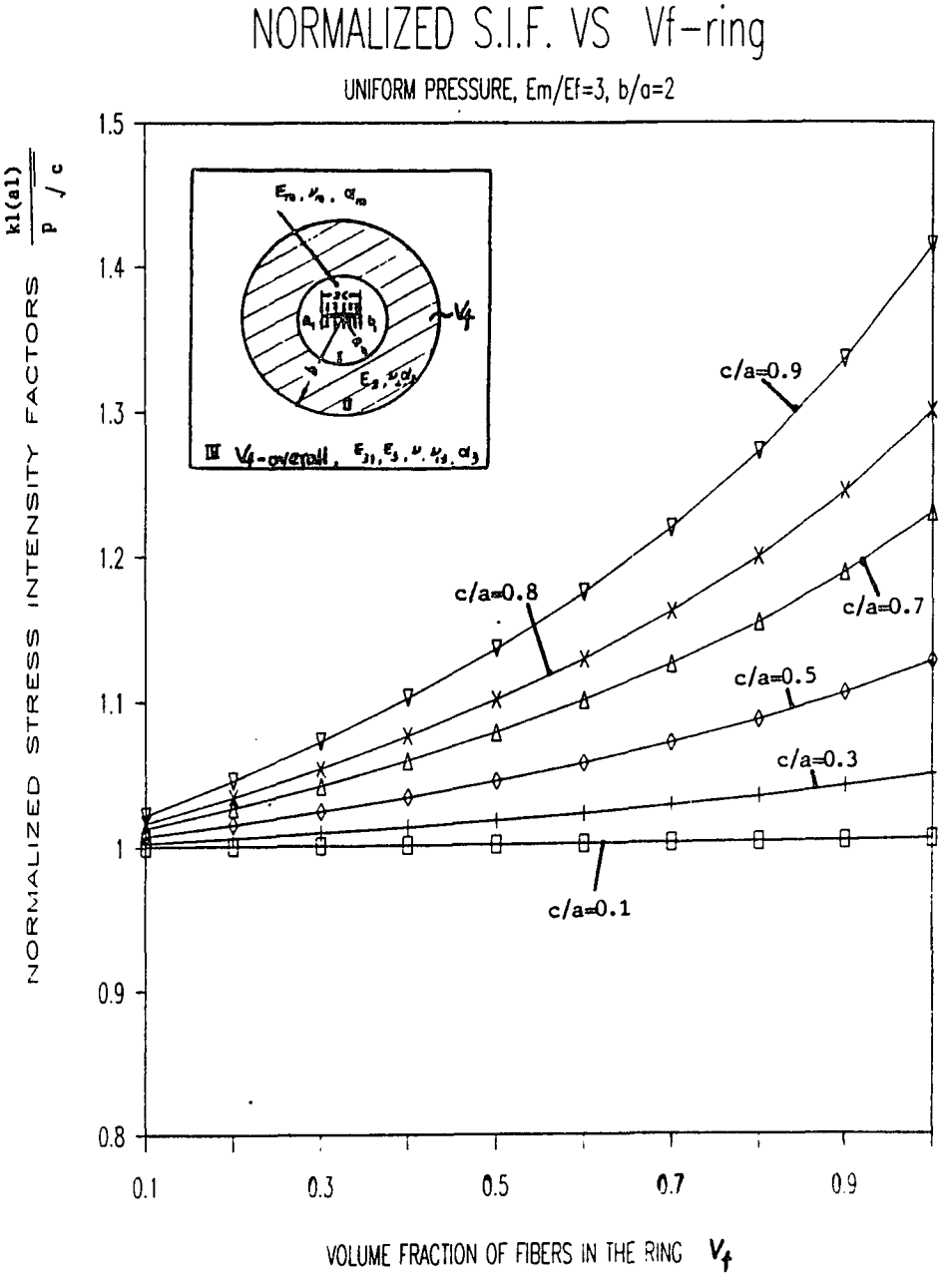
NORMALIZED S.I.F. VS Vf-ring
UNIFORM PRESSURE, Em/Ef=3, b/a=2
NORMALIZED STRESS INTENSITY FACTORS k1(a1) / p √c
1.5
1.4
1.3
1.2
1.1
1
0.9
0.8
0.1
0.3
0.5
0.7
0.9
c/a=0.9
c/a=0.8
c/a=0.7
c/a=0.5
c/a=0.3
c/a=0.1
VOLUME FRACTION OF FIBERS IN THE RING Vf

Fig. 68

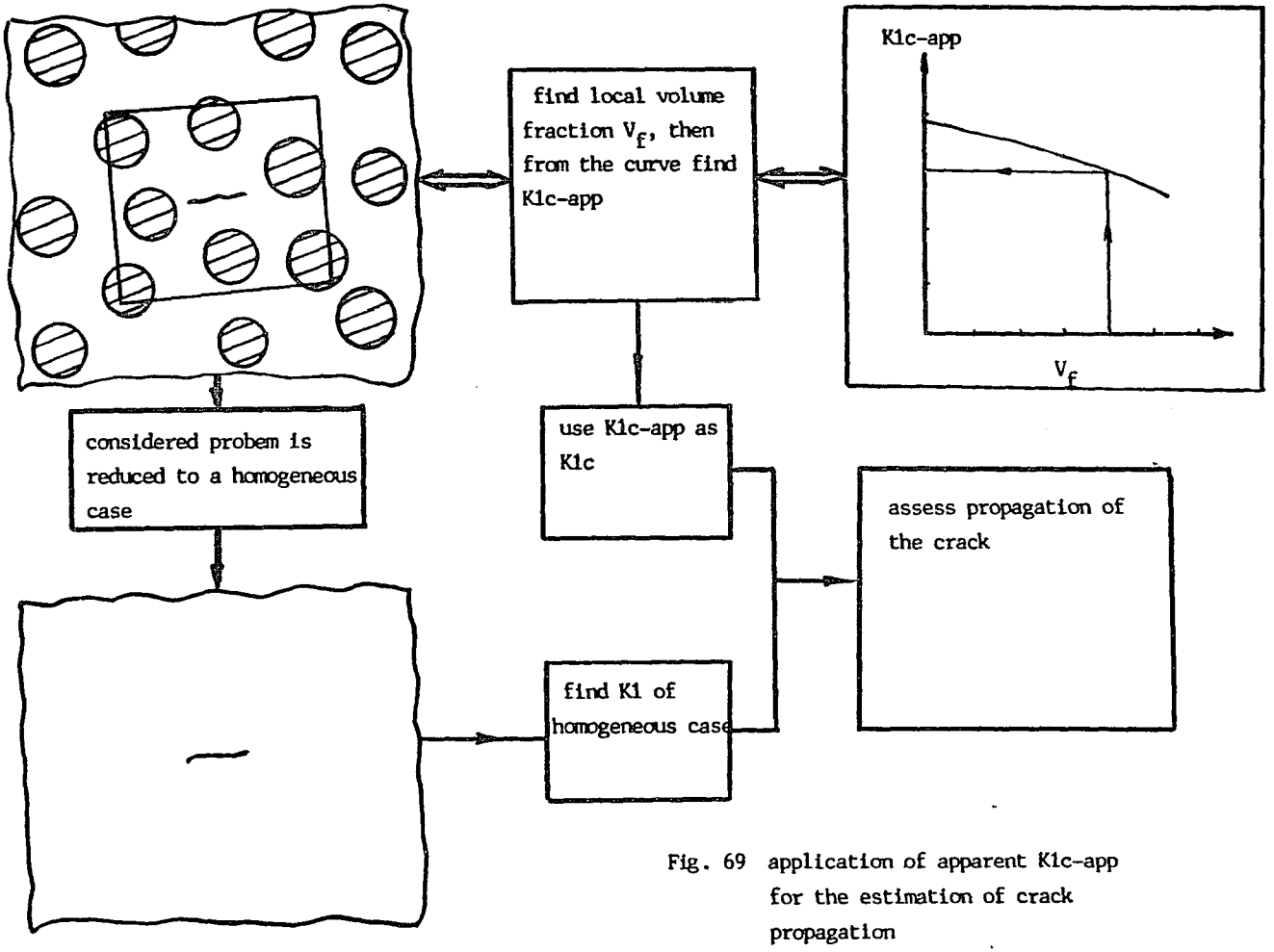

Fig. 69 application of apparent Klc-app for the estimation of crack propagation

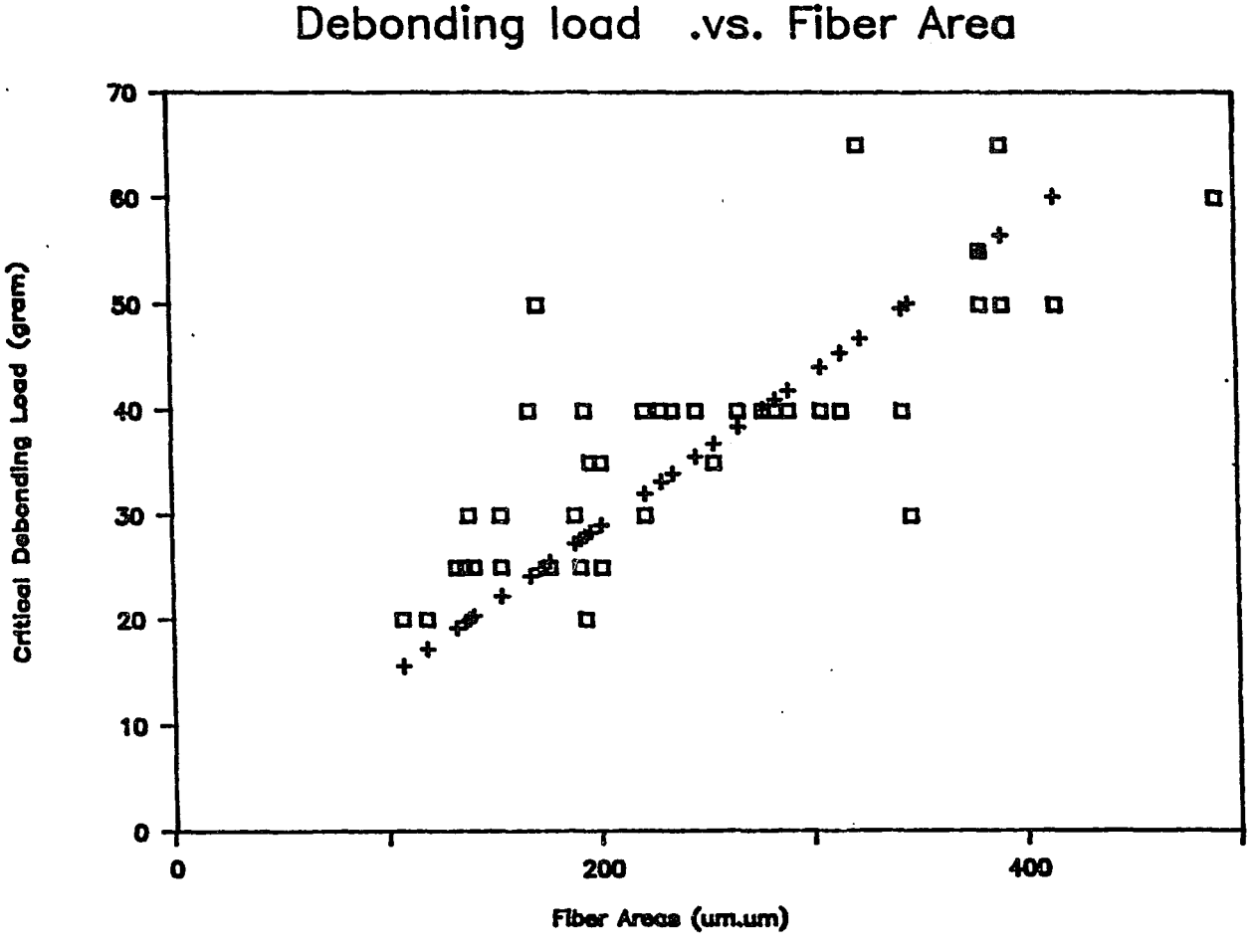
Debonding load .vs. Fiber Area
Critical Debonding Load (gram)
70
60
50
40
30
20
10
0
0
200
400
Fiber Areas (um.um)

Fig. 70

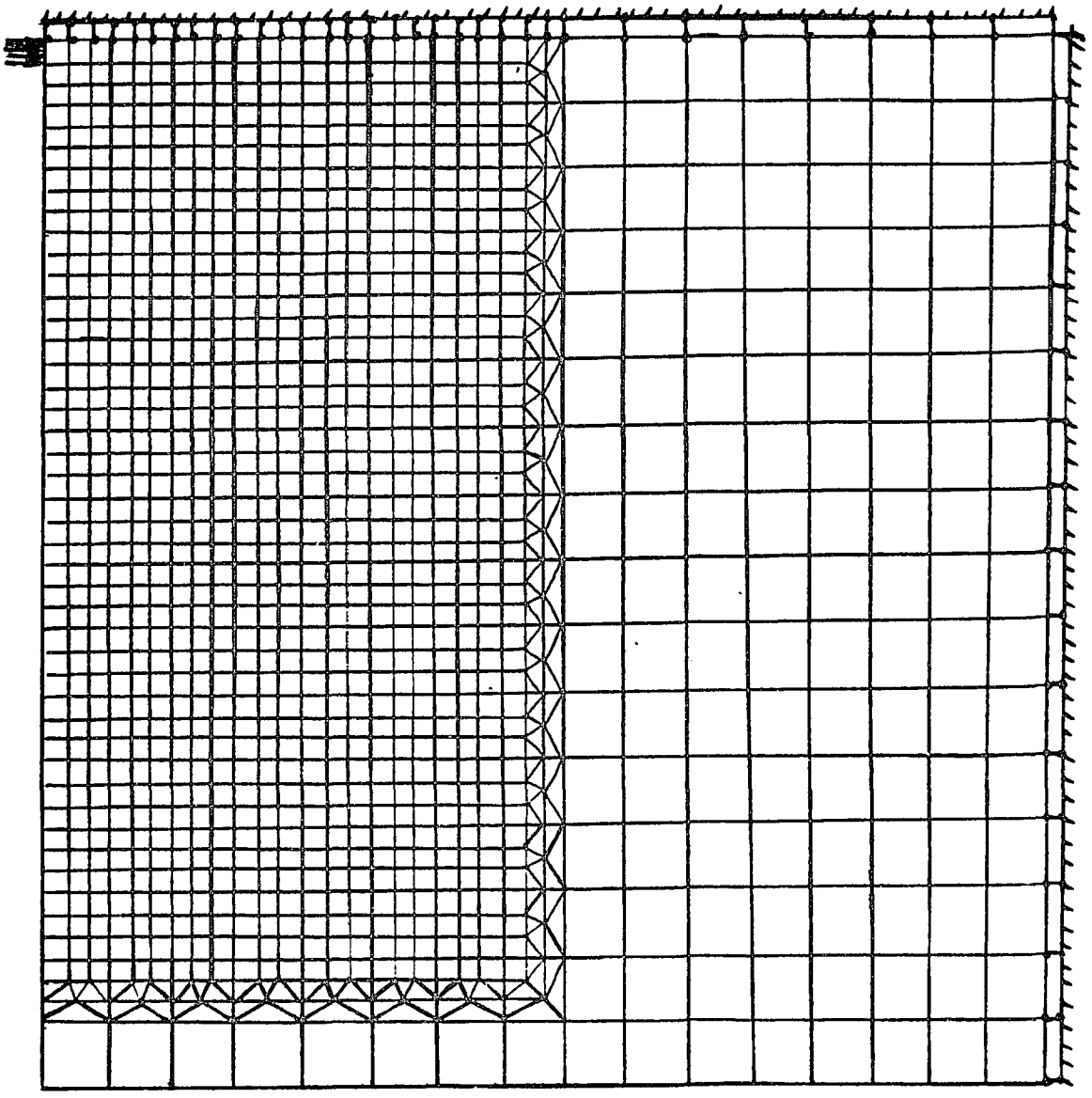

finite element mesh
(debonding model)

Fig. 71

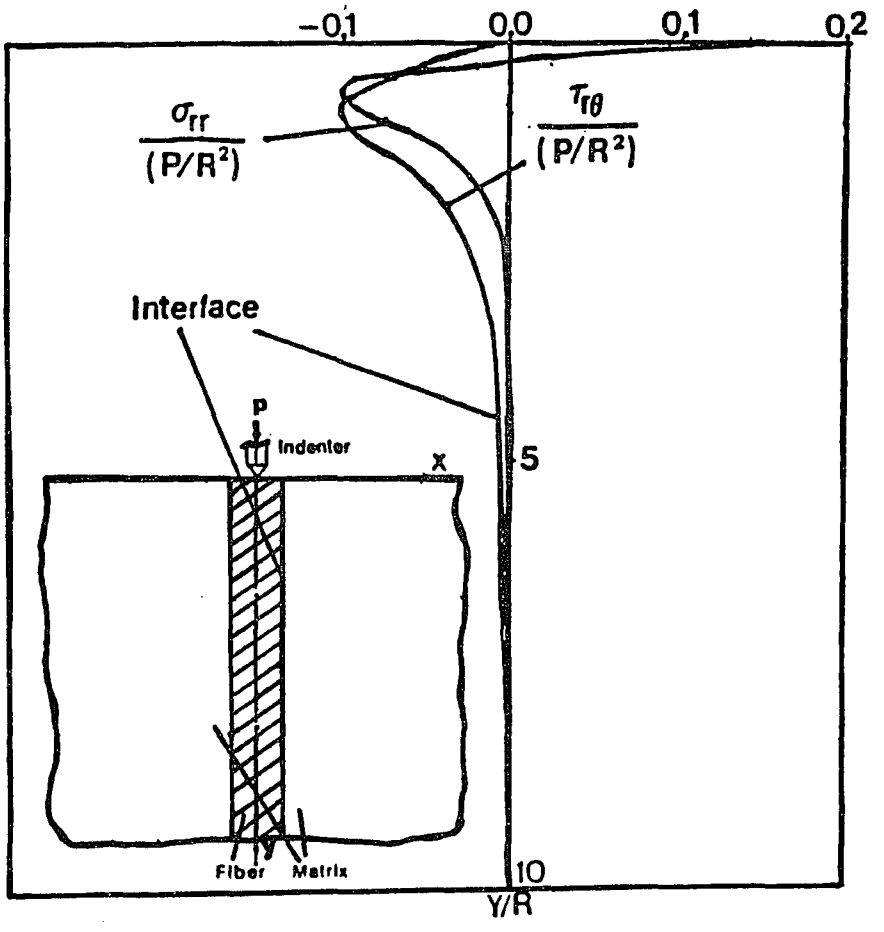

Stress distributions on the interface along the fiber axial direction under debonding loading

Fig. 72

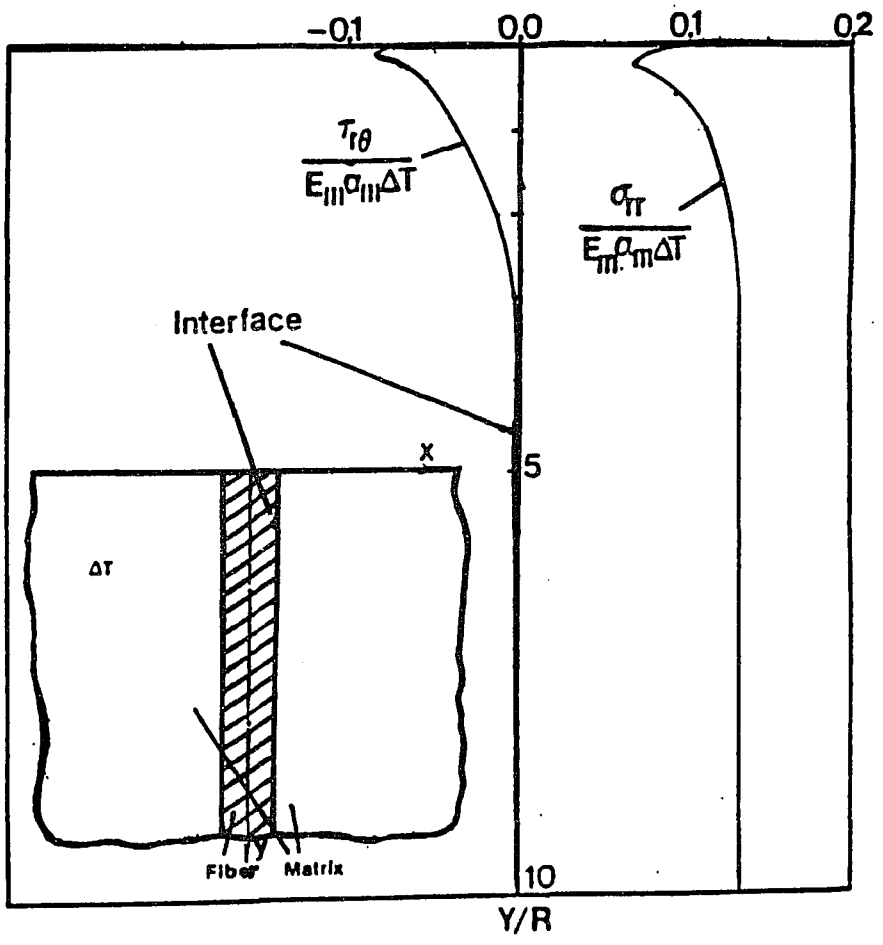

Stress distributions on the interface along the fiber axial direction under high temperature

Fig. 73

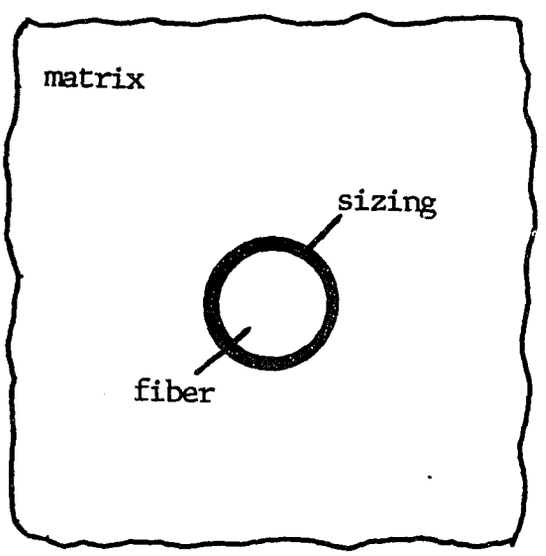

Fig. 74 sizing effect

APPENDIX I
SOLUTION OF UNCRACKED RING MODEL PROBLEMS

The definition of ring model has been given in chapter II. In brief, ring model consists of the following three domains:

1) circular disk domain, $r \leq a$, matrix material with Young's modulus E_m, Possion's ratio ν_m, thermal expansion coefficient α_m.

2) annular domain, $a \leq r \leq b$, composite, isotropic material with Young's modulus E_2, Possion's ratio ν_2 and thermal expansion coefficient α_2.

3)infinitely extended domain, $b \leq r$, composite, assumed mechanically transversely isotropic and thermally isotropic material, constitutive equation can be found in chapter IV and definitions for the engineering constants of this domain are as follows:

E : Young's modulus in x_1-x_2 plane (see Fig. 3)

E_3: Young's modulus in x_3 direction (see Fig. 3)

ν : Poisson's ratio in x_1-x_2 plane (see Fig. 3)

ν_{31} : Poisson's ratio for transverse strain in any direction in x_1-x_2 plane due to stress in x_3 direction (see Fig. 3).

Accordingly, $\frac{\nu_{31}}{E_3} = \frac{\nu_{13}}{E}$

G_3: shear modulus in plane parallel to x_3 axis.

FORMULATION OF THE PROBLEM

To formulate the problem under consideration, Michell's general solutions are referred to. After assuming proper stress functions for the disk, ring and infinite domains, and matching stresses and displacements at the interfaces the constants in the stress functions can be determined. The stresses and displacements in all the three domains are also determined. In this chapter both mechanical (uniaxial traction) and thermal loading cases are considered.

Assumption of solutions for disk, ring and infinite domains

a. Disk

For the problem under consideration stresses and displacements satisfy the following symmetry conditions:

$$\sigma_{rr}(r,\theta) = \sigma_{rr}(r,-\theta)$$

$$\sigma_{\theta\theta}(r,\theta) = \sigma_{\theta\theta}(r,-\theta)$$

$$\sigma_{r\theta}(r,\theta) = -\sigma_{r\theta}(r,-\theta)$$

$$u_r(r,\theta) = u_r(r,-\theta)$$

$$u_\theta(r,\theta) = -u_\theta(r,-\theta)$$

After taking regularity and symmetry conditions into consideration, stresses and displacements for the disk domain can be assumed as

$$\sigma_{rr1}(r,\theta)=2c_{01}-2a_{21}\cos 2\theta \quad (1)$$

$$\sigma_{\theta\theta 1}(r,\theta) = 2c_{01}+(2a_{21}+ 6b_{21}r^{2})\cos 2\theta \quad (2)$$

$$\sigma_{r\theta 1}(r,\theta) = (2a_{21}+ 6b_{21}r^{2})\sin 2\theta \quad (3)$$

displacements are found to be

$$u_{r1}(r,\theta)=\frac{1-\nu_1^2}{E_1}\left[\frac{2(1-2\nu_1)}{1-\nu_1}c_{01}r-\left(\frac{2}{1-\nu_1}a_{21}r+b_{n1}\frac{4\nu_1}{1-\nu_1}\right)r^{3}\right)\cos 2\theta]+$$

$$(1+\nu_1)\alpha_1\Delta Tr + S_2\cos\theta \quad (4)$$

$$u_{\theta 1}(r,\theta)=\frac{1-\nu_1^2}{E_1}\left(\frac{2}{1-\nu_1}a_{21}r+b_{21}\frac{6-4\nu_1}{1-\nu_1}r^{3}\right)\sin 2\theta\Big\} - S_2\sin\theta \quad (5)$$

c. Ring

Stresses and displacements in the ring can be assumed as:

$$\sigma_{rr2}(r,\theta)=\frac{b^{2}}{r^{2}}+2c_{02} - (a_{22}+ 6c_{22}r^{-4}+ 4d_{22}r^{-2})\cos 2\theta \quad (6)$$

$$\sigma_{\theta\theta 2}(r,\theta)=-\frac{b_{02}}{r^2}+2c_{02}+(2a_{22}+12b_{22}r^2+6c_{22}r^{-4})\cos 2\theta \qquad (7)$$

$$\sigma_{r\theta 2}(r,\theta)=2(a_{22}+3b_{22}r^2-3c_{22}r^{-4}-d_{22}r^{-2})\sin 2\theta \qquad (8)$$

$$u_{r2}(r,\theta)=\frac{1-\nu_2^2}{E_2}\left[-\frac{b_{02}}{1-\nu_2}\frac{1}{r}+\frac{2(1-2\nu_2)}{1-\nu_2}c_{02}r-\left(\frac{2}{1-\nu_2}a_{22}r+\frac{4\nu_2}{1-\nu_2}\right.\right.$$

$$\left.\left.b_{n2}r^3-\frac{2}{1-\nu_2}c_{22}r^{-3}-4d_{22}r^{-1}\right)\right]\cos 2\theta\Bigg\}+(1+\nu_2)\alpha_2\Delta Tr+S_3\cos\theta \qquad (9)$$

$$u_{\theta 2}(r,\theta)=\frac{1-\nu_2^2}{E_2}\left(\frac{2}{1-\nu_2}a_{22}r^1+\frac{6-4\nu_2}{1-\nu_2}b_{22}r^3+\frac{2}{1-\nu_2}c_{22}r^{-3}+\frac{-2+4\nu_2}{1-\nu_2}d_{22}\right.$$

$$\left.r^{-1}\right)\sin 2\theta \qquad (10)$$

d. Infinite domain

Stresses for the infinite domain can be assumed as

$$\sigma_{rr3}(r,\theta)=\frac{\sigma_0}{2}+\frac{b_{03}}{r^2}-\left(\frac{\sigma_0}{2}+6c_{23}r^{-3}+4d_{23}r^{-2}\right)\cos 2\theta \qquad (11)$$

$$\sigma_{\theta\theta 3}(r,\theta)=\frac{\sigma_0}{2}-\frac{b_{03}}{r^2}+\left(\frac{\sigma_0}{2}+6c_{23}r^{-3}\right)\cos 2\theta \qquad (12)$$

$$\sigma_{r\theta 3}(r,\theta)=-\left(-\frac{\sigma_0}{2}+6c_{23}r^{-3}+2d_{23}r^{-2}\right)\sin 2\theta \qquad (13)$$

where σ_0 is uniaxial traction acting at infinity in y direction, displacements can be written as :

$$u_{r3}(r,\theta)=\frac{1}{E'}\left[-(1+\nu')\frac{b_{03}}{r}+\frac{\sigma_0}{2}(1-\nu')r+[2(1+\nu')c_{23}r^{-3}+4d_{23}r^{-1}-\right.$$

$$\left.\frac{\sigma_0}{2}(1+\nu')r]\cos 2\theta\right]+\quad(1+\nu_{31})\alpha_3\Delta T \qquad (14)$$

$$u_{\theta 3}(r,\theta)=\frac{1}{E'}[2(1+\nu')c_{23}r^{-3}+2(-1+\nu')d_{23}r^{-1}+\frac{\sigma_0}{2}(1+\nu')r]\sin 2\theta \qquad (15)$$

e. Boundary condition

Having assumed the basic form of solutions, the unknown constants in those equations can be determined by substituting them into the following continuity conditions:

$$\sigma_{rr1}(a,\theta) = \sigma_{rr2}(a,\theta) \qquad (16)$$

$$\sigma_{r\theta 1}(a,\theta) = \sigma_{r\theta 2}(a,\theta) \qquad (17)$$

$$u_{r1}(a,\theta) = u_{r2}(a,\theta) \qquad (18)$$

$$u_{\theta 1}(a,\theta) = u_{\theta 2}(a,\theta) \qquad (19)$$

$$\sigma_{rr2}(b,\theta) = \sigma_{rr3}(b,\theta) \qquad (20)$$

$$\sigma_{r\theta 2}(b,\theta) = \sigma_{r\theta 3}(b,\theta) \qquad (21)$$

$$u_{r2}(b,\theta) = u_{r3}(b,\theta) \qquad (22)$$

$$u_{\theta 2}(b,\theta) = u_{\theta 3}(b,\theta) \qquad (23)$$

By substituting eqns (1-15) into eqns (16-23), we obtain two sets of simultaneous equations as follws:

$$2c_{01} - \frac{b_{02}}{a^2} - 2c_{02} = 0 \qquad (24)$$

$$\frac{2(1-2\nu_1)(1+\nu_1)}{E_1} ac_{01} + \frac{(1+\nu_2)}{E_2} \frac{1}{a} b_{02} - \frac{2(1-2\nu_2)(1+\nu_2)}{E_2} ac_{02} =$$

$$[(1+\nu_2)\alpha_2 - (1+\nu_m)\alpha_m]\Delta Ta \qquad (25)$$

$$\frac{b_{02}}{b^2} + 2c_{02} - \frac{b_{03}}{b^2} = \frac{\sigma_0}{2} \qquad (26)$$

$$-\frac{(1+\nu_2)}{E_2} \frac{1}{b} b_{02} + \frac{2(1+\nu_2)(1-2\nu_2)}{E_2} bc_{02} + \frac{(1+\nu')}{E'} \frac{1}{b} b_{03} =$$

$$\frac{\sigma_0(1-\nu')}{2E'} b + [(1+\nu_{31})\alpha_3 - (1+\nu_2)\alpha_2]\Delta Tb \qquad (27)$$

$$2a_{21} + 6a^2 b_{21} - 2a_{22} - 6a^2 b_{22} + 6a^{-4} c_{22} + 2a^{-2} d_{22} = 0 \qquad (28)$$

$$-2a_{21} + 2a_{22} + 6a^{-4} c_{22} + 4a^{-2} d_{22} = \qquad (29)$$

$$-\frac{2(1+\nu_1)}{E_1}aa_{21}-4\nu_1\frac{1+\nu_1}{E_1}a^3b_{21}+\frac{2(1+\nu_2)}{E_2}aa_{22}+4\nu_2\frac{1+\nu_2}{E_2}a^3b_{22}-\frac{2(1+\nu_2)}{E_2}a^{-3}c_{22}-$$

$$4(1-\nu_2)\frac{1+\nu_2}{E_2}a^{-1}d_{22}=0 \qquad (30)$$

$$\frac{2(1+\nu_1)}{E_1}aa_{21}+(6-4\nu_1)\frac{1+\nu_1}{E_1}a^3b_{n1}-\frac{2(1+\nu_2)}{E_2}aa_{22}-(6-4\nu_2)\frac{1+\nu_2}{E_2}a^3b_{22}-\frac{2(1+\nu_2)}{E_2}a^{-}$$

$$^3c_{22}-(4\nu_2-2)\frac{1+\nu_2}{E_2}a^{-1}d_{22}=0 \qquad (31)$$

$$-\frac{2(1+\nu_2)}{E_2}ba_{22}-4\nu_2\frac{1+\nu_2}{E_2}b^3b_{22}+\frac{2(1+\nu_2)}{E_2}b^{-3}c_{22}-4(1-\nu_2)\frac{1+\nu_2}{E_2}b^{-1}d_{22}-$$

$$-\frac{2(1+\nu_2)}{E_2}ba_{22}-4\nu_2\frac{1+\nu_2}{E_2}b^3b_{22}+\frac{2(1+\nu_2)}{E_2}b^{-3}c_{22}-4(1-\nu_2)\frac{1+\nu_2}{E_2}b^{-1}d_{22}-$$

$$\frac{22(1+\nu')}{E'}b^{-3}c_{23}-\frac{1}{E'}b^{-1}d_{23}=-\frac{2(1+\nu')}{E'}b\sigma_0 \qquad (32)$$

$$\frac{2(1+\nu_2)}{E_2}ba_{22}+(6-4\nu_2)\frac{1+\nu_2}{E_2}b^3b_{22}+\frac{2(1+\nu_2)}{E_2}b^{-3}c_{22}+(4\nu_2-2)\frac{1+\nu_2}{E_2}b^{-1}d_{22}-$$

$$\frac{2(1+\nu')}{E'}b^{-3}c_{23}+\frac{2(1-\nu')}{E'}b^{-1}d_{23}=\frac{2(1+\nu')}{E'}b\sigma_0 \qquad (33)$$

$$-2a_{22}-\qquad 6b^{-4}c_{22}-4b^{-2}d_{22}+6b^{-4}c_{23}+4b^{-2}d_{23}=-\frac{\sigma_0}{2} \qquad (34)$$

$$2a_{22}+6b^{2}b_{23}- 6b^{-4}c_{22}-2b^{-2}d_{22} + 6b^{-4}c_{23}+2b^{-2}d_{23} =\frac{\sigma_0}{2} \quad (35)$$

After solving the simultaneous equations, stresses and displacements in all the three domains are determined and given by eqns(1-15). If $\Delta T=0$, $\sigma_0\neq 0$, solution is reduced to that for uniaxial traction case, If $\sigma_0=0$, $\Delta T\neq 0$, solution is reduced to that for thermal loading case. When both of them are not zero, the solution is for combined mechanical and thermal loadings.

BIBLIOGRAPHY

1. Schioler, 1. J. and Stoglich, J. J., "Ceramic Matrix Composites: A Literature Review", Ceramic Bulletin, Vol. 65, No.2, pp. 287-292, ed. by Schioler, L. J., 1986.

2. Rice, R.W.,"Fractograghic Identification of Strength Controlling Flaws and Microcracking" in Fracture Mechanics of Ceramics, Vol. 1, ed. by Bradt, R. C., Hasselman, D. P. H. and Lange, F. F., Plenum Press, New York, pp. 323-345, 1974.

3. Rice, R.W., Frieman, S.W., Pohanka, R.C., Mecholsky, J.J. and Wu, C.C., "Microstructural Dependence of Fracture Mechanics Parameters in Ceramics" in Fracture Mechanics of Ceramics, Vol.4, ed. by Bradt, R. C., Hasselman, D. P. H. and Lange, F. F., Plenum Press, New York, pp. 840-876, 1978.

4. Rice, R.W., "Microstructural Dependence of Mechanical Behavior of Ceramics" in Treatise on Materials Science and Technology, Vol. II, Properties and Microstructure, ed. by McCrone, R.K., Academic Press, New York, pp. 199-381, 1977.

5. Rice, R.W., Pohanka, R.C., McDonough, W.J., "Effect of Stresses from Thermal Expansion Anisotropy, Phase Transformations and Second Phases on the Strength of Ceramics", Journal of American Ceramic Society, Vol. 63, pp. 703-710, 1980.

6. Rice, R.W., "Processing Induced Sources of Mechanical Failure in Ceramics" in Processing of Crystalline Ceramics, ed. by Palmour,

H., III, Davis, R.F., Hare, T.M., Plenum Press, New York, pp. 303-319, 1978.

7. Baratta, F.I., "Stress Intensity Factor Estimates for a Peripherically Cracked Spherical Void and a Hemispherical Surface Pit", Journal of American Ceramic Society, Vol. 61, pp. 490-493, 1978.

8. Evans, A.G., Biswas, D.R. and Fulrath, R. M., "Some Effects of Cavities on the Fracture of Ceramics: I, Cylindrical Cavities," Journal of American Ceramic Society, Vol. 62, pp. 95-100, 1979.

9. Evans, A.G., Biswas, D.R. and Fulrath, R. M., "Some Effects of Cavities on the Fracture of Ceramics: II, Spherical Cavities," Journal of American Ceramic Society, Vol. 62, pp. 101-106, 1979.

10. Clarke, F. J. P., Acta Met., Vol. 12, pp. 139,1964.

11. Kuszyk, J. A. and Bradt, R. C., Journal of American Ceramic Society, Vol. 56, pp. 420, 1973.

12. Matsuo, Y. and Sasaki, H., Journal of American Ceramic Society, Vol. 49, pp. 229, 1966.

13. Davidge, R. W. and Tappin, G., Journal of Materials Science, Vol. 3, pp. 297, 1968.

14. Evans, A. G., "Microfracture from Thermal Expansion Anistropy - I. Single Phase System," Acta Met., Vol. 26, PP. 1845-1853, 1978.

15. Kristic, V. D., "Critical Grain Size/Preexisting Flaw Size Relation in Anisotropic Brittle Solids," Journal of American Ceramic Society, Vol. 66, pp. 726-729, 1983.

16. Clarke, D. R., "Microfracture in Brittle Solids Resulting from Anisotropic Shape Changes," Acta Met., Vol. 18, pp. 913-924, 1980.

17. Fu, Y., Evans, A. G. and Kriven, W. M., "Microcrack Nucleation in Ceramics Subjected to Phase Transformation," Journal of American Ceramic Society, Vol. 67, pp. 626-630, 1984.

18. Lawn, B. R. and Swain, M. V., "Microfracture Beneath Point Indentations in Brittle Solids," Journal of Materials Science, Vol. 10, pp. 113-122, 1975.

19. Green, D. J., "Microcracking Mechanisms in Ceramics," in Fracture Mechanics of Ceramics, Vol. 5, pp. 457-478, ed. by Bradt, R. C., Evans, A. G., Hasselman, D. P. H. and Lange, F. F., Plenum Press, New York, 1983.

20. Rice, R. W. and Lewis, D., III, "Limitation and Challenge in Applying Fracture Mechanics to Ceramics," in Fracture Mechanics of Ceramics, Vol. 5, ed. by Bradt, R. C., Evans, A. G., Hasselman, D. P. H. and Lange, F. F., Plenum Press, New York, pp. 659-676, 1983.

21. Davidge, R. W., "Mechanical Behavior of Ceramics," Cambridge University Press, 1979.

22. Lange, F. F., "Criteria for Crack Extension and Arrest in Residual Localized Stress Field Associated with Second Phase

Particles," in Fracture Mechanics of Ceramics, Vol. 2, ed. by Bradt, R. C., Hasselman, D. P. H. and Lange, F. F., Plenum Press, New York, 1974

23. Davidge, R.W. and Green, J.J., "The Strength of Two-Phase Ceramic-Glass Materials", Journal of Materials Science, Vol.3, pp.629-634, 1968.

24. Evans, A. G., "The Role of Inclusions in the Fracture of Ceramic Materials," Journal of Materials Science, Vol. 9, pp. 1145-1152, 1974.

25. Ito, Y. M., Rosenblatt, M., Cheng, L. Y., Lange, F. F. and Evans, A. G., "Cracking in Particulate Composites due to Thermomechanical Stress," International Journal of Fracture, Vol. 27, pp. 483-491, 1981.

26. Wilkens, M. L., "Calculation of Elastic-Plastic Flow," Lawrence Livermore, UCRL-7322, 1969.

27. Ito, Y. M., Rosenblatt, M., Perry, F. W. and Eggum, G. E., "Analysis of Water Drop Erosion Mechanisms," Air Force Materials Laboratory, AFML-77-219, 1977.

28. Green, D. J., "Stress-Induced Microcracking at Second Phase Inclusions," Journal of American Ceramic Society, Vol. 64, pp. 138-141, 1981

29. Cook, R.F., Lawn, B.R. and Fairbanks, C.J., "Microstructure-Strength Properties in Ceramics:I, Effect of Crack Size on

Toughness", Journal of American Ceramic Society, 68[11], pp. 604-615, 1985.

30. Michalske, Terry. A. and Hellmann, John. R., "Strength and Toughness of Continuous-Alumina-Fiber-Reinforced Glass-Matrix Composites", Journal of American Ceramic Society, Vol 71, No 9, pp. 725-731, 1988.

31. Mecholsky, J. J., "Evaluation of Mechanical Property Testing Methods for Ceramic Matrix Composites", Ceramic Buttetin, Vol. 65, No.2, pp. 315-321, ed. by Schioler, L. J., 1986.

32. Prewo, K. M., Brennan, J. J. and Layden, G. K., "Fiber Reinforced Glass and Glass-Ceramics for High Performence Applications", Ceramic Buttetin, Vol. 65, No.2, pp. 305-313, ed. by Schioler, L. J., 1986..

33. Niihata, K., Nakahira, A., Uchiyyama, T. and Hirai, T., "High-Temperature Mechanical Properties of Al_2o_3-SiC Composites", Fracture Mechanics of Ceramics, Vol. 5, pp. 103-116, ed. by Bradt, R. C., Evans, A. G., Hasselman, D. P. H. and Lange, F. F., Plenum Press, New York, 1983.

34. Marshall, D. B. and Evans, A. G., "Failure Mechanisms in Ceramic-Fiber/Ceramic-Matrix Composites", Journal of American Ceramic Society, Vol 68, No 5, pp. 225-231, 1985.

35. Marshall, D. B., "An Indentation Method for Measuring Matrix-Fiber Frictional stresses in Ceramic Composites", Communication of American Ceramic Society, c 259-260, 1984.

36. Marshall, D. B. and Evans, A. G., "The Tensile Strength of Uniaxially Reinforced Ceramic Fiber Composites", in Fracture Mechanics of Ceramics, Vol. 5, pp. 1-15, ed. by Bradt, R. C., Evans, A. G., Hasselman, D. P. H. and Lange, F. F., Plenum Press, New York, 1983.

37. Faber, K. T., Advani, S. H., Lee, J. K., Jinn and J. T., "Frictional Stress Evaluation Along the Fiber-Matrix Interface in Ceramic Matrix Composites", Journal of American Ceramic Society, 69 [9], c 208-209, 1986.

38. Hsueh, C. H., "Analytical Evaluation of Interfacial Shear Strength for Fiber-Reinforced Ceramic Composites", Journal of American Ceramic Society, 71[6], pp. 490-493, 1988.

39. Shetty, D. K., "Shear-Lag Analysis of Fiber Push-Out (Indentation) Tests for Estimate Interfacial Friction Stress in Ceramic-Matrix Composites", Journal of American Ceramic Society, 71[2], c 107-109, 1988

40. Grande, D. H., Mandell, J. F. and Hong, K. C. C., "Fiber-Matrix Bond Strength Studies of Glass, Ceramic, and Metal Matrix Composites", Journal of Materials Science, Vol. 23, pp 311-328, 1988.

41. Delale, F., "Critical Fiber Size For Microcrack Suppression in Ceramic-Fiber/Ceramic-Matrix Composites", Engineering Fracture Mechanics, Vol. 31, pp. 145-155, 1988.

42. Atkinson, C., "The Interaction Between A Crack and An Inclusion", International Journal of Engineering and Science, 1972, Vol. 10, pp 127-136.

43. Erdogan, F. and Gupta, G. D., "The Inclusion Problem With A Crack Crossing the Boundary", International Journal of Fracture, Vol. 11, No 1, pp. 13-27, 1975.

44. Toya, M., "A Crack Along the Interface of A Circular Inclusion Embedded in A Infinite Solid", Journal of Mechanics and Physics of Solids, Vol. 22, pp 325-348, 1974.

45. ANSYS, Swanson Analysis System, Inc, Houston, PA.

46. Dundurs, J. and Mura, T., "Interaction Between An Edge Dislocation and A Circular Inclusion", Journal of Mechanics and Physics of Solids, Vol. 12, pp 177-189, 1964.

47. R.W. Little, Elasticity, Prentice Hall, Englewood Cliffs, New Jersey. (1973).

48. Gradshteyn, I. S. and Ryzhik, I. M., "Table of Integrals, Series, and Products", ACADEMIC PRESS, New York, 1980.

49. Muskhelishvili, N. I., Singular Integral Equations. P. Noordhoff N. V., Groningen, Holland, 1953.

50. Erdogan, F., "Mixed Boundary Value Problems in Mechanics", in Mechanics Today, Vol. 2, pp. 1-86, 1986.

51. Erdogan, F. and Gupta, G. D., "ON the Numerical Solution of Singular Integral Equations", Quarterly of Applied Mathematics, Vol. 29, pp. 525-534, 1972.

52. F. Delale and F. Erdogan, "Stress Intensity Factors in a Hollow Cylinder Containing a Radial Crack", International Journal of Fracture, Vol. 20, pp. 251-265, 1982.

53. D.P. Rooke and J. Tweed, "The Stress Intensity Factors of a Radial Crack in a Finite Rotating Elastic Disk", International Journal of Engineering and Science, Vol.10(8), pp. 709-714, 1972.

54. D.P. Rooke and J. Tweed, "The Stress Intensity Factors of an Edge Crack in a Finite Rotating Elastic Disk", International Journal of Engineering and Science, Vol.11, pp. 279-283, 1973.

55. J. Tweed and D.P. Rooke, "The Stress Intensity Factor of an Edge Crack in a Finite Elastic Disk", International Journal of Engineering and Science, Vol.11, pp. 65-73, 1973.

56. O.L. Bowie and D.M. Neal, "A Modified Mapping Collocation Technique for Accurate Calculation of Stress Intensity Factors", International Journal of Fracture, Vol.6, pp. 199-206, 1970.

57. M. Isida, "Arbitrary Loading Problems of Doubly Symmetric Regions Containing a Central Crack, Engineering Fracture Mechanics, Vol.7(3), pp. 505-514, 1975.

58. Delale, F. and Xu, Y. L., "Stress Field of a Circular Disk Containing an Edge Dislocation and its Application to the

Solution of Disk Crack Problems"", to appear on Bullitin of Istanbul Technical University.

59. Lawn, B. and Wilshaw, R., "Review: Indentation Fracture: Principles and Applications", Journal of Materials Science, Vol. 10, pp. 1049-1081, 1975.

60. Evans, A. G., "Fracture Toughness: The Role of Indentation Techniques", in Fracture Mechanics Applied to Brittle Materials, ASTM STP 678, edited by S.W. Freiman, pp 112-115, 1979.

61. Marion, R. H., "Use of Indentation Fracture to Determine Fracture Toughness", in Fracture Mechanics Applied to Brittle Materials, ASTM STP 678, edited by S.W. Freiman, pp 103-111, 1979.

62. Xu, Y. L., Delale, F. and Liaw, B. M.,"Effect of Temperature and Fiber Distribution on Matrix Microcracking in Ceramic Matrix Composites", submitted to ASME, Journal of Engineering Materials and Technology.

63. Delale, F., Xu, Y. L., and Liaw, B. M., "High Temperature Effect in Ceramic Matrix Composites", in Visco-Plastic Behavior of New Materials, ed. D. Hui and T. J. Kozik, ASME, 1989.

64. Erdogan, F. and Biricikogln, V., "Two Bonded Half Planes with a Crack Going Through the Interface", International Journal of Engineering and Science, Vol. 11, pp. 745- 766, 1973.

65. Muskhelishvili, N. I., Some Basic Problems of the Mathematical Theory of Elasticity, (English translation by Radok, J. R. M.), P. Noordhoff N. V., Groningen, Holland, 1953.

66. Milne-Thomson, L. M., Plane Elastic Systems, Springer-Verlag, Berlin.

67. Kelly, J. L. and Wilhoit, J.C., "The Stresses Produced by Uniform Radial and Lateral Displacement of Two Circular Holes in An Infinite Plate", Proceedings of the Fourth U.S. National Congress of Applied Mechanics, Vol.1, pp. 635-644, 1962.

68. Lawn, B. R. and Fuller, Journal of Materials Science, Vol. 10, pp. 2016-2024, 1975.

69. Delale, F. and Liaw, B. M., Research Proposal.

70. Delale, F. and Liaw, B. M., Research Annual Report (1988).

71. Dundurs, J. and Sendeckyj, G.P., "Edge Dislocation inside a Circular Inclusion", Journal of Mechanics and Physics of Solids, Vol. 13, pp. 141-147, 1965.

72. ABAQUS Manuals, Hibbit, Karlsson & Sorensen, Inc., Providence, RI.

73. Delale, F. and Liaw, B.M., " Microcracking and Toughness of Ceramic-Fiber/Ceramic-Matrix Composites Under High Temperature", Technical Report, AFOSR-87-0288, The City College, December 1989.

74. Delale, F. and Xu, Y. L., "Effect of Fiber Interaction on Microcracking in Ceramic Matrix Composites", presented on ASME WAM, 1990.

75. Delale, F., Xu, Y. L., and Liaw, B. M., "Microcracking in Ceramic Composites Under High Temperature", published in Proceedings of 5th Japan-US Conference on Composite Materials, Tama-City, Tokyo, Japan, June 1990.